의학박사 학위논문

Mechanism of Improved Glucose Homeostasis after Metabolic Surgery

대사 수술을 통한 포도당 항상성 호전의 기전

2019 년 07 월

서울대학교 대학원

의학과 중개의학 전공

안 창 호

A thesis of the Degree of Doctor of Philosophy

대사 수술을 통한 포도당 항상성 호전의 기전

Mechanism of Improved Glucose Homeostasis after Metabolic Surgery

July 2019

Department of Translational Medicine

Seoul National University

College of Medicine

Chang Ho Ahn

Mechanism of improved glucose homeostasis after metabolic surgery

by
Chang Ho Ahn

A thesis submitted to the Department of Translational Medicine in partial fulfillment of the requirements for the Degree of Doctor of Philosophy in Translational Medicine at Seoul National University College of Medicine

July 2019

Approved by Thesis Committee:

Professor _____Chairman
Professor _____Vice chairman
Professor _____
Professor _____
Professor _____

ABSTRACT

Obesity increases the risk of metabolic, cardiovascular, musculoskeletal diseases and even some types of cancer. Among various complications of obesity, type 2 diabetes mellitus (T2DM) is the prototype of metabolic complications. Obesity is the primary contributor to the development of T2DM. Despite of tremendous efforts to bring better treatment for obesity and diabetes, there are still significant unmet needs.

Metabolic surgery is a surgical treatment to reduce body weight and improve glucose metabolism. Unlike other pharmacologic treatment for obesity and diabetes, metabolic surgery demonstrated superior clinical efficacy and longer durability. Furthermore, metabolic surgery can induce remission of T2DM which is defined as achieving normoglycemia without any anti-diabetic medication. By unraveling the mechanism of metabolic surgery to improve metabolic homeostasis, we can develop new insights into glucose metabolism and better treatments.

To elucidate the molecular mechanism of metabolic surgery, two rodent models of metabolic surgery were used. First, ileal transposition (IT) is an experimental surgery which translocate a segment of distal ileum into proximal jejunum. The metabolic effects of IT were investigated in diet-induced obese rats. IT improved glucose tolerance by augmenting postprandial insulin and GLP-1 secretion. IT also increased pancreatic β-cell mass which was thought to be associated with increased GLP-1 secretion. However, IT did not have significant effect on body weight and insulin sensitivity. On histologic

examination, the transposed ileum showed hypertrophic change and increased enteroendocrine cell density positively stained for GLP-1 and GLP-1/GIP. Then, an unbiased transcriptomic analysis was applied on the transposed ileum to investigate the adaptive process of the intestine after IT. Using microarray analysis of the transposed ileum at week-1 and week-4 after surgery, I could demonstrate that the transposed ileum undergoes a dynamic adaptation process after IT. Functional enrichment analysis and network analysis further characterized the major components of each stage, which were structural adaptation at week 1 and metabolic and immune adaptations at week 4.

Secondly, a mouse model of vertical sleeve gastrectomy (VSG) was constructed to investigate the effects of VSG in glucose metabolizing tissues including liver, fat and muscle. Vertical sleeve gastrectomy removes lateral 80% of the stomach and leaves only tube like remnant of the stomach. I examined gene expression profiles of liver, fat and muscle in VSG mice compared with sham and sham pair-fed (sham-PF) mice using RNA sequencing analysis at 8 weeks after surgery. VSG improved glucose tolerance significantly than sham, but only marginally than sham-PF. Unexpectedly, gene expression profiles of liver, fat, and muscle tissues were significantly different between VSG and sham-PF, which was more distinct than the comparison between sham and sham-PF, suggesting the weight-loss independent effects on gene expression of peripheral tissues are more robust than weight-loss dependent effects. In addition, immune response-related gene ontology and pathways were consistently un-regulated in the three organs. In further analysis, the immune

response in adipose tissue was characterized as up-regulation of M2 phenotype macrophage and B lymphocytes.

In summary, IT in rats and VSG in mice could demonstrate the metabolic improvements after metabolic surgery. The intestine undergoes dynamic adaptation process after surgery which can have implications in metabolic homeostasis with structural and functional changes. The glucose metabolizing peripheral tissues, liver, fat and muscle, showed both weight-loss dependent and independent changes in gene expression. The immune response was the common pathway enriched in the three organs after metabolic surgery.

Keywords: metabolic surgery, ileal transposition, vertical sleeve gastrectomy, microarray, RNA sequencing, gut adaptation, M2-macrophage, B lymphocytes

Student number: 2016-30012

CONTENTS

LIST OF TABLES AND FIGURES

General introduction

Chapter 1

Chapter 2

Discussion

General Introduction

1. The unmet needs in the treatment of obesity and diabetes.

Obesity is pandemic in this modern society. The prevalence of obesity is consistently increasing and nearly tripled since 1975 (1). Korea is no exception to this obesity epidemic. The prevalence of obesity was 34.7% by body mass index (BMI) ≥25 kg/m^2, and 6.0% by BMI ≥30 kg/m^2 in 2017, Korea (2). Obesity increases the risk of metabolic diseases (type 2 diabetes mellitus, fatty liver and dyslipidemia), cardiovascular diseases (hypertension, myocardial infarction and stroke), musculoskeletal disease, depression and even several types of cancer (3). Besides these medical consequences of obesity, obesity affects the social functioning of an individual such as lower quality of life, unemployment, and lower productivity (3). Various medical organizations including World Obesity Federation have declared obesity as a chronic progressive disease, not just a risk factor for other diseases (4). Among various complications of obesity, the prototype metabolic disease associated with obesity is type 2 diabetes mellitus (T2DM). Diabetes mellitus is characterized by hyperglycemia resulting from defects in insulin secretion, insulin action, or both (5). Among subtypes of diabetes mellitus, T2DM is a diabetes mellitus not caused by the destruction of pancreatic β-cells or other specific causes (6). The risk of T2DM increases linearly with increasing BMI (7). Through its

progressive course, T2DM can lead to various complications resulted from the damages in the vasculature system.

Lifestyle changes focused on healthy diet and increased physical activity are the first line treatment for the obesity and diabetes. With lifestyle changes, patients can lose about 5 to 10% of their body weight. However, it is extremely hard to maintain the reduced body weight. Most patients start to regain body and return to their previous weight (8). In addition to the lifestyle changes, various pharmacological attempts have been made for obesity treatment. There are currently available agents including locaserin, bupropion/naltrexone, phentermine/topiramate, orlistat and liraglutide (9). However, their clinical efficacy is limited around 3 to 6% of weight loss except 10% weight loss for phentermine/topiramate, and long term safety is not proven yet. Several previously approved anti-obesity medications are withdrawn from the market due to serious cardiovascular or psychologic side effects.

There is also a hurdle in the treatment of diabetes. Although many newer glucose lowering medications are developed, none has been shown to reverse the progressive course of diabetes. In fact, nearly 50% of patients with T2DM fail to achieve adequate glycemic control by the criteria of hemoglobin A1c <7% both in Korea and US (10, 11).

2. Metabolic surgery for the treatment of obesity and diabetes

2.1. Historical background of metabolic surgery

The surgical attempts to lose body weight date back to mid 1950s (12). Early attempts were to cause malabsorption of nutrients by bypassing a part of intestine where the nutrient absorption occurs (Figure 1-1A, B). In 1953, Varco et al. carried out the first intestinal bypass in humans. He anastomosed the proximal jejunum to the distal ileum, left only a small segment of the small intestine exposed to nutrients (13). These intestinal bypass procedures could achieve significant and durable weight loss. However, these procedures led to serious complications including diarrhea, dehydration, vitamin deficiency, protein malnutrition, metabolic bone diseases, liver failure, and even death (12).

Another approach was to restrict the nutrient intake by partitioning the stomach (Figure 1-1C, D). Purely restrictive procedures were first reported in 1973 by Printen and Mason (14). Their procedure was evolved to vertical banded gastroplasty which is a vertical partition of the stomach that creating a chamber. However, these procedures showed weight regain during the long term follow-up period and complications including band erosion, dysphagia, and inability to tolerate solid foods were also reported. Gastric banding was another attempt to restrict the food intake, in which a band was placed tightly around the superior aspect of the stomach to partition it (15). Then, it was evolved to adjustable gastric band (AGB) surgery using silicone adjustable band (16).

To maximize weight loss while minimizing complications, various modifications from above mentioned surgeries were made. At the same time, the combination of restrictive and malabsorptive proecedures were also tried. Procedures with limited clinical efficacy and high rate of complication quickly

lost popularity. In a worldwide report 2013, currently 4 types of surgeries are the most popular metabolic surgery accounting for more than 95% of all the surgery cases globally (17). The 4 surgeries are Roux-en-Y gastric bypass (RYGB), vertical sleeve gastrectomy (VGS), adjustable gastric banding (AGB), and biliopancreatic diversion (BPD), in the order of popularity.

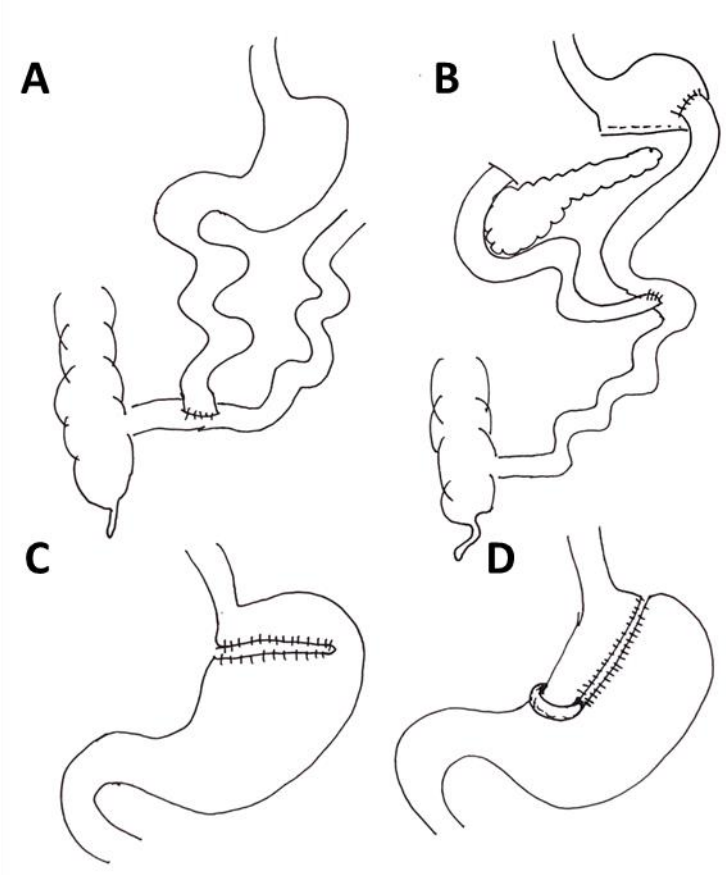

Figure 1-1. Diagrams of past bariatric procedures

Intestinal bypass procedures: (A) jejunoileal bypass and (B) biliopancreatic diversion. Gastroplasty procedures: (C) horizontal gastroplasty and (D) vertical banded gastroplasty. Adapted from Moshiri et al. (18).

2.2. Current practice of metabolic surgery

The two most popular procedures currently are RYGB and VSG. AGB showed lower efficacy and BPD showed higher rate of complication and malnutrition than RYGB or VSG.

VSG was developed by Dr. Gagner (12). VSG resects lateral portion of the stomach on the side of greater curvature removing more than 80% of the stomach volume and leaving tube-like remnant stomach (Figure 1-2A). Originally, VSG was performed in a part of two-stage surgery combining initial VSG and intestinal bypass as a next step for high risk patient who cannot tolerate a complex surgery at once (19). It was noted that many of these patients did well enough with SG alone that they did not want the second component of the two stage surgery (20). Eventually, VSG became a successful stand-along procedure.

RYGB is more complex procedure than VSG, which combining resection of the stomach and bypass of the small intestine (Figure 1-2B). RYGB developed from the observations that patients who had subtotal gastrectomy for cancer lost considerable amount of body weight. In RYGB, the stomach is divided into the upper stomach pouch, which is 15–30 ml in volume, and the lower, gastric remnant (21). The upper stomach pouch is then anastomosed to the mid-jejunum through a gastrojejunal anastomosis in a Roux-en-Y fashion. A jejuno-jejunal anastomosis between the excluded biliopancreatic limb and the alimentary limb is made at 75–150 cm distal to the gastrojejunostomy. The gastric remnant and biliopancreatic limb is no longer exposed to food. Gastric, pancreatic and biliary secretions flow in the biliopancreatic limb and mix with

food at the jejuno-jejunal anastomosis. Nowadays both RYGB and VSG can be performed laparoscopically and have low rate of surgical complication and mortality.

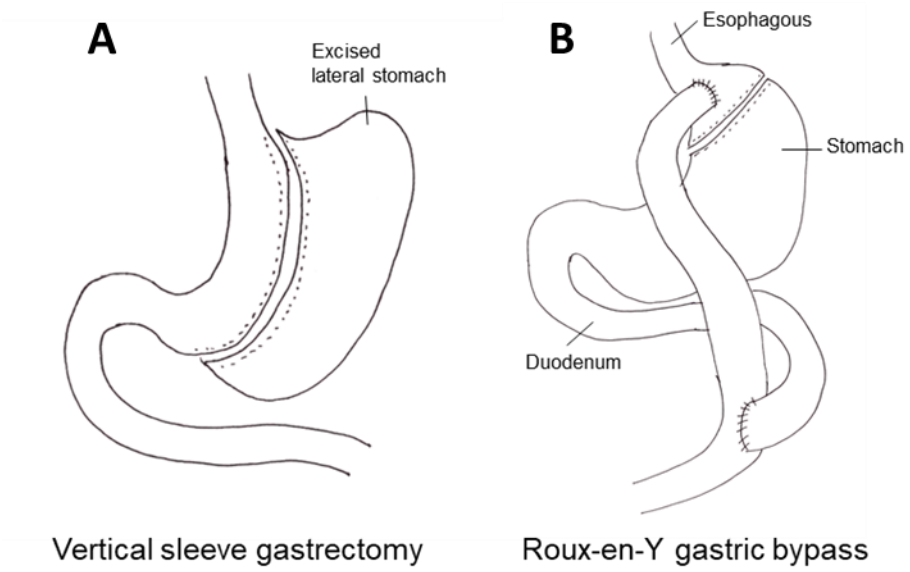

Figure 1-2. The two most popular bariatric surgeries currently

(A) vertical sleeve gastrectomy and (B) Roux-en-Y gastriv bypass. Adapted from Madsbad et al. (22).

2.3. Superior efficacy and long durability of metabolic surgeries in the treatment of obesity and diabetes

In a meta-analysis of observational studies, diabetes remission rates of each surgery were 92.8% (85.3-97.2%) for RYGB, 85.5% (72.7-94.1%) for VSG and 67.6% (49.5-82.8%) for AGB (23). The reduction of BMI was -14.3 (-19.2 to -9.6) for RYGB, -12.1 (-14.0 to -10.3) for VSG and -7.7 (-9.4 to -6.0) for AGB, respectively.

Swedish Obese Subjects (SOS) study was a landmark clinical study which demonstrated the long term effects of metabolic surgeries (24). It was a nonrandomized, prospective, controlled study. Obese individuals (BMI ≥34 kg/m^2 in men and ≥38 kg/m^2 in women) who were undergoing metabolic surgery (19% AGB, 69% vertical banded gastroplasty and 12% RYGB) were enrolled (n = 2010), and matched to conventionally treated control individuals with obesity (n = 2037). In patients who underwent surgery, the maximum weight loss was generally reached after 1–2 years, with stabilization of weight loss from baseline at 25% and 14% below the baseline weight for RYGB and AGB, respectively after 10 years. All-cause mortality was reduced by 24% in 15 years of follow-up.

The Longitudinal Assessment of Metabolic Surgery (LABS) study was a multicenter observational cohort study in USA and included 2,458 adults undergoing metabolic surgery (70.7% RYGB, 24.8% AGB and 4.5% other procedures) (25). After 7 years of follow-up, the mean weight loss was 28.4% for RYGB and 14.9% for AGB. Diabetes remission rates were 60.2% for RYGB and 20.3% for AGB.

The Surgical Treatment and Medications Potentially Eradicate Diabetes Efficiently (STEMPEDE) trial was a randomized, controlled, nonblinded, single-center study comparing VSG, RYGB and intensive medical treatment for the effects on improving hyperglycemia (26). There were more rapid, larger and more sustained reductions in the levels of glycated hemoglobin, fasting plasma glucose, and BMI in the RYGB and VSG group than medical treatment group. The diabetes remission rate defined as glycated hemoglobin <6.5% without diabetes medication was 0, 30.6 and 23.4% for medical treatment, RYGB and VSG, respectively at 5-year follow-up. In the two surgical group, BMI was reduced from 36.0 to 29.3 kg/m^2 for VSG and 37.0 to 28.9 kg/m^2 for RYGB, while it was only reduced from 36.4 to 34.0 kg/m^2 after medical treatment. In addition, the difference of BMI between RYGB and VSG was small but statistically significant (P = 0.01). This randomized controlled trial demonstrated that metabolic surgery was superior to intensive medical therapy in terms of glycemic control, weight reduction, medication reduction, improvement in lipid levels, and quality of life which was sustained for 5 years. Interestingly, the outcome of body weight and glycemic control was similar between the subjects with BMI over 35 kg/m^2 and below 35 kg/m^2, suggesting the benefits of metabolic surgery are not only applied to severely obese patients but also to the patients with moderate obesity.

2.4. The need to understand the underlying mechanism of metabolic surgeries

The results of prospective observational studies or randomized trials have consistently shown that metabolic surgeries including RYGB and VSG are highly effective for body weight and glucose control. They can even induce the remission of T2DM which is unlikely to be achieved by medical treatment. This clinical success of metabolic surgeries raised a large interest to the underlying mechanism of these surgeries. By unraveling the underlying mechanism of metabolic surgeries, we can better understand the physiology of body weight control and glucose metabolism, and eventually develop new noninvasive treatments for obesity and T2DM beyond metabolic surgeries.

3. Food restriction and malabsorption are not the main mechanism of metabolic surgery

Initially, it was speculated that weight loss after metabolic surgery was due to mechanical restriction and, for procedures that involve bypass of the intestine, malabsorption of ingested food (27). However, a large series of evidences suggested that the food restriction or malabsorption are not the mechanism of the metabolic surgery.

The most obvious evidence why food restriction is not the mechanism of metabolic surgery is that the eating behavior after metabolic surgery is in contrast with that after dieting. While on a low-calorie diet, patients report an increase in hunger and a decrease in satiety along with changes in hormone levels controlling energy intake (28). However, after RYGB and VSG, patients feel less hunger and early satiety, even though they were on a diet with lower

calorie than before surgery and had a significant weight loss (29, 30). RYGB was also reported to affect brain reward systems in eating behavior (31) and taste sensation (32), suggesting more complex effects of RYGB on food intake than just a restriction. In animal studies, RYGB and VSG reduce the daily calorie intake compared to sham surgery initially during early postoperative period, but eventually animals undergone RYGB or VSG increase the daily food intake to the similar level as sham control animals (Figure 1-3) (33-35). Another evidence is an observation of pregnant rat underwent VSG. The rat could increase the daily food intake during lactation to meet the increased calorie requirement as similar to control rat (36). These animal studies provide direct evidences that mechanical restriction of food intake is not the mechanism how metabolic surgery induce weight loss.

About malabsorption of nutrients after metabolic surgery, AGB and VSG simply do not induce malabsorption (37). In RYGB, malabsorption of carbohydrate and protein was not reported, but some extent of lipid malabsorption (around 10% of ingested) was reported (38). Malabsorption of micronutrients including vitamins, calcium, zinc, and iron can occur after RYGB (39). However, it is not clear whether these malaborption of micronutrients have a clinical impact after RYGB.

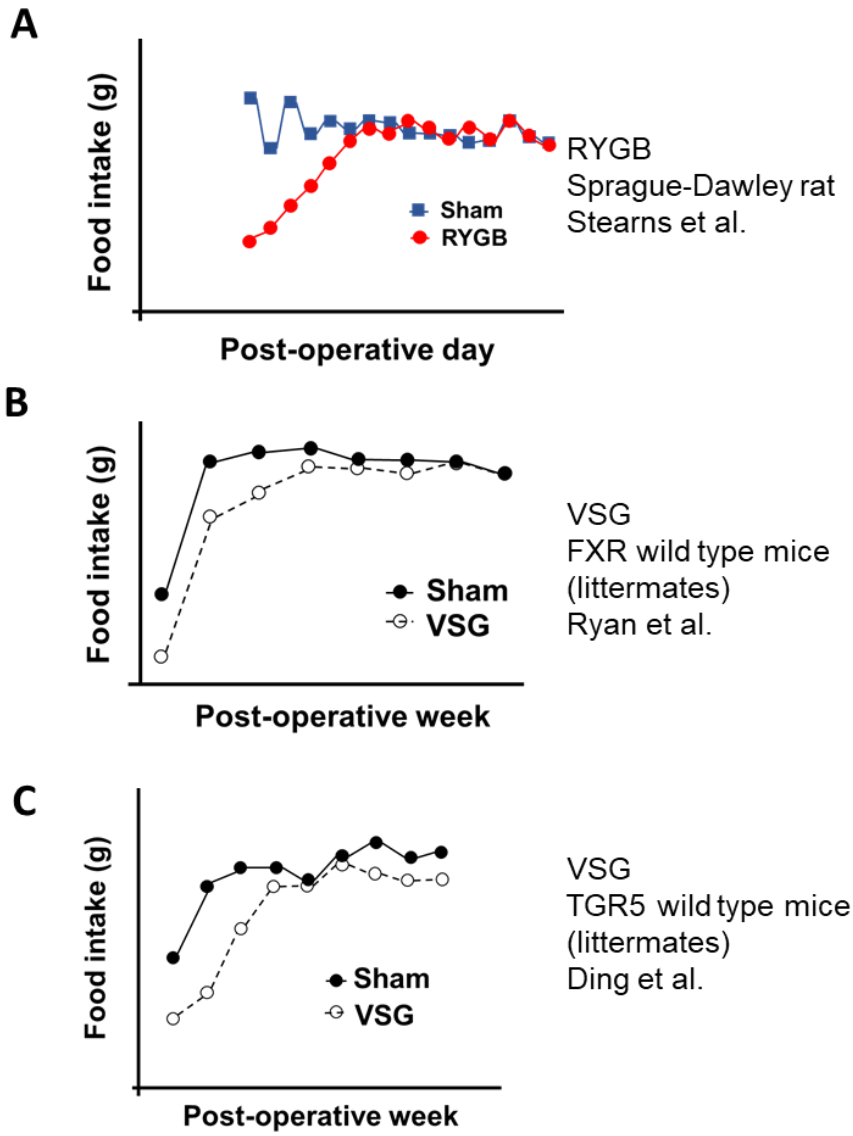

Figure 1-3. Food intake graphs from different rodents studies of RYGB or VSG

Studies performed by (A) Stearns et al. (33), (B) Ryan et al. (34), and (C) Ding et al. (35). The three studies used different rodent strains and performed by different study groups. They all showed similar results of initial reduction of food intake after metabolic surgery for 2 to 3 weeks, then catch up to the similar extent as control animal.

4. Weight loss-dependent and independent effects of metabolic surgery on glucose metabolism

Another issue is whether there is a weight-loss independent mechanism of metabolic surgery to improve glucose metabolism. Body adiposity is a major determinant of an individual's insulin sensitivity. Insulin sensitivity decreases and the incidence of diabetes increases with higher BMI (40-42). Calorie restriction and subsequent weight loss have potent effects on insulin sensitivity and overall glucose metabolism. Only about 5% weight loss reduced the incidence of diabetes by 58% and this effect lasted even after the regain of body weight (43). Thus, it has long been argued that whether diabetes remission is mainly due to weight loss-dependent or weight loss-independent effects of metabolic surgery, because it can direct the researchers where to focus on to elucidate the mechanism of metabolic surgery (44).

4.1. The evidences support the importance of weight loss-dependent effects of metabolic surgery

The argument that weight loss-dependent mechanism is the main mechanism of diabetes remission after metabolic surgery can be divided into two part: first, the very low calorie diet shortly after the surgery explains early improvements in hepatic insulin sensitivity; second, long term weight loss is the major determinant to improve peripheral insulin sensitivity. Low calorie diet has very rapid effects on hepatic glucose metabolism. Low calorie diet (~1100 kcal/day) can reduce basal glucose production and intrahepatic

triglyceride content only within 48 hours, and the insulin sensitivity measured by HOMA-IR improved by 40% (45). In a study of 11 T2DM patients who had RYGB and 14 T2DM patients who were matched for BMI, HbA1c and given very low calorie diet (VLCD, 500 kcal/day), glucose disposal, acute insulin response and disposition index measured by frequently sampled intravenous glucose tolerance test had a similar improvement in the two groups after mean 21 days, suggesting VLCD and RYGB had similar acute effects on insulin sensitivity and pancreatic β-cell function (46).

It is difficult to directly compare the effects of long term weight loss between surgical and non-surgical treatment. Although there is no direct comparison, for indirect comparison, the relationship between peripheral insulin sensitivity measured by hyperinsulinemic euglycemic clamp and BMI was plotted for patients who had metabolic surgery to see whether the insulin sensitivity improves beyond that expected from BMI (47). The results from hyperinsulinemic euglycemic clamp in 220 non-diabetic lean, overweight and obese subjects constituted a curvilinear reference line. The relationship between BMI and insulin sensitivity reported in previous studies of LAGB and RYGB was on the reference line of non-diabetic controls, suggesting that weight loss itself is a primary determinant of the improvement in peripheral insulin sensitivity after long term weight loss.

4.2. The evidences support the importance of weight loss-independent effects of metabolic surgery

Unlike human studies, in animal studies, we can control confounding factors including weight loss, calorie intake, nutrients source and surgical stress. Especially using weight matched sham control animal, we can directly investigate the weight loss-independent effects. In RYGB and VSG rats, the glucose tolerance and insulin sensitivity after intraperitoneal glucose or insulin challenge were improved than sham control as similar extent as pair-fed rats (48). However, the postprandial insulin and GLP-1 secretion after oral glucose challenge, and hepatic insulin sensitivity measured by hyperinsulinemic euglycemic clamp were greatly increased in RYGB and VSG rats than sham or pair-fed rats. In db/db mice, VSG lowered blood glucose and triglyceride level significantly more than pair-fed mice at early postoperative period (7 days after surgery) (49). Using RNA sequencing analysis of liver tissue, VSG was shown to differentially affect the gene expression of liver compared to pair-fed mice, where the expression of bile acid related genes were mainly changed (50). A recent study, using ex vivo analysis of pancreatic islet, VSG improved glucose-stimulated insulin secretion more than pair-fed mice, and transcriptome analysis of the islet showed differential gene expressions pattern in calcium signaling and insulin secretion pathways in VSG compared to pair-fed mice (51). In addition to the evidences from animal studies, experts also suggests possible clinical evidences that support weight loss-independent mechanism in human metabolic surgery (Table 1-1) (44, 47).

There is still a continuing argument about the importance or existence of weight loss-independent effects in metabolic surgery. Thus a comprehensive analysis

on the weight loss-independent effects is necessary for deeper understanding of metabolic surgery.

Table 1-1. The clinical evidences that support weight loss-independent mechanism in human metabolic surgery

Very rapid T2DM remission after RYGB or VSG (52)
Greater improvements in glucose homeostasis after RYGB or VSG than similar weight loss after AGB (53)
Different pattern of postprandial insulin and other hormone response after oral mixed meal or glucose load
Occasional development of late-onset β-cell hyperactivity and hypoglycemia (54)

5. Mechanisms how metabolic surgery induces diabetes remission

5.1. Perspective on insulin sensitivity

Insulin sensitivity can be estimated by various measures in human. HOMA-IR is an index of insulin sensitivity that is calculated from plasma glucose and insulin levels of fasting state and mainly reflects hepatic insulin sensitivity (55). After various metabolic surgeries, including RYGB, AGB and VSG, HOMA-IR decreases even within days after surgery and remains at the lower level for more than 18 months after surgery with about 50% reduction from baseline (56).

Hyperinsulinemic euglycemic clamp is a gold standard method to estimate the whole body insulin sensitivity (57). During the clamp, supraphysiologic dose of insulin is infused and, simultaneously, variable rate of glucose is infused and adjusted to maintain the plasma glucose level in an euglycemic range. The glucose infusion rate, which reflects how much glucose is needed to maintain the euglycemia under the hyperinsulinemic condition, is the measure of whole body insulin sensitivity. Not like HOMA-IR which reflects a fasting state, hyperinsulinemic euglycemic clamp sets a body to a different homeostatic point. It is assumed that by the hyperinsulinemia hepatic glucose production is suppressed and the glucose infusion rate reflects glucose disposal by peripheral tissues including skeletal muscle and adipose tissue. The peripheral insulin sensitivity measured by hyperinsulinemic euglycemic clamp does not change during very early postoperative period (2 to 4 weeks) with

moderate weight loss (~10%) after RYGB. However, it increased markedly after greater weight loss (20 to 40%) 6-16 months after surgery by 50 to 150% increase (47). In a longitudinal study of 10 T2DM and 10 NGT subjects who underwent RYGB, hepatic insulin sensitivity significantly increased even at 1 week after surgery (58). However, peripheral insulin sensitivity was not improved at 1 week after surgery, but improved at 3 months and even more at 1 year after surgery. VSG similarly improved insulin sensitivity compared with RYGB in a study of subjects with matched (20%) weight loss after surgery (59). These can be summarized that metabolic surgery acutely improve hepatic insulin sensitivity followed by long term improvement in peripheral insulin sensitivity (Figure 1-4).

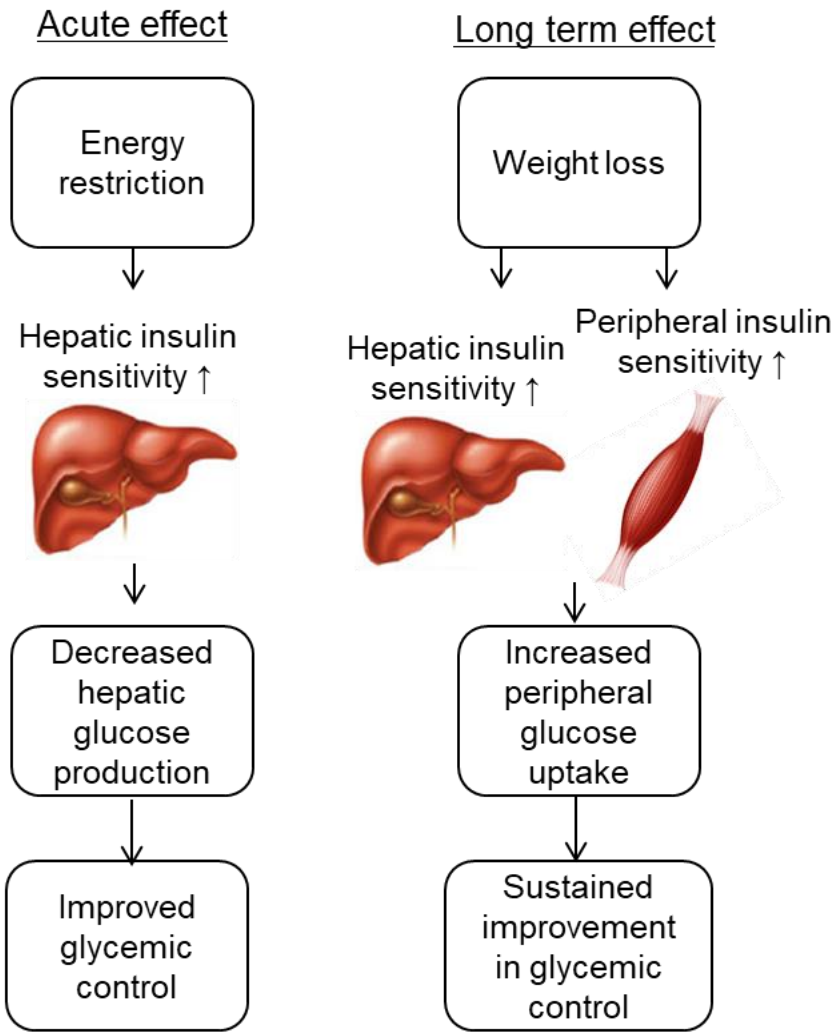

Figure 1-4. Effect of metabolic surgery on insulin sensitivity evolved from acute to long term period

Modified from Dirksen et al. (60).

5.2. Perspective on pancreatic β-cell function

After RYGB and VSG, the postprandial plasma glucose and insulin profile show a characteristic pattern (Figure 1-5). The glucose level reaches higher and faster peak than before surgery and decreases more steeply to return to baseline level (22). Insulin profile is similar to this. Plasma insulin level has faster and higher peak and steeper fall thereafter. This suggests that the physiology of postprandial glucose handling and insulin secretion is markedly changed after metabolic surgery. This is probably caused by the different rate of glucose absorption and the different GLP-1 response profile after surgery (22).

If we measure the total amount of insulin secretion after glucose challenge by calculating area under the curve (AUC) of insulin level, it usually decreased after metabolic surgery due to large improvements in insulin sensitivity. Thus, it is an inappropriate measure to estimate pancreatic β-cell function after surgery. The disposition index, which is insulin secretion multiplied by insulin sensitivity is consistently increased after RYGB and VSG in various studies, but this was mainly by the increase of insulin sensitivity (47). In a longitudinal study, RYGB increased insulin secretion only after oral glucose load, not after iv glucose load, measured by incremental AUC of C-peptide, insulinogenic index and disposition index (58). In a study of porcine RYGB model, not just β-cell function, but also β-cell mass and GLP-1 receptor expression in pancreatic islet were increased than sham-operated animal (61). Postprandial GLP-1 secretion is largely increased after RYGB and VSG, and GLP-1 has been reported to have beneficial effects on β-cell function and

survival. Improvement in insulin sensitivity and resolution of hyperglycemia can lead to significant attenuation of glucotoxocity, which is one of the main contributors to β-cell dysfunction in T2DM. These can be a mechanism how metabolic surgery improves pancreatic β-cell function.

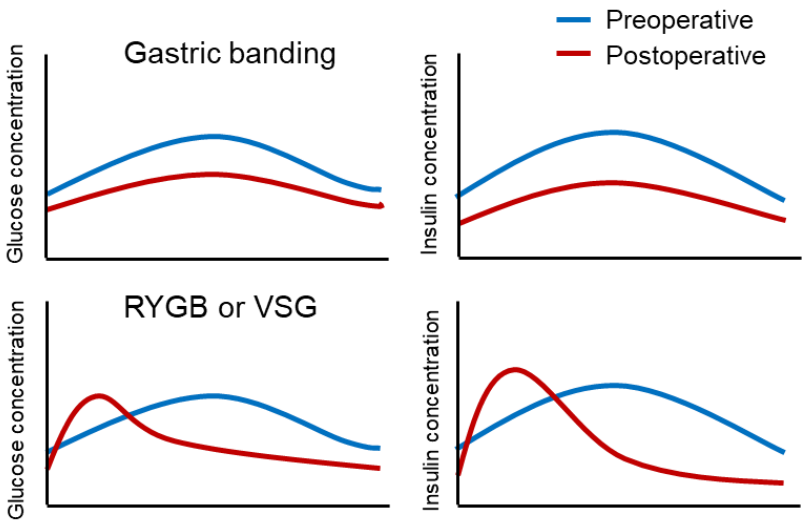

Figure 1-5. The characteristic pattern of postprandial glucose and insulin level in patients underwent RYGB or VSG and gastric banding

Modified from Madsbad et al. (22).

6. Need of systematic approach to investigate the underlying mechanism of metabolic surgery

The unprecedented success of RYGB and VSG in treatment of morbid obesity and T2DM aroused much attention to the molecular mechanism of these surgeries to improve whole body metabolism. Interestingly, there are clear evidences supporting that food restriction and malabsorption, the initial goal that surgeries tried to achieve, are not the major mechanism of how metabolic surgery induce significant weight loss. This led to further studies on gut-brain pathways and regulation of gut hormones. Yet, the mechanism has not been clearly elucidated, and it is suggested to rely on the complex interplay of different organs including the gut, pancreatic islet, liver, adipose tissue, skeletal muscle and more. Thus, it is necessary to employ a systematic approach to investigate the underlying mechanism of metabolic surgery.

In addition, an unbiased approach can be advantageous for this purpose. Previous hypothesis-driven biased approaches to uncover the pivotal molecular pathway of metabolic surgery were failed. GLP-1, ghrelin, melanocortin receptor, and GDF15 pathways were not essential for mediating the effects of VSG (62-65). Even though, an unbiased approach has a strength especially in hypothesis generation step, it can explore the various aspects of molecular changes systematically.

In this study, we employed an unbiased systematic analysis of tissue transcriptome to explore the molecular aspects of metabolic surgery.

Chapter 1.

Metabolic effects of ileal transposition and the adaptive process of the transposed distal ileum

Background and objectives of chapter 1

RYGB is an effective metabolic surgery that can induce robust weight loss and even remission of type 2 diabetes. It is composed of complex alterations in gut physiology characterized by restricted stomach volume, bypass of proximal small intestine (duodenum and upper jejunum), and expedited delivery of unabsorbed nutrients to the distal small intestine). In other words, the stomach, proximal small intestine and distal small intestine are the three key parts of the intestine involved in the effects of RYGB. Among them, the distal small intestine can have a crucial role because gut hormones involved in energy homeostasis and glucose metabolism, such as glucagon like peptide-1 (GLP-1) and peptide YY (PYY), are mainly secreted from the distal small intestine. However, it is difficult to dissect the individual effect of each intestinal part in RYGB.

Ileal transposition (IT) is an experimental surgical procedure that is used to investigate the role of the distal small intestine in RYGB (66). IT translocates a segment of the distal ileum to the upper jejunum distal to the Treitz ligament, which enables a large amount of ingested nutrients to be exposed to the translocated distal ileal tissue, and improves glucose tolerance in both obese and nonobese diabetic rat models (66). I aimed to investigate the role of the distal small intestine performing IT in diet-induced obese rat model, a physiologic model of obesity and T2DM.

In addition to the metabolic effects of IT, I had another objective to examine the adaptive process of the distal small intestine after surgery. The

intestine is a highly plastic organ with large potential of transformation to adapt a new physiologic states such as bowel resection (67). The small intestine undergoes morphological and functional changes after RYGB, and these changes can serve a pivotal role in the metabolic improvements after metabolic surgery (68). In a rat model of IT, compared to the ileum *in situ* (IIS), the transposed ileum (ITR) showed morphological changes, including lengthening of the villi and thickening of the muscle, which was dubbed the jejunization process (69, 70). Real-time PCR analysis of the ITR showed increased expression of the *Gcg* and *Pyy* genes, accompanied by higher plasma levels of glucagon-like peptide-1 (GLP-1) and peptide YY (PYY) (71). These studies demonstrated altered structure and endocrine function of the ITR. However, systematic analysis of the adaptive processes of ITR has rarely been performed. Since the gut adaptation process incorporates many aspects of gut physiology, an unbiased systematic analysis can enable the understanding of such diverse characteristics of the gut adaptation process. Thus, I performed transcriptome analysis of the ITR from IT surgery and of the IIS from sham surgery at two different postoperative time points (weeks 1 and 4) to investigate the gut adaptation process after IT.

Materials and Methods

1. Animals

For the investigation of the metabolic effects of IT, diet-induced obese rats were used. Male Sprague-Dawley (SD) rats aged 6 weeks old were purchased (Orient Bio Inc. Sungnam, Korea). After 1 week of acclimation period, rats were individually housed and fed high fat diet (60% of total calories from fat, D12492, Research Diets, Inc. New Brunswick, NJ). After 12 weeks of high fat diet feeding, rats were randomized into IT or sham surgery.

For the investigation of the intestinal adaptation after IT, chow-fed non-obese rats were used. Male Sprague-Dawley rats aged 13 to 14 weeks were individually housed and fed a standard chow diet (Purina rat and mouse chow, Purina Korea, Seoul, Korea) *ad libitum*. Rats were randomly selected for sham or IT surgery. For gene expression analysis, rats were sacrificed at 1 and 4 weeks postoperatively. Thus, the study groups consisted of IT and sham groups of postoperative 1-week and 4-week models. The ITR and IIS were harvested from the IT and sham surgery rats, respectively, and fixed in a 10% formalin solution for histologic analysis or frozen in liquid nitrogen and stored at -70 ℃ for RNA isolation. To investigate long-term morphological changes in the ITR, the IT-operated rats were killed at 1, 4, 8, 12 and 16 weeks after IT surgery, and the ITR was harvested. Histologic examination and immunohistochemistry of GLP-1 and GIP were done for the harvested ileal tissues.

2. Surgical Techniques

The detailed protocol of surgery was described in our previous study (70). Briefly, IT or sham surgery was performed after overnight fast under general anesthesia with 2% isoflurane. In the IT surgery, the distal ileal segment located between 5 and 15 cm proximal to the ileocecal valve was resected with intact mesentery and transposed at 10 cm distal to the ligament of Treitz in an isoperistaltic fashion. In the sham surgery, 3 corresponding transections of the intestine (2 for the distal ileum and 1 for the upper jejunum) were made and repaired *in situ*. The intestinal anastomosis was made with 6–0 Vicryl. Ceftriaxone (50 mg/kg) was given intramuscularly immediately before laparotomy as a prophylactic antibiotic. Meloxicam (1.5 mg/kg) was given subcutaneously after surgery for postoperative pain control. No oral intake was allowed for 24 hours after surgery, and then, liquid meal and water were provided gradually. From postoperative day 3, the standard chow diet and water were given *ad libitum*. The mortality rates were 18.8% (3/16) and 16% (4/25) for 1-week and 16-week models, respectively.

3. Insulin tolerance test

Insulin tolerance test was conducted 6 weeks after surgery. After 4 hours of fasting, insulin (0.75 units/kg) i.p. was administered. A drop of blood sample was drawn by tail vein cutting at 0, 15, 30, 60, 90, 120 minutes after insulin injection. Blood glucose levels were measured by a glucometer (OneTouch, LifeScan Inc., Milpitas, CA).

4. Oral glucose tolerance test

Oral glucose tolerance test was conducted 6 weeks after surgery. After overnight fast, a glucose load (1.5 g/kg) in 50% dextrose solution was administered by oral gavage. Blood samples were drawn by tail vein cutting at 0, 15, 30, 60, 90, 120, and 180 minutes after oral glucose load. All the blood samples were placed on ice immediately and centrifuged for plasma separation. The plasma was stored at -80 for further analysis.

5. Biochemical analysis

The plasma concentration of insulin, glucagon, total glucose-dependent insulinotropic polypeptide (GIP), and peptide YY (PYY) were measured by Millipex Map rat metabolic magnetic bead panel kit (No. RMHMG-84K, Millipore, Billerica, MA). Plasma total GLP-1 level was measured by a ELISA kit (Millipore).

6. Histology and immunohistochemistry

The tissue sections of ITR and IIS were stained with hematoxylin and eosin. The villi length and muscle thickness were measured using light microscopy. For immunofluorescence staining, after deparaffinization and antigen retrieval processes, the slides were incubated with an anti-GIP antibody diluted 1:50 (CSB-PA445787, Flarebio Biotech LLC, College Park, MD, USA) at 4 °C overnight and then with the Alexa Fluor 594 goat anti-rabbit secondary antibody diluted 1:1000 (A-11037, Thermo Fisher Scientific, Rockford, IL, USA) for 1 hour at room temperature. Subsequently, the slides were incubated with an anti-GLP-1 antibody diluted 1:200 (HYB 147-06, Antibody Shop,

Gentofte, Denmark) overnight and with the Alexa Fluor 488 donkey anti-mouse secondary antibody diluted 1:1000 (A-21202, Thermo Fisher Scientific, Rockford, IL, USA) for 1 hour. Nuclear staining was performed using 6-diamidino-2-phenylindole (DAPI) (ImmunoBioScience, Mukilteo, WA, USA). Finally, the slides were examined with a fluorescence microscope (Leica DMI 4000B, Bensheim, Germany).

Three pancreas tissue sections starting from the middle of the paraffin block were made with 150 μm distance for each rat. The sections were incubated overnight with anti-insulin antibody diluted 3:800 then with HRP conjugated anti-rabbit secondary antibody diluted 1:100 for 1 hour. The scanned images of slides were analyzed to measure the area of insulin-positive cells and total pancreas tissue by ImageJ software (NIH, Bethesda, MD).

7. Microarray experiments

The ileal tissue samples stored at -70 °C were used for the isolation of RNA. Total RNA was isolated from the tissues using an RNeasy Mini kit (Qiagen, Valencia, CA, USA). The integrity of the isolated RNA was analyzed using an Agilent 2100 Bioanalyzer (Agilent Technologies, Palo Alto, CA, USA), and the RNA integrity number (RIN) of all the RNA samples was higher than 9.4, which is larger than the recommended RIN of 8.5 for microarray analysis according to the Agilent protocol for microarray experiments. RNA was reverse transcribed and amplified with the Low Input Quick Amp Labeling Kit (Agilent Technologies, Palo Alto, CA, USA). Complementary RNA was hybridized onto the Agilent rat chip, which includes 62,976 probes

corresponding to 19,297 annotated genes. The differentially expressed genes (DEGs) were defined as false discovery rate ≤ 0.05 and fold-change ≥ 1.5. The detailed analytical methods of gene expression data and network analyses are described in Supplementary Methods.

8. Analysis of gene expression data

The probe intensities were normalized at the log_2-scale using the quantile normalization method (72). The probes were annotated with Lumi 1.8.3. The expressed genes were identified as previously described (73). To identify differentially expressed genes (DEGs) between the ITR and IIS among the expressed genes, integrative statistical hypothesis testing was performed as previously described (73). Briefly, Student's t-test and the log_2-median-ratio test were performed to compute T-values and log_2-median-ratios for all the genes. Empirical distributions of the null hypothesis for T-values and log_2-median-ratios were estimated by performing random permutations of samples and then applying the Gaussian kernel density estimation method to T-values and log_2-median-ratios resulting from the random permutations. The adjusted P values of each gene in the t-test and log_2-median-ratio test were computed by two-tailed tests using their corresponding empirical null distributions. The P values from the two tests were then combined with Stouffer's method (74); false discovery rates (FDRs) for the combined P values were then computed using the Storey method (75); and the DEGs were identified as genes with a FDR ≤ 0.05 and an absolute log_2-fold-change larger than 0.58 (1.50-fold). Functional enrichment analysis of DEGs was performed using DAVID

software (76). Gene ontology biological processes (GOBPs) enriched by the DEGs were identified as those with $P < 0.05$.

9. Network analysis

To construct a network model for the DEGs, I first selected a subset of the DEGs involved in the representative processes associated with the effects of IT surgery. I then collected protein-protein interactions for the selected genes from four public interactome databases: BIND (Biomolecular Interaction Network Database) (77), HPRD (Human Protein Reference Database) (78), BioGRID (Biological General Repository for Interaction Datasets) (79), and MINT (Molecular INTeraction Database) (80). To map human proteins to rat proteins, I used the human-rat ontology information in the rat genome database (RGD) (81). The initial network model for the selected DEGs was visualized using Cytoscape (82). The nodes in the network model were arranged based on the information (their cellular localizations and associated pathways and activation/inhibition information for interactions) in the Kyoto Encyclopedia of Genes and Genomes (KEGG) pathway database (83) such that the nodes involved in the same pathways are located near one another.

10. Real-time PCR analysis

The expression levels of representative DEGs associated with the effects of IT surgery were validated using quantitative real-time PCR (qRT-PCR). Complimentary DNA was generated using Superscript II reverse transcriptase (Invitrogen, Carlsbad, CA, USA). qRT-PCR was performed with

specific primers using SYBR master mix (Takara, Shiga, Japan) and the ABI 7500 real-time PCR system (Applied Biosystems, Foster City, CA, USA). The glyceraldehyde-3-phosphate dehydrogenase (GAPDH) expression level was used as the internal control. Nucleotide sequences of the primers are shown in Table 2-1.

Table 2-1. Primers for qRT-PCR

Gene	Forward primer	Reverse primer
Gapdh	ATG ACT CTA CCC ACG GCA AG	TAC TCA GCA CCA GCA TCA CC
G6pc	GTG TCC GTG ATC GCA GAC C	GAC GAG GTT GAG CCA GTC TC
Slc2a2	GTC CAG AAA GCC CCA GAT ACC	TGC CCC TTA GTC TTT TCA AGC T
Hk3	CTC CAG GCT GGT GTC AGT GA	CTC CGA TTG CAA AAA GGT GAC T
Ccl5	CCA GAG AAG AAG TGG GTT CA	AGC AAG CAA TGA CAG GAA AG
Il1b	CAC CTC TCA AGC AGA GCA CAG	GGG TTC CAT GGT GAA GTC AAC
Jak3	GGA GAG TGA GGC GCA TGT GAA GAT	CAG ATT GGC GGG AGA AGA TGT TGT
Stat1	TGA GTT CCG ACA CCT GCA ACT GAA	AGG TGG TCT CAA GGT CAA TCA CCA
Tlr2	TCT TGA TGG CTG TGA TAG G	CCG AGG GAA TAG AGG TGA
Slc27a2	TTT CAG CCA GCC AGT TTT G	TCT CCT CGT AAG CCA TTT CC

Acadm	ACC AAG ACG GCT ACA ATG ATG	TGA GGC AGA AGC TAA GGT TGA
Col1a1	GCT CCT CTT AGG GGC CAC T	CCA CGT CTC ACC ATT GGG G

11. Statistical analysis

The homeostasis model assessment of insulin resistance (HOMA-IR) was calculated as follows: HOMA-IR = (fasting insulin [μU/mL] x fasting glucose [mg/dL]) /405. The insulinogenic index was used to estimate insulin secretion and was calculated as follows: (insulin [30 min] – insulin [0 min])/(glucose [30 min] – glucose [0 min]). The area under the curve (AUC) was calculated by the trapezoidal rule. With the exception of the microarray data, all other data are shown as the mean ± SEM. Serial data of body weights, food and water intake, glucose, and hormone levels were analyzed by two-way repeated measures ANOVA with Tukey's post hoc test. When comparing two groups, statistical significance was determined using Student's t-test or Mann-Whitney U test. When more than two groups were compared, one-way analysis of variance with Tukey's post hoc test was used. A P value <0.05 was considered statistically significant.

Results

1. Effects of IT on body weight, food intake, and metabolic parameters

The mortality rate was 40% (6/15) in IT group and 22.2% (2/9) in sham group. Although I matched body weights between IT and sham group before surgery, the baseline body weight of survived rats was slightly higher in IT group (Figure 2-1). When I analyze the percent change of body weight compare to the preoperative body weight, IT showed significantly higher decrease of percent body weight only during 2 to 3 weeks after surgery than sham. The body weight increased after that to the similar level as preoperative body weight. The food intake was only reduced during the 2nd week after surgery in IT compared to sham. It was not different between IT and sham from postoperative week 3.

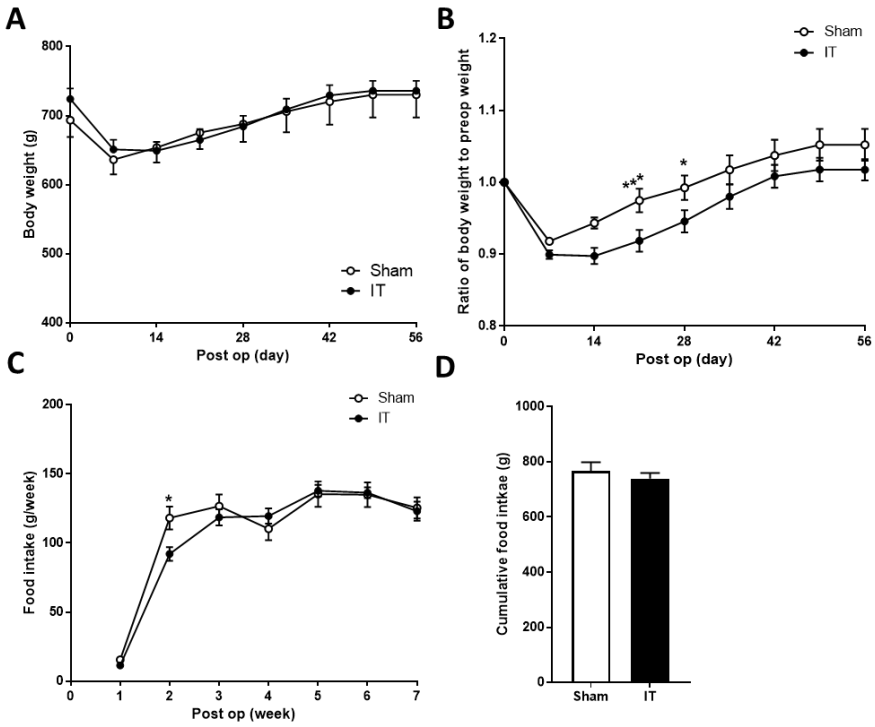

Figure 2-1. Body weight and food intake after surgery

(A) Body weight and (B) change of body weight from baseline after surgery. (C) weekly food intake and (D) cumulative food intake after surgery.

*P value <0.05 between IT and sham using RM-ANOVA with Tukey's post-hoc test.

The plasma glucose level was significantly lower in IT than sham after oral glucose challenge (Figure 2-2). Insulin level was higher in sham along with significantly higher insulinogenic index which reflects the acute insulin response after glucose challenge. However, the HOMA-IR and insulin tolerance test were not different between IT and sham, which suggests no significant difference in insulin sensitivity between the two groups.

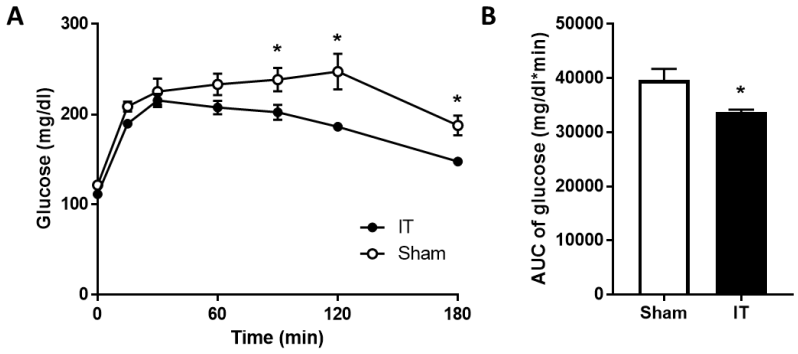

Figure 2-2. Oral glucose tolerance test

Plasma levels of (A) glucose and (B) AUC of glucose. *P < 0.05 for IT vs. sham.

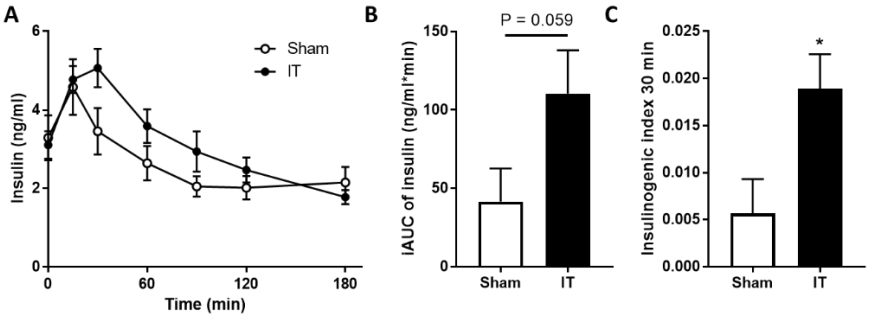

Figure 2-3. Plasma insulin levels during oral glucose tolerance test

Plasma levels of (A) insulin, (B) AUC of insulin and (C) insulinogenic index 30 minutes during oral glucose tolerance test. *P < 0.05 for IT vs. sham.

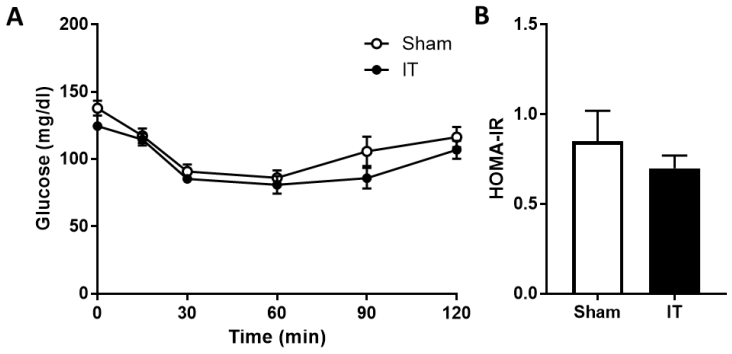

Figure 2-4. Insulin tolerance test

(A) Plasma glucose levels of insulin tolerance test. (B) HOMA-IR index.

During OGTT, plasma total GLP-1 and PYY were much higher in IT than sham. GIP was not different between the groups, and glucagon level showed only a trend of increase in IT (Figure 2-3).

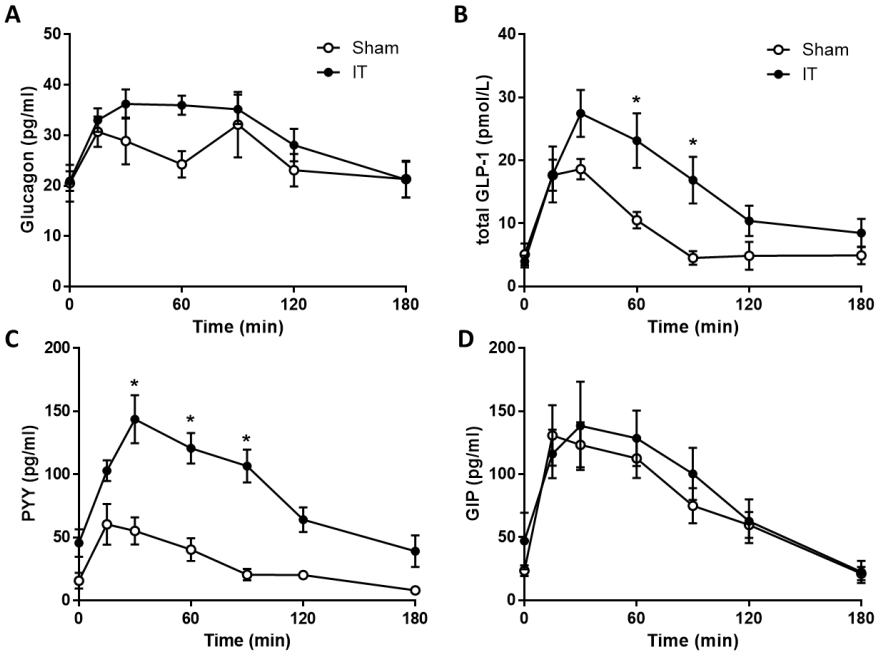

Figure 2-5. Hormone levels during oral glucose tolerance test

Plasma levels of (A) glucagon, (B) total GLP-1, (C) PYY, and (D) GIP during OGTT. *P < 0.05 for IT vs. sham.

2. IT increased enteroendocrine cell density in the transposed ileum

I, then, examined the histomorphology of ITR see whether the above effects of IT in gut hormone secretion was accompanied by the change of the distal ileum tissue in microscopic level. In H&E stain, ITR showed a distinct hypertrophy in both the diameter and thickness (Figure 2-4). The substructures including the length of villi, crypt depth, and muscle thickness were all significantly increased in the transposed ileum of IT group compared to the ileum in situ of sham group.

I stained the ileal tissue with anti-GLP-1 and anti-GIP antibody to examine the density of enteroendocrine L- and K-cells in the transposed ileum. The density of L-cell was increased in the transposed ileum (Figure 2-4). Interestinly, the density of K/L cell, both GLP-1 and GIP positive cell, was increase by more than three folds, which suggests possibility of dynamic transition in the enteroendocrine cell population in the transposed ileum.

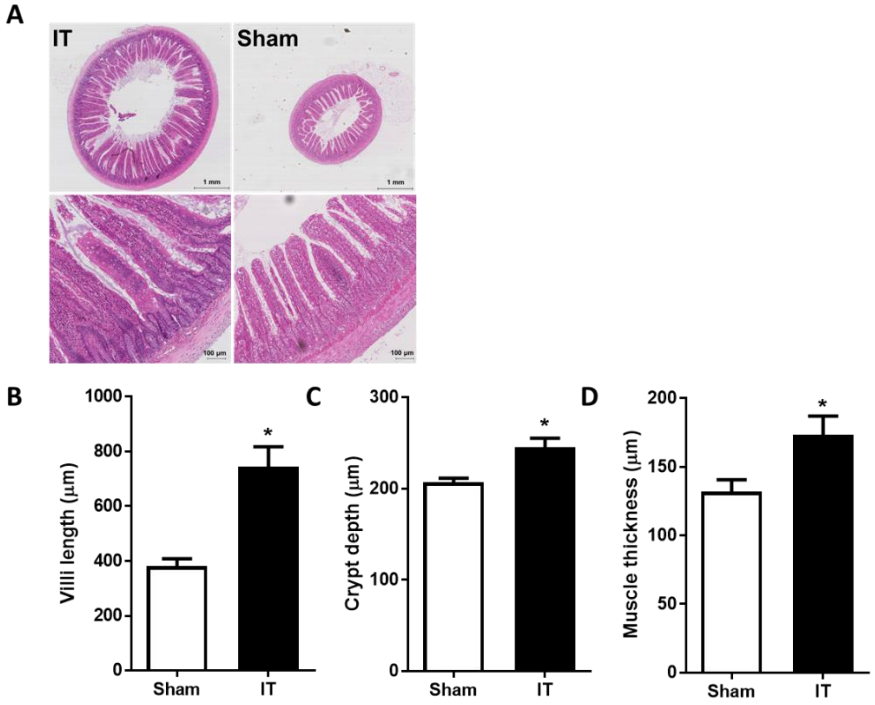

Figure 2-6. Histology of the transposed ileum

(A) Representative images of H&E slides, (B-D) measurements of microscopic structure of intestine including (B) villi length, (C) crypt depth, and (D) muscle thickness. *P < 0.05 for IT vs. sham.

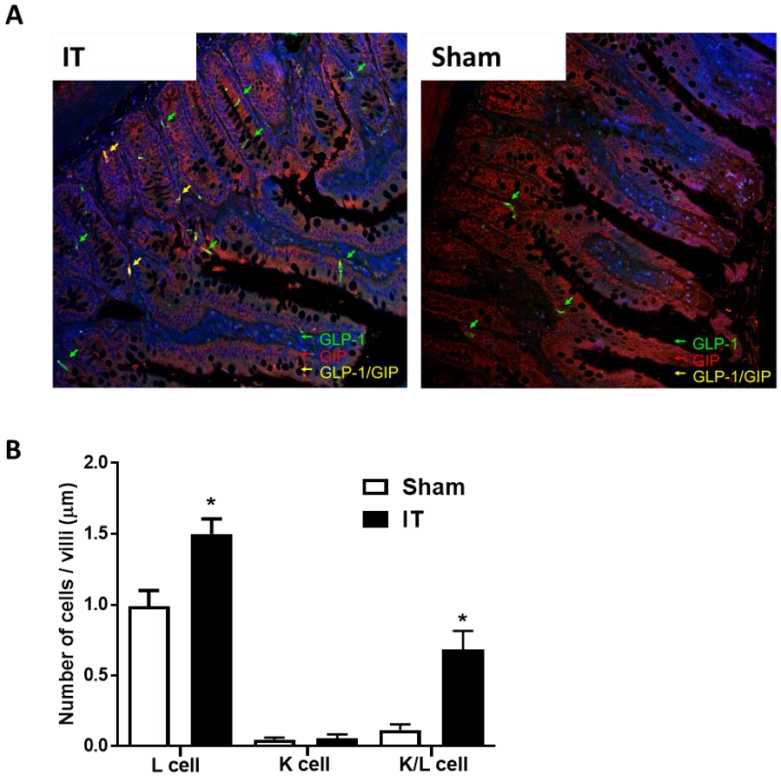

Figure 2-7. Enteroendocrine cell density of the transposed ileum

(A) Representative images of immunofluorescent staining of ileal tissue. (B) number of each type of enteroendocrine cells. *P < 0.05 for IT vs. sham.

3. IT increased pancreatic β-cell mass

To examine the effects of the IT on the pancreatic β-cell mass, I stained the pancreas section with anti-insulin antibody. The relative β-cell area was significantly higher in IT than sham (Figure 2-5). Reflecting the modest degree of hyperglycemia in DIO rat, the structure of pancreatic islet showed no distinctive change in both groups.

From above-mentioned findings, I focused on the transposed ileum for further investigation, because the increased gut hormone secretion and insulin secretion was thought to be the major determinant of improved glucose tolerance after IT. I first examined the temporal changes in the ITR at different time points after surgery. Secondly, I performed microarray analysis on ITR and IIS to systematically analyze the adaptation process of the intestine.

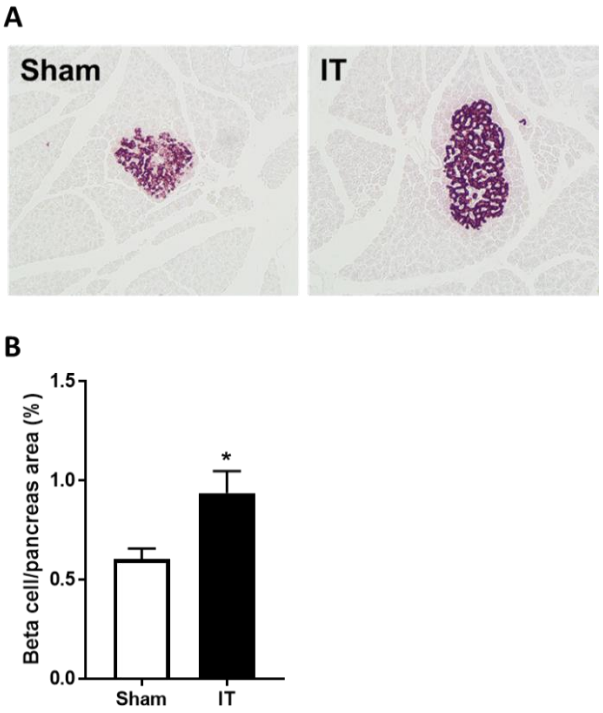

Figure 2-8. Pancreatic β-cell area

(A) Representative images anti-insulin staining of pancreas section. (B) relative beta cell area in each group. *P < 0.05 for IT vs. sham.

4. Morphologic changes in the transposed ileum during the long-term postoperative period

The villi length and muscle thickness increased from 1 to 4 weeks (Figures 2-6 A-C). However, they showed no further significant changes until 16 weeks. In addition, I examined the density of enteroendocrine K- and L-cells in the ITR at 1, 4, 8 and 16 weeks after surgery. The density of L-cells increased from 1 to 8 weeks, and that of K/L-cells increased 1 to 4 weeks (Figure 2-6 D-F).

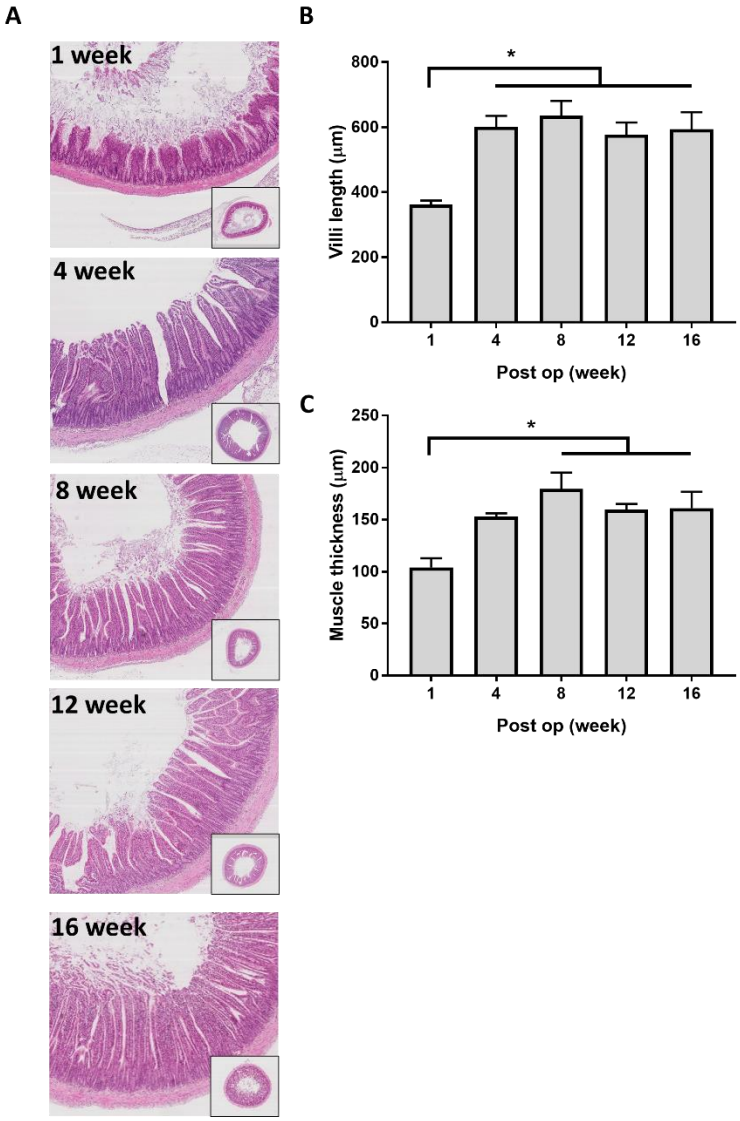

Figure 2-9. Morphologic changes in the transposed ileum in the long-term postoperative period

(A) Hematoxylin and eosin-stained section of the transposed ileum at 1 to 16 weeks after IT. Comparison of villi length (B) and muscle thickness (C) of the transposed ileum (n = 4 ~ 5) in the IT groups at 1, 4, 8, 12 and 16 weeks after surgery. *P <0.05 by one-way ANOVA with Tukey's post hoc test.

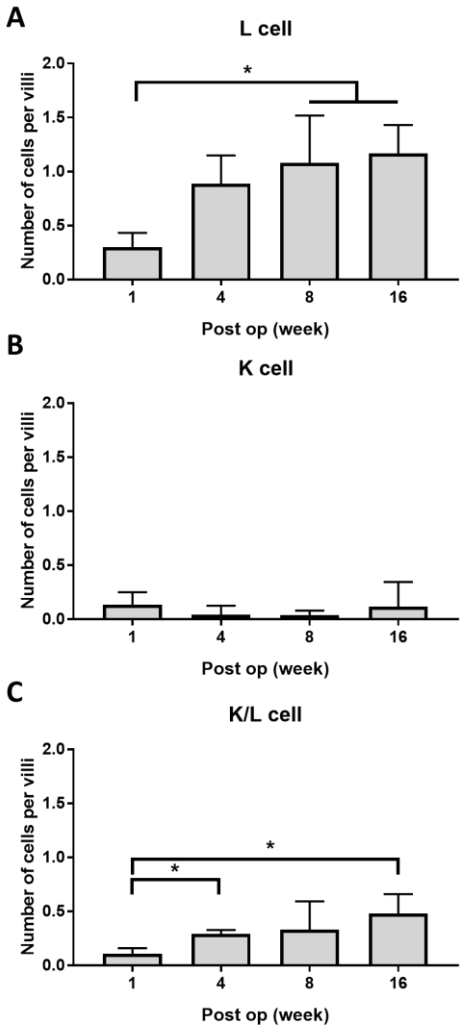

Figure 2-10. Enteroendocrine cell densities in the transposed ileum in the long-term postoperative period

Comparison of the densities of L- (A), K- (B), and K/L-cells (C) in the transposed ileum in the IT groups at 1, 4, 8, and 16 weeks after surgery (N = 4 for 1, 4, 8, and 12-week and 5 for 16-week). *P <0.05 by one-way ANOVA with Tukey's post hoc test.

5. Global gene expression profiling of postoperative 1-week and 4-week models

To systematically examine the molecular nature underlying the aforementioned effects of IT, I performed gene expression profiling of the distal ileum samples from four rats in the IT and sham groups at 1 and 4 weeks after surgery (Figure 2-7A). The two time points were determined based on the above observations of the apparent metabolic improvements at week 4 and no further morphologic changes after week 4. Principal component analysis (PCA) showed that the difference was largest between weeks 1 and 4. In addition, the separation between the IT and sham groups was also apparent at both weeks 1 and 4, although the separation between the IT and sham groups was larger at week 4 than week 1 (Figure 2-7B). Similar patterns were observed in the hierarchical clustering of the gene expression data (Figure 2-7C). To identify the genes governing this distinction, I compared gene expression profiles and selected a total of 1,792 DEGs between the IT and sham groups in weeks 1 and 4 (Figure 2-7D). Of the genes involved in the enteroendocrine system, Gip, Gcg, and Fxr were found to be up-regulated in weeks 1 and 4 (Figures 2-7E and F).

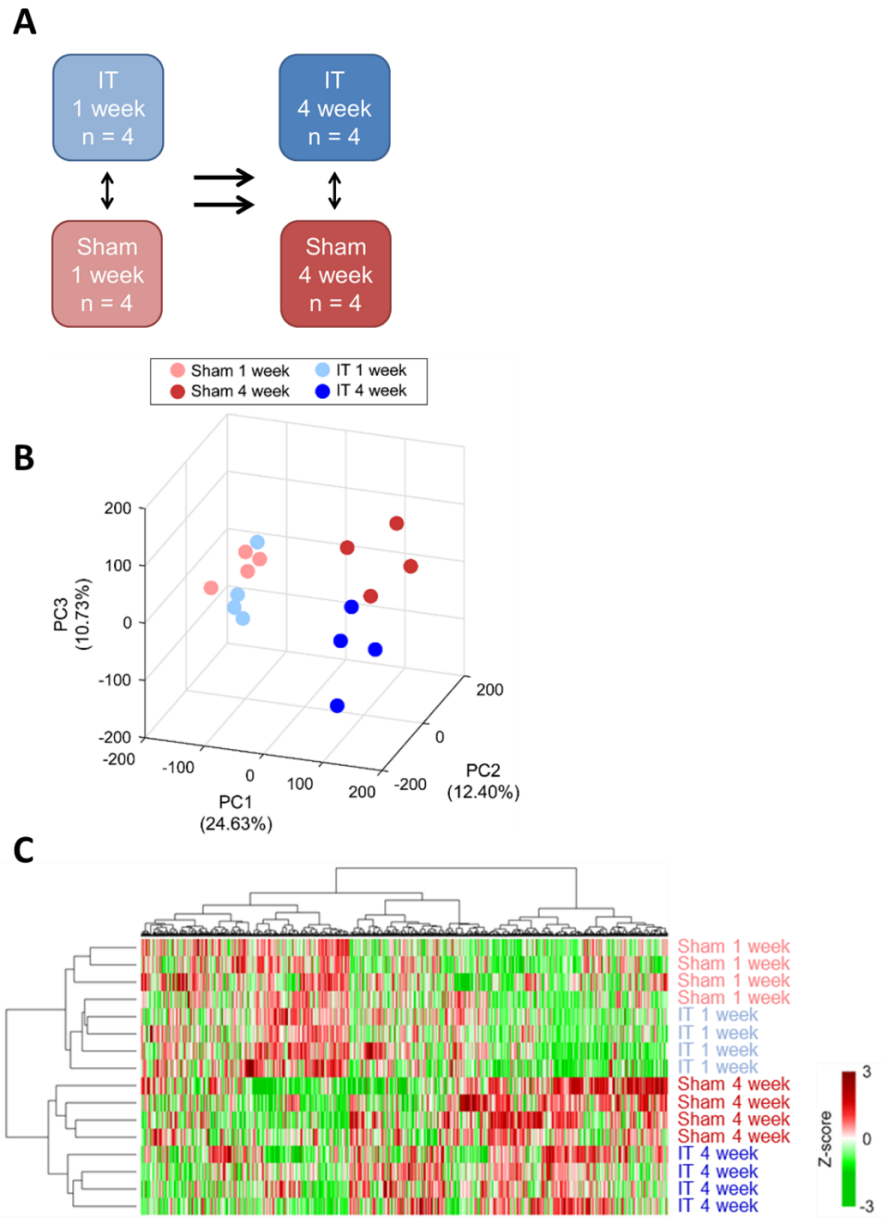

Figure 2-11. Clustering of the microarray data between IT and sham groups

(A) Schematic diagrams for tissue microarray analysis. One or four weeks after surgery, gene expression profiling of distal ileum tissues obtained from four independent rats in each group was performed. 3-D score plots obtained from

principal component analysis (PCA) (B) and heat maps showing gene expression patterns obtained from hierarchical clustering (Euclidean distance as a dissimilarity measure and ward linkage method) (C). Percentages in parentheses indicate percentages of variance captured by the first three principal components (PC1-3). Red and green represent an increase and decrease, respectively, in the expression level of each gene with respect to its median expression level in week 1 or 4. The color bar denotes the gradient of $\log_2$-fold-changes of gene expression levels in individual samples with respect to its median expression level.

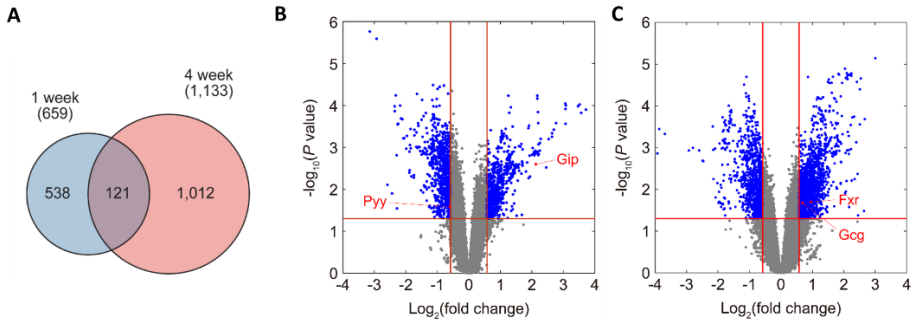

Figure 2-12. Differentially expressed genes between the IT and sham groups

(A) Venn diagram showing relationships between DEGs in weeks 1 and 4. Numbers in parentheses indicate the number of DEGs in weeks 1 and 4. Volcano plots showing DEGs in weeks 1 (B) and 4 (C). X- and Y-axes represent the $\log_2$-fold-change and the $-\log_{10}$(P value), respectively. Blue and red dots indicate DEGs and genes previously known to be up-regulated after bariatric surgery.

6. Cellular processes altered in postoperative 1-week and 4-week models

To systematically investigate the DEGs, I categorized them into eight clusters (C1-8) based on their up- and down-regulation patterns in weeks 1 and 4 (Figure 2-8A). Interestingly, 93.2% of the DEGs showed up- or down-regulation uniquely in week 1 or 4. Moreover, among the 121 shared DEGs between weeks 1 and 4, only 45 and 24 (57.0% of 121) were commonly up- and down-regulated, respectively. These data suggest that the differential expression of genes by transposition of the distal ileum drastically changes during the course of the early adaptation period. Next, to understand cellular processes associated with the DEGs, I performed enrichment analysis of gene ontology biological processes (GOBPs) for genes in C1-8 using DAVID (76). Among C1-8, I focused on GOBPs enriched by four major clusters (C2, C4, C5 and C7) including more than 10% (179 DEGs) of the total number of DEGs. The up-regulated genes in C2 and C4 were mainly associated with cellular processes related to structural adaptation (extracellular matrix organization and cell adhesion), nutrient absorption (response to nutrient and lipid transport), and immune adaptation (wound healing, inflammatory response, neutrophil chemotaxis, macrophage and leukocyte activation, and T cell differentiation) of the ITR (Figure 2-8B). Of note, the processes related to structural adaptation and nutrient absorption were up-regulated predominantly in week 1, while the processes related to immune adaptation were up-regulated predominantly in week 4. On the other hand, the down-regulated genes in C5 were mainly associated with fatty acid beta-oxidation and glucose homeostasis, which were

related to metabolic adaptations of the ITR (Figure 2-8B). These metabolic processes were down-regulated predominantly in week 4. These data suggest dynamic regulation of structural, metabolic and immune adaptations in the early postoperative period after IT.

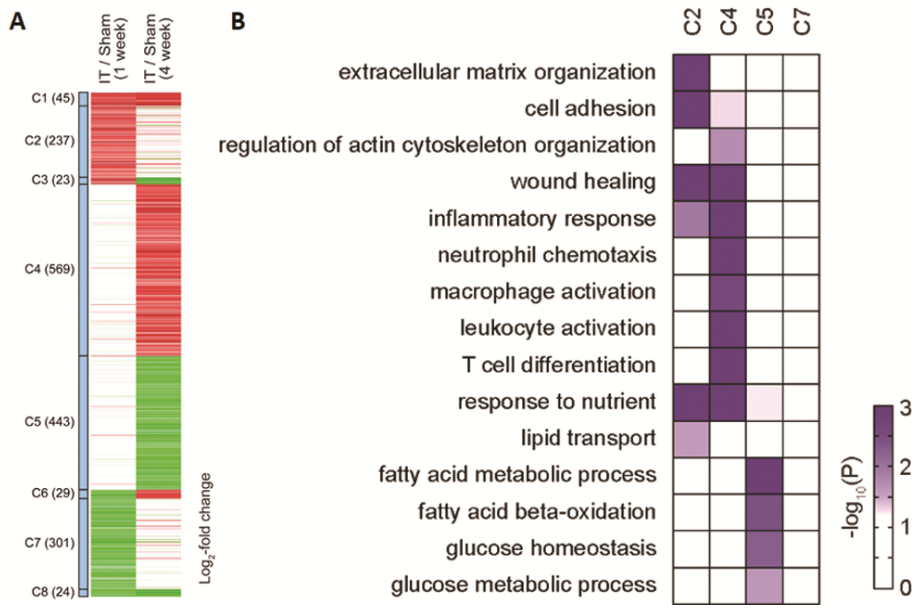

Figure 2-13. Clusters of DEGs and their associated cellular processes

(A) Eight clusters (C1-8) of DEGs defined by up- and down-regulation patterns from the comparison of the IT and sham groups (IT/Sham) in weeks 1 and 4. Numbers in parentheses indicate the number of DEGs belonging to the corresponding cluster. Red and green represent increased and decreased expression levels of each gene in the IT groups compared to the sham groups in week 1 or 4. The color bar indicates the gradient of $\log_2$-fold-changes between the IT and sham groups. (B) Heat map showing cellular processes (gene ontology biologic processes) enriched by genes in four major clusters (C2, C4, C5 and C7). The color bar denotes the gradient of $-\log_{10}(P)$, where P is the significance of the enrichment obtained by the EASE score method in DAVID.

7. Network models of the adaptation processes after IT

The GOBP enrichment analysis indicated that IT affected cellular pathways associated with structural, metabolic and immune adaptations of the ITR. To examine these cellular pathways, I built network models that describe the interactions among the DEGs involved in the aforementioned processes. The network model for structural adaptation (Figure 2-9A) showed that extracellular matrix proteins (Col1a2/4a1/6a1, Fn1 and Lama2/c1) and their interacting integrins (Itga1/a5/a7) and plasma membrane proteins (Flna and Cav1) were up-regulated at week 1, suggesting their potential roles in the intestinal adaptation after IT (84). This observation is consistent with the prominent histologic change of the ITR from 1 to 4 weeks.

The network for immune adaptation (Figure 2-9B) showed that many cytokines (Il1a, Il1b, Il17a and Il22) and chemokines (Ccl3, Ccl5, Ccl17, Ccl19, Ccl21, Ccl22, Cxcl1 and Cxcl10), their receptors (Il2rb, Il6r, Il21r, Il22ra1, Ccr5, Ccr9, Cxcr3, Cxcr4 and Cxcr6), their downstream signaling molecules (Jak3 and Stat1) in the JAK-STAT pathway and toll-like receptors (Tlr2 and Tlr4) were elevated predominantly in week 4. Then, I examined which types of immune cells were more affected after IT by comparing the differential expression of marker genes for diverse types of immune cells in weeks 1 and 4. The expression of marker genes for T cells, B cells, neutrophils, and macrophages increased in week 4 relative to that of marker genes for other immune cells (Figure 2-9C). Interestingly, among the marker genes of T cells, those for Th17 cells, not Th1 and Th2 cells, were significantly up-regulated in week 4 (Figure 2-9C).

Finally, the network model for metabolic adaptation (Figure 2-9D) showed that glucose transporter (Scl2a2/Glut2), hexose kinase 3 (Hk3), and enolase 3 (Eno3) in the glycolytic pathway were elevated from week 1, whereas G6pc in the gluconeogenesis pathway was down-regulated. On the other hand, fatty acid transporter (Slc27a2) and enzymes for fatty acid metabolism (Cpt1b, Acadm, Acaa1a and Acaa1b) were down-regulated at week 4. In contrast, amino acid transporters (Slc7a9 and Scl1a5) were upregulated at week 4.

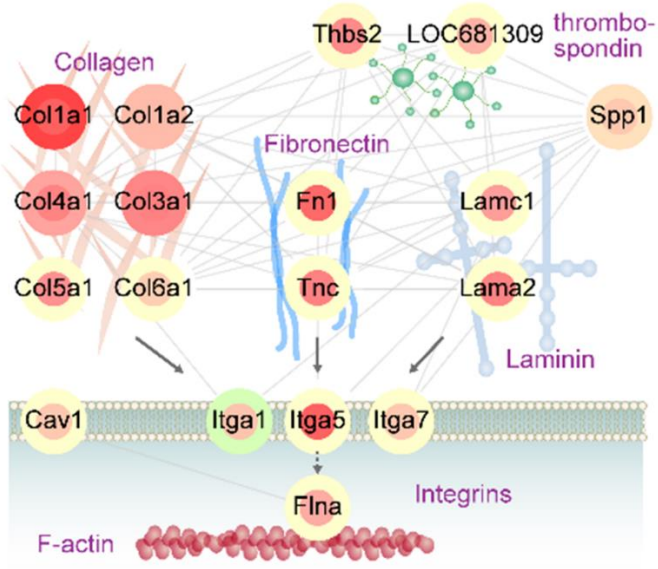

Figure 2-14. Network model for the structural adaptation after IT

Node center and border colors represent increased (red) and decreased (green) expression levels in the IT groups compared to the sham groups in weeks 1 (center) and 4 (border; see the legend for node center and border). Solid and dotted arrows/inhibition symbols represent direct and indirect activation/inhibition, respectively, obtained from KEGG pathway databases. Gray lines indicate protein-protein interactions obtained from interactome databases (Methods). Plasma membranes are denoted by thick gray lines, cytoplasm by a blue background, and extracellular matrix or lumen by a white background.

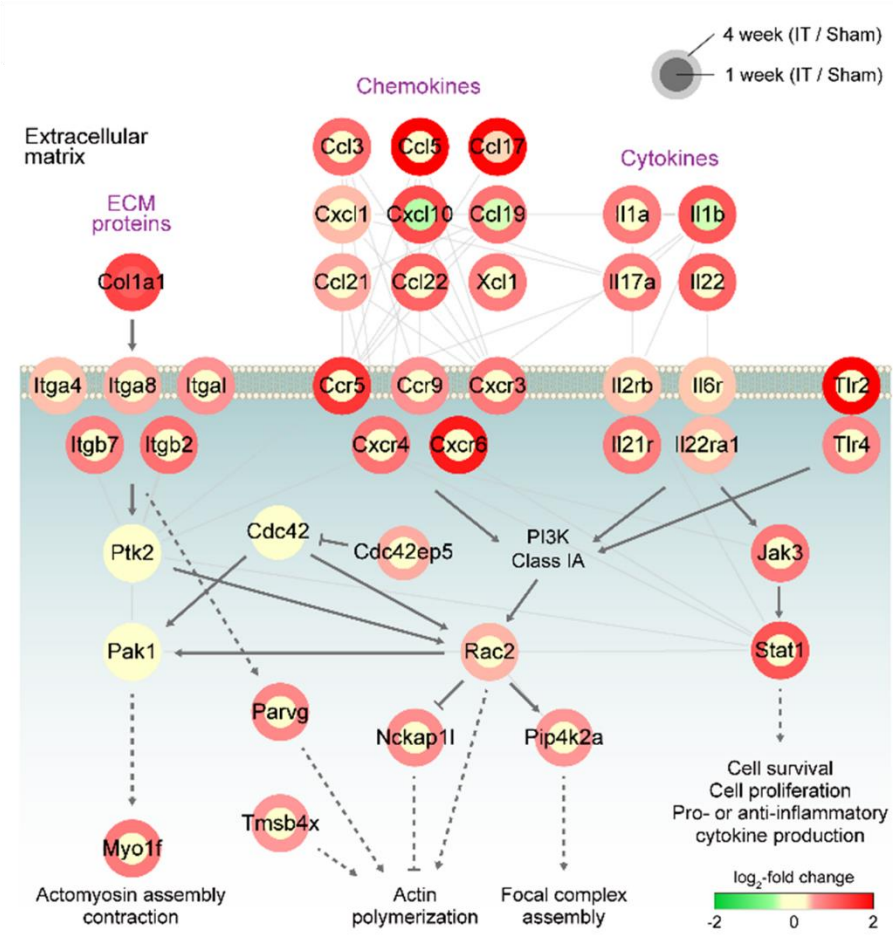

Figure 2-15. Network model for the immune adaptation after IT

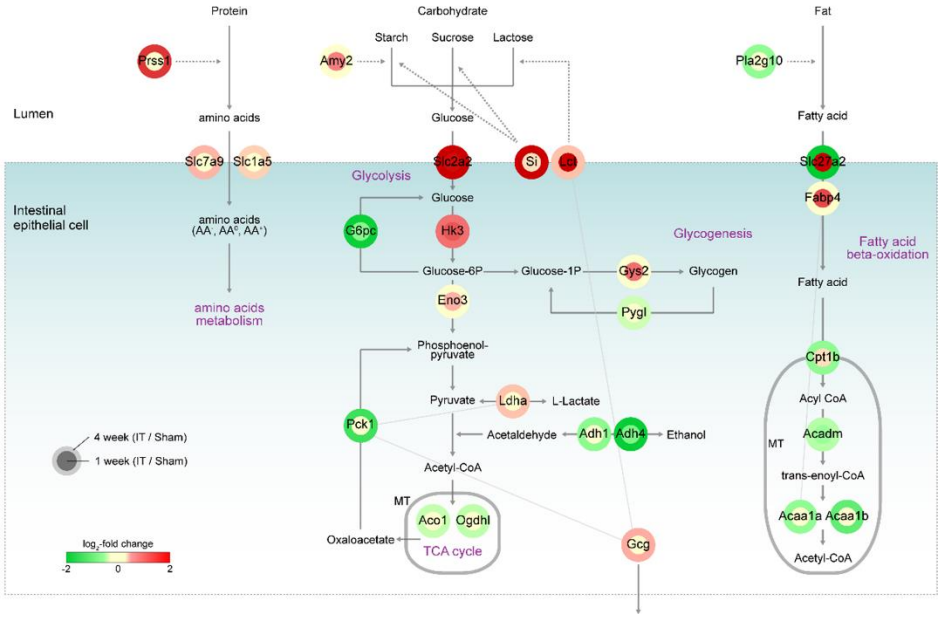

Figure 2-16. Network model for the metabolic adaptation after IT

8. Validation of differential expression of genes involved in the adaptation processes

To validate IT-induced alterations of the aforementioned pathways, I examined differential expression of the following representative genes in the network models by qRT-PCR: Col1a1 in structural adaptation using the 1-week model; Ccl5, Il1b, and Tlr2 in immune adaptation using the 4-week model; and G6pc, Glut2, Hk3, Slc27a2, and Acadm in metabolic adaptation using the 4-week model. The increased or decreased expression of these genes was consistent with the results obtained from microarray experiments (Figure 2-10). Log_2-fold-changes of these genes in individual samples were significantly correlated with those obtained from microarray experiments (Supplementary Figure 2-11).

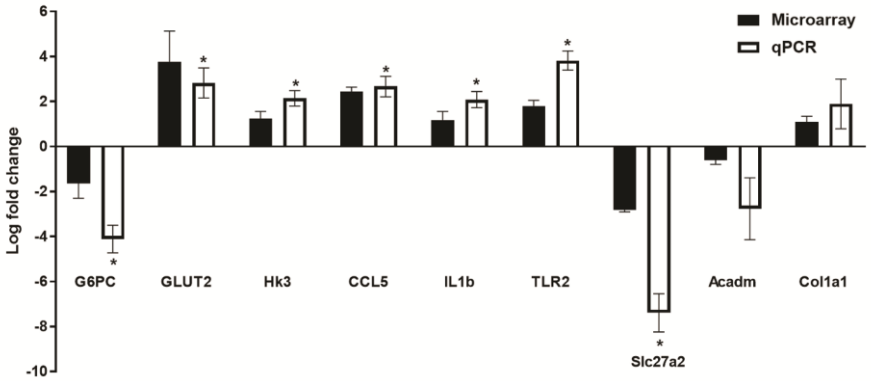

Figure 2-17. Validation of the differential expression of representative genes in the key cellular pathways affected by bariatric surgery using qRT-PCR analysis

Data are shown as the mean ± SEM of the log_2-fold-change between the IT and sham groups (IT/Sham). n = 4 for each group in the microarray experiments and n = 4 ~ 6 in each group for the qRT-PCR analyses. Gene expression was validated in the 4-week model, except for *Col1a1*. *P <0.05 comparing the IT and sham groups by Student's t-test.

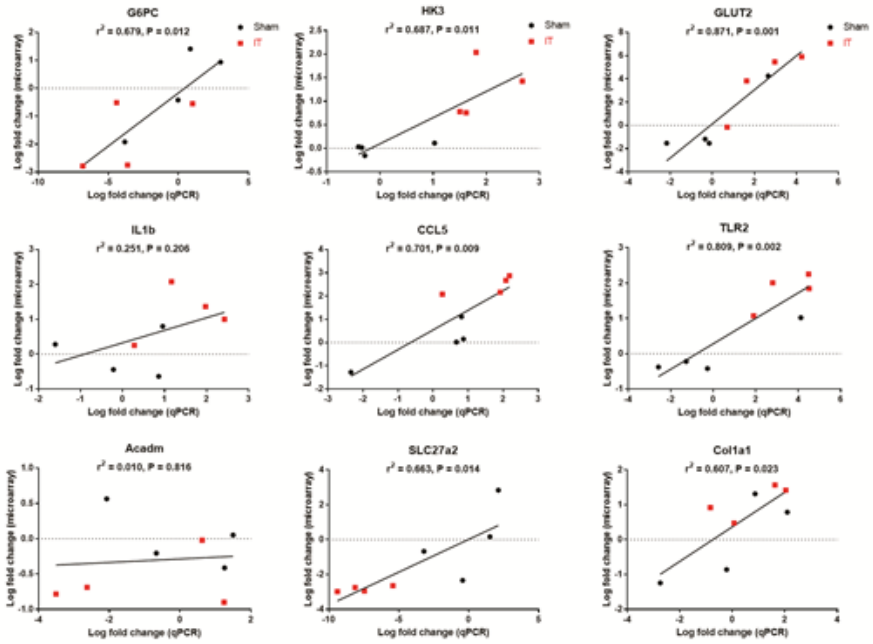

Figure 2-18. Correlation between the key gene expression levels measured by microarray and RT-PCR

Data are presented as the log_2-fold-change compared to the mean value of the control group (sham group). Linear regression analysis was performed to calculate Pearson's correlation coefficient and the P value.

Discussion of chapter 1

I investigated the metabolic effects of IT in diet-induced obese rats. IT only induced transient body weight loss compared to sham, and had no significant effect on insulin sensitivity. On the other hand, glucose stimulated insulin secretion was significantly improved along with the increased postprandial GLP-1 and PYY secretion. In terms of insulin sensitivity and pancreatic β-cell function, IT mainly affected pancreatic β-cell function.

About the effects of IT on body weight, previous studies reported somewhat mixed results (66). IT significantly reduced body weight in studies of Zucker rats (85, 86), while it did not in studies of UCD-T2DM rats and diet-induced obese rats (69, 87-89). This can be explained by that the effects of IT can be different among these obese rat models. However, this can also suggest that the effect of IT on body weight is modest, if any. In the two studies showed significant difference in body weight after IT, the magnitude of difference was less than 10% compared to sham control at 8 weeks after surgery. In our study, when I see the change of body weight from preoperative level, IT group had significantly lower body weight at 3 and 4 weeks after surgery, but the difference lost statistical significance from then. Our study support that the sole effect of the distal small intestine may not be enough to induce large body weight loss like RYGB.

Postprandial insulin secretion significantly increased after IT, along with the increased pancreatic β-cell area. Among the gut hormones I measured, GLP-1 and PYY showed significant increase after oral glucose challenge. After

IT, the transposed ileum is exposed to relatively high amount of undigested food material. This nutrient delivery makes the transposed ileum into a new physiologic circumstances and induces so called 'jejunization process'. Villi length, muscle thickness, and crypt death were all higher in IT than sham. Furthermore, I showed that the enteroendocrine cell density was increased after IT compared to sham. This could contribute to the increase in the gut hormone secretion. Interestingly, not only the density of L-cell, but also the density of K/L cell was significantly increased after IT. GIP-producing K cells are most abundant in the proximal small intestine and GLP-1-producing L cells are most abundant in the distal small intestine and the colon (90). The K/L cell might be an intermediate phenotype of enteroendocrine cells to adapt to the changed gut environments. The increased GLP-1 secretion can be the major contributor to the increased pancreatic β cell area. GLP-1 relieves ER stress of pancreatic β cell, which is the major mechanism of β cell failure in insulin resistant state (91). Collectively, after IT, through the adaptive change of the transposed ileum, GLP-1 secretion was increased, and this can contribute to the postprandial insulin secretion and pancreatic β cell survival.

In the longitudinal histologic analysis of the ITR, morphologic changes were significant until postoperative week 4. The distribution of GLP-1 positive L-cells and both GLP-1 and GIP positive K/L-cells also demonstrated a significant increase during this early postoperative period and no further increase thereafter. Gene expression analyses showed the differential regulation of genes involved in structural, metabolic and immune adaptations

over time. Structural adaptation predominantly occurred at week 1, while metabolic and immune adaptations predominantly occurred at week 4.

According to functional enrichment and network analyses, the most enriched cellular process was extracellular matrix organization, represented by the up-regulation of collagen, fibronectin, and laminin for structural adaptation in postoperative week 1. Consistent with this finding, histologic analysis showed that villi length and muscle thickness increased predominantly from week 1 to 4. In a previous study, after resection of 80% of the small intestine in rats, the hyperplastic process of the remnant small intestine was nearly complete by 1 week after surgery (92), supporting our finding of structural adaptation at a very early stage after IT.

Our analyses also showed that immune adaptation was apparent at week 4. Cytokines, chemokines and their receptors are up-regulated in ITR. The intestine is an important immunologic organ where the immune system contact with gut microbiome. Metabolic surgery including RYGB has huge impact on the composition of gut microbiome, and this can lead to altered gut immune response (93).

The network model for metabolic adaptation showed up-regulation of the glucose transporter *Slc2a2*/*Glut2*, with a 3.7-fold increase in week 1 and a 63.6-fold increase in week 4. GLUT2 can be recruited to the apical membrane of the intestinal epithelium under conditions of high glucose levels in luminal contents (94). After IT, the ITR is exposed to a luminal content with high concentrations of monosaccharides, which might stimulate the expression of GLUT2 in the epithelium of the ITR. In addition, GLUT2 is involved in glucose

sensing and incretin secretion. In an *ex vivo* study of the rat small intestine, a GLUT2 inhibitor decreased the secretion of GIP, GLP-1, and PYY (95). In mice lacking GLUT2, postprandial secretion of GLP-1 was impaired (96).

There were several limitations in this study of IT model. First, the surgical mortality was considerable. To optimize the surgical protocol, I practiced the surgery before the main experiment. However, the mortality was about 40% in IT group even in the main experiment. This might affect the outcome of the surgery. Second, sham surgery could also cause some physiologic changes in the small intestine. In the sham surgery, there was three anastomosis of the small intestine. This might lead to stricture and decreased bowel motility. If there was another sham surgery group not incorporating bowel anastomosis, it would be possible to differentiate such an effect. Third, since IT showed only a minimal effect on body weight and insulin sensitivity, I could not comprehensively study the mechanism how metabolic surgery affect insulin sensitivity. Fourth, in current study, microarray was done using the full thickness of ileal tissue. Thus, it was unable to differentiate whether the changes of gene expression is come from epithelium or other layers.

Considering these limitations, I further planned to study another model of metabolic surgery with more clear effect on body weight, such as VSG. In addition, I also planned to use mouse as an animal model, because the homology of mouse genome and human genome has been more extensively studied than rat genome, and by using transgenic mouse model I can characterize a specific molecular pathway.

Chapter 2.

Effects of vertical sleeve gastrectomy on the gene expression of liver, fat and muscle and their implications in glucose homeostasis

Background and objectives of chapter 2

Vertical sleeve gastrectomy (VSG) is currently the most popular procedure of bariatric surgery. It has several advantages including, simpler surgical procedure, lower rate of complication, and lower rate of micronutrient malnutrition than RYGB. Despite that VSG does not bypass any part of the intestine, the metabolic effects of VSG seemed non-inferior to RYGB. In a randomized controlled trial comparing VSG, RYGB and intensive medical treatment, glycated hemoglobin and BMI were not significantly different between RYGB and VSG at 1 year after surgery (97). The diabetes remission rates of RYGB and VSG in observational studies were not significantly different as 92.8% and 82.5%, respectively (23).

The effects of VSG are combined effects of augmented insulin secretion and improved insulin sensitivity. Insulin sensitivity is consisted of hepatic and peripheral insulin sensitivity. The skeletal muscle and adipose tissue are the major organ contribute to the peripheral insulin sensitivity. After VSG, the hepatic and peripheral insulin sensitivity are both significantly improved, but the time course the improvement is different between each other. Thus, to understand the glucose metabolism after VSG, it is necessary to investigate the physiology of liver, skeletal muscle and adipose tissue systematically. Previously, Seeley et al. performed transcriptome analysis of liver and ileum in mouse model of VSG (34, 50). They could reveal the altered bile acid metabolism pathway in both tissues. However, there was lack of systematic analysis of glucose metabolic in peripheral tissues. With RNA

sequencing analysis the underlying molecular pathways of VSG can be capitulate. At the same time by having not only sham control group, but also pair-fed group, I can investigate the impact of weight-loss dependent and independent mechanism on gene expression of peripheral organs.

Materials and methods

1. Animals

Six week old male C57BL/6N mice were purchased from Orient Bio, Seongnam, Korea. After 1 week of acclimation period, mice were fed 60% high fat diet (D12492, Research Diets, New Brunswick, NJ) for 12 weeks, and were then randomly divided into 3 body weight-matched groups: sham, sham-pair feeding (sham-PF) and VSG groups. The mice were housed 3 or 4 mice per cage and then individually from 8 weeks before surgery. The housing environment was maintained in a controlled temperature (25°C) and 12-hour light/dark cycle (light off at 2000 h). All procedures for animal use were approved by the Institutional Animal Care and Use Committee of Seoul National University.

2. Surgery

Mice were fasted for 18 hours before surgery. The surgical area of the abdomen was dehaired with thioglycolic acid cream (Niclean). After induction of isoflurane anesthesia, the abdomen was disinfected with povidone-iodine solution and midline laparotomy was done. The lateral stomach was excised along with a virtual line from gastroesophageal junction to pylorus-duodenum junction leaving a tubular remnant of the stomach. The remaining stomach was approximated and sutured with 6-0 vicryl. After visual inspection of the stomach suture, if a leakage was suspected, I made additional sutures. After suturing, the intraperitoneal cavity was washed with warm saline 3 or 4 times.

Dry gauge was gently applied to remove any remaining fluid in the cavity. The abdominal fascia and skin was closed using 6-0 vicryl and 6-0 nylon, respectively. Antibiotics (ceftriaxone 50 mg/kg) was administered before surgery and daily until postoperative day 2. Normal saline 20 ml/kg was administered after surgery. Anagesics (meloxicam 1 mg/kg) was administered after surgery and until postoperative day 2. No oral intake was allowed for 24 hours. Water was provide for 24 hours followed by 5 days of liquid diet (Newcare, Wellife, Korea). On postoperative day 6, 1 gram of high fat diet was reintroduced with liquid diet. If the mouse looked grossly well and had eaten the high fat diet, then liquid diet was removed and high fat diet was given ad libitum. The body weight and food intake was monitored daily. The sham-PF group was matched to VSG group one by one and given the amount of food eaten by the VSG mouse.

3. Insulin tolerance test

Mice fasted for 4 hours was given an intraperitoneal injection of insulin (0.75 IU/kg). Blood glucose was measured from the tip of tail vein at baseline, 15, 30, 60 and 90 minutes after the injection with a glucometer (AccuCheck, Roche diagnostics, Indianapolis, IN).

4. Glucose tolerance test

The mice had both intraperitoneal glucose tolerance test (IPGTT) and oral glucose tolerance test (OGTT) 1 week apart. Mice fasted for 12 hours overnight was given 20% dextrose (1 g/kg) by intraperitoneal injection or oral

gavage. Blood glucose was measured from the tip of tail vein at baseline, 15, 30, 60, and 120 minutes after glucose administration with a glucometer (AccuCheck, Roche diagnostics, Indianapolis, IN).

5. Glucose-stimulated insulin and GLP-1 secretion in vivo

On a separate day at least 1 week apart from any blood measurement, mice fasted for 12 hours overnight was given 20% dextrose (1 g/kg) by oral gavage. Before and 15 minutes after the oral gavage, approximately 100 μl of blood was obtained by retro-orbital sampling. Blood was cold-centrifuged and plasma was stored at -80°C for the measurement of insulin and GLP-1. Plasma insulin and GLP-1 level were measured by ELISA (#90080 and #81508, respectively, CrystalChem, Downers Grove, IL).

6. Indirect calorimetry

The O2 consumption, CO2 production and locomoter activity were measured using a comprehensive lab monitoring system (CLAMS, Columbus Instruments, Columbus, OH). Mice from each group were placed in the CLAMS chambers for 4 days. The measurement data after 24 hours of acclimation period was used for further analysis. The rawdata file was analyzed using the CalR application (https://calrapp.org).

7. RNA sequencing

After euthanasia, liver, epididymal adipose and soleus muscle tissue were isolated from sham, sham-PF and VSG mice. Tissues were stored in RNA

later solution (Invitrogen) at -20 °C. Total RNA was extracted using RNeasy Plus Universal kits (Qiagen). RNA quality was checked based on RNA integrity number (RIN). All samples had RIN over 9.0. cDNA library was constructed with the TruSeq RNA library kit using 1 μg of extracted RNA. The protocol consisted of polyA-selected RNA extraction, RNA fragmentation, random hexamer primed reverse transcription and 100nt paired-end sequencing by Illumina HiSeq4000. Sequence reads were aligned to the mouse reference genome (mm10) and gene expression values were calculated from aligned reads using RSEM-1.2.31. Differentially Expressed Genes (DEGs) were determined using DESeq2 package. DEG was defined as raw p-value <0.05 and fold-change <1.5. Enrichment analysis for gene ontology biologic process and KEGG pathway was done using DAVID. The scheme of RNA sequencing analysis is summarized in figure 3-1.

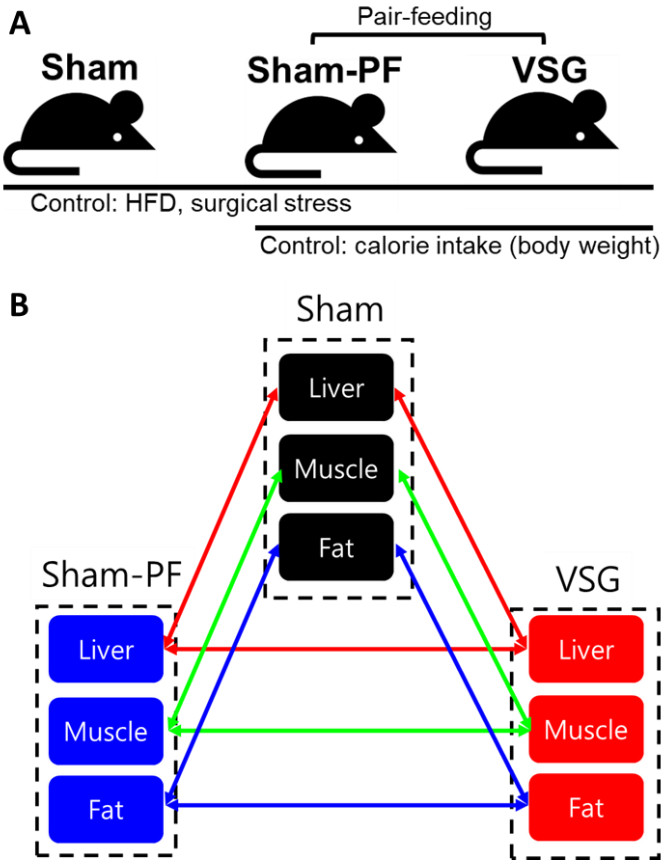

Figure 3-1. The scheme of the mouse study.

(A) The grouping strategy and (B) the scheme of RNA sequencing analysis.

8. Western blotting

Fresh frozen mouse adipose tissues were minced and lysed using RIPA buffer supplemented with protease inhibitors. Protein concentration was determined using Pierce BCA protein assay kit, and 20 μg of protein per lane was seperated using Mini-PROTEAN TGX gel (Bio-Rad). The protein was transferred onto PVDF membranes (Millipore, Billerica, MA). The membrane was incubated with primary antibody overnight at 4 °C. After washing with Tris-buffered saline with Tween (TBST) buffer, the membrane was re-incubated with secondary antibody for 1 hour. The primary antibodies used were against Cxcl13 (AF470-SP, R&D systems) and β-actin (8H10D10, Cell Signaling). The secondary antibodies were anti-goat, anti-mouse conjugated with HRP. Specific protein bands were detected by using the enhanced chemiluminescence kit (Thermo, Rockford, IL).

9. Isolation of stromal vascular fraction Flow cytometry

Dissected epididymal adipose tissue was chopped in DMEM media with 1 mg/ml collagenase P and 5% BSA. After 45 minutes of shaking incubation at 37 °C, any debris were filtered using nylon mesh. The stromal vascular fraction (SVF) was separated via centrifugation (500 g 10 minutes). The SVF was washed and incubated with antibodies for further flow cytometry analysis. For the analysis of macrophage population, the SVF was stained with following antibodies:CD11b-FITC (BD 557396), F4/80-Bv421 (BD 565411), CD206-APC (BD 565250), and MHC II-PE (BD 562010). For the analysis of lymphocyte population, the SVF was stained with following antibodies: CD19-

APC-Cy7 (BD 561043) and CD3-PE-Cy5 (BD 561108). Samples were analyzed using a BD FACSCanto and the FACSDiva software (BD Biosciences). Data were processed with FlowJo software (Tree Star).

10. Statistical analysis

Data in the graph are presented as mean ± SEM, otherwise indicated. The area under the curve (AUC) was calculated by the trapezoidal rule. Time-series data were analyzed using repeated measures ANOVA followed by Sidak's post-hoc test. Three group comparisons were done using one-way ANOVA followed by Tukey's post-hoc test. Data were analyzed using Prism (GraphPad, San Diego, Ca). P value < 0.05 was considered significant.

Results

1. Metabolic effects of VSG

1.1. Body weight was reduced by VSG, but food intake was only reduced during early postoperative period

After surgery all mice lost significant amount of body weight during early postoperative period (Figure 3-2). VSG lost slightly more body weight than sham during liquid diet period, and had lower body weight regain thereafter. This resulted in significant weight difference between the two groups, and this difference was maintained during the whole postoperative monitoring period. The body weight of sham-PF group was initially paralleled with sham group during the liquid diet period. Then, the body weight of sham-PF group followed that of VSG group after the initiation of pair feeding. Until the last monitoring period, the body weight of sham-PF was almost same as that of VSG group.

It was unable to measure the exact amount of liquid diet consuming due to loss by cage handling. The food intake was well matched between VSG and sham-PF group (Figure 3-2). However, during the 6th and 7th week after surgery, sham-PF had slightly lower amount of food than VSG (P value = 0.180 and 0.086, by t-test, 6 and 7 week respectively). Comparing VSG and sham, VSG reduced food intake only during early postoperative period until week 3. After that the food intake was similar between the groups.

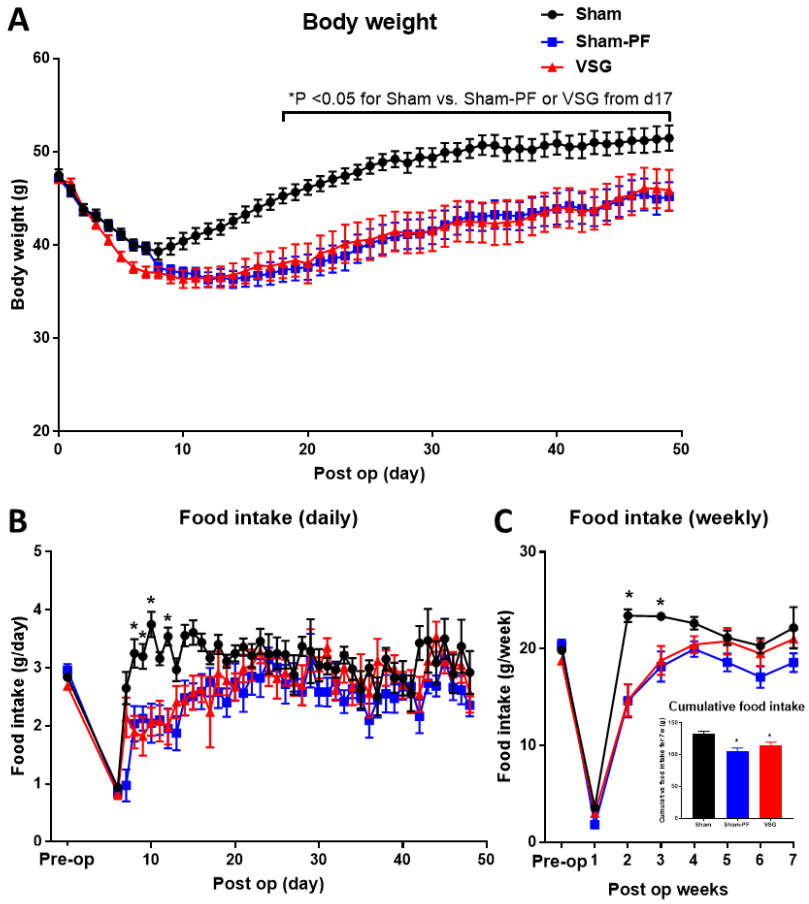

Figure 3-2. Body weight and food intake after VSG

(A) Body weight, (B) daily food intake and (C) weekly food intake after surgery and an inlet for the cumulative food intake of entire study period. *P value <0.05 for VSG vs. sham

1.2. VSG improved glucose tolerance after oral and intraperitoneal glucose challenge

I tested the glucose tolerance by both oral and intraperitoneal challenge 1 week apart. Both VSG and sham-PF groups demonstrated improved glucose tolerance than sham group (Figure 3-3). However, for the VSG group, the pattern of blood glucose level was different between oral and intraperitoneal challenge. After oral glucose challenge, VSG mice showed higher peak of blood glucose at 15 min than sham-PF and steeper decline nearly to the baseline level at 30 min. This was not seen after intraperitoneal challenge, and the blood glucose level was similar between VSG and sham-PF during IPGTT (Figure 3-3).

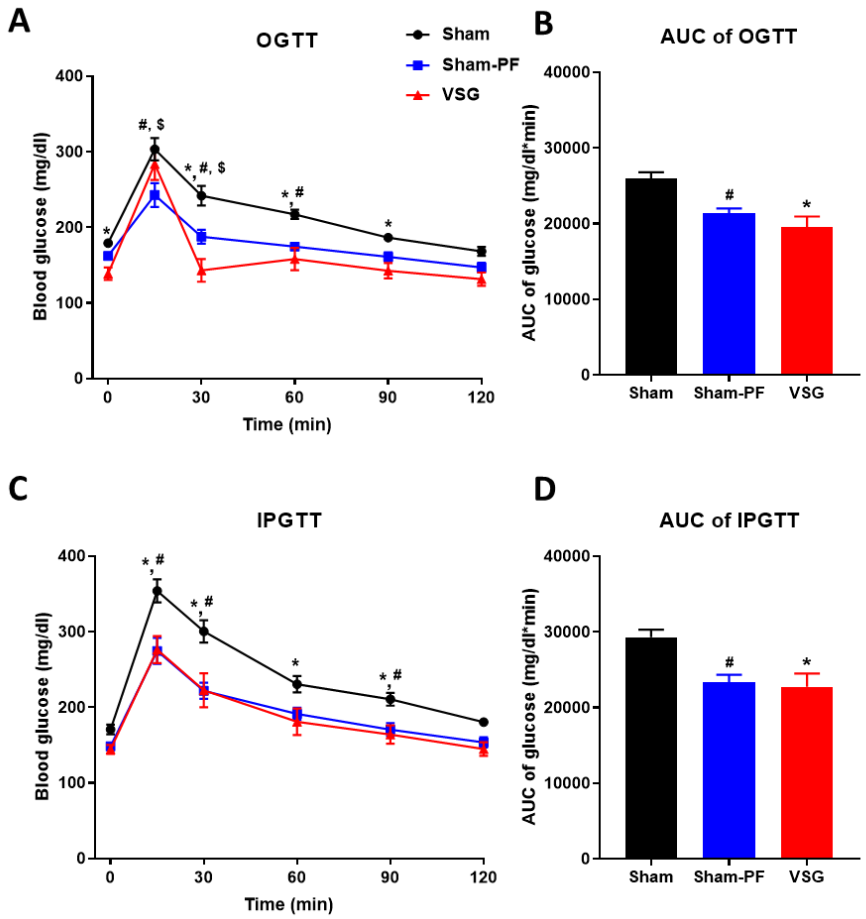

Figure 3-3. Glucose tolerance test

(A) Blood glucose level and (B) AUC of glucose level during OGTT. (C) Blood glucose level and (D) AUC of glucose level during IPGTT. #P <0.05 for sham vs. sham-PF $P <0.05 for sham-PF vs VSG *P value <0.05 for VSG vs. sham

1.3. VSG increased postprandial insulin and GLP-1 secretion

I had sampled peripheral blood at baseline and 15 minutes after oral glucose load for hormone measurements. Postprandial insulin level was significantly higher in VSG group than both sham and sham-PF (Figure 3-4). Insulinogenic index which was increment of insulin divided by increment of glucose was significantly higher in VSG than sham, which was also higher than sham-PF with marginal significance (P = 0.070).

Postprandial plasma GLP-1 level was higher in VSG group than both sham and sham-PF group (Figure 3-4). Fasting GLP-1 level was not significantly different among the groups.

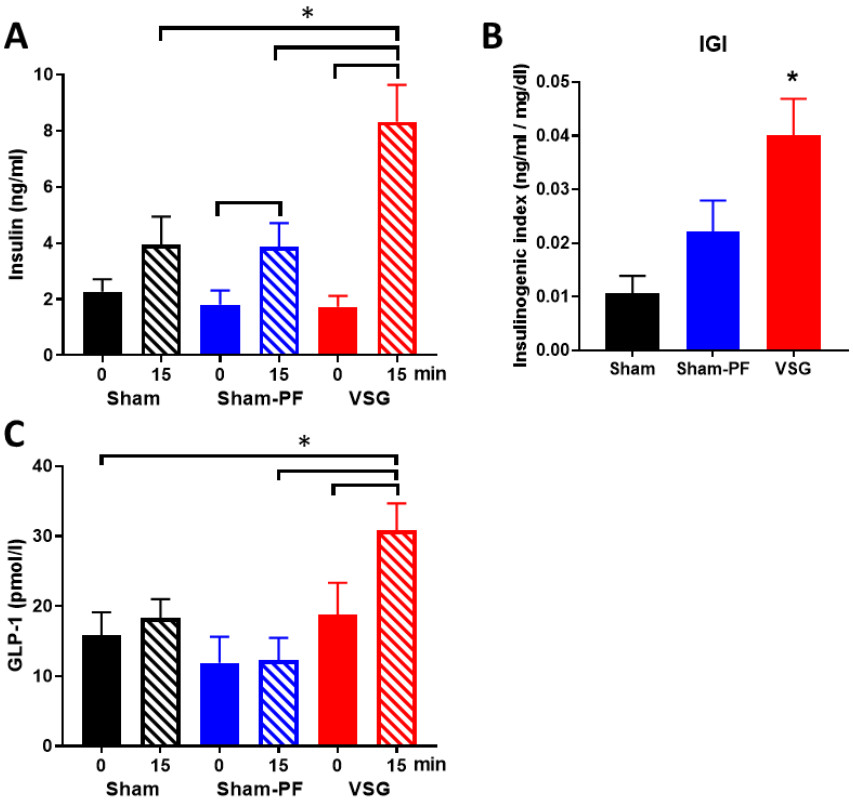

Figure 3-4. Glucose stimulated insulin secretion

(A) Plasma insulin level, (B) insulinogenic index and plasma total GLP-1 level after oral glucose challenge. *P value <0.05 for VSG vs. sham

1.4. VSG improved insulin sensitivity

I measured dynamic insulin sensitivity with insulin tolerance test. After intraperitoneal injection of insulin, rapidly decreased in VSG group which was significantly larger amount than both sham and sham-PF group at 15 minutes (Figure 3-5). Besides 15-minute measurements, plasma glucose level was similar between VSG and sham-PF, which was lower than sham group. HOMA-IR index which mainly reflects hepatic insulin sensitivity at fasting state was significantly lower in VSG group than sham.

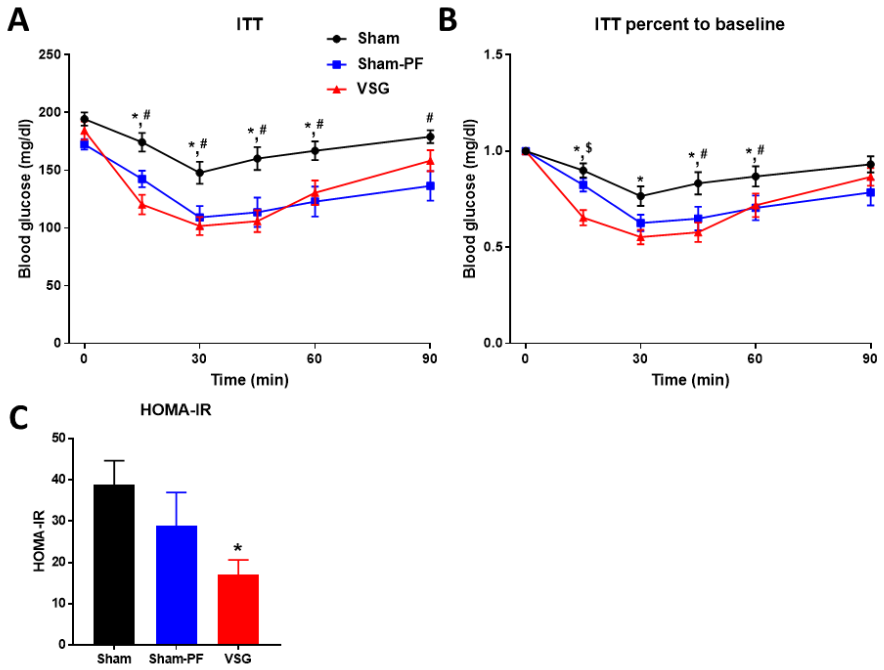

Figure 3-5. Insulin tolerance test and HOMA-IR

(A) Blood glucose level during insulin tolerance test. (B) Blood glucose level as a ratio to baseline value. (C) HOMA-IR. *P <0.05 for sham vs. VSG #P <0.05 for sham vs. sham-PF $P <0.05 for sham-PF vs VSG

1.5. VSG increased energy expenditure, but did not change respiratory exchange ratio

To see whether energy expenditure was changed after surgery, I put the mice in the metabolic cage. The energy expenditure was significantly increased in VSG group than sham group considering total body weight (Figure 3-6). Sham-PF was similar with VSG group, but the statistical significance for the differences between sham and VSG was not reached. However, the respiratory exchange ratio was not different among the groups.

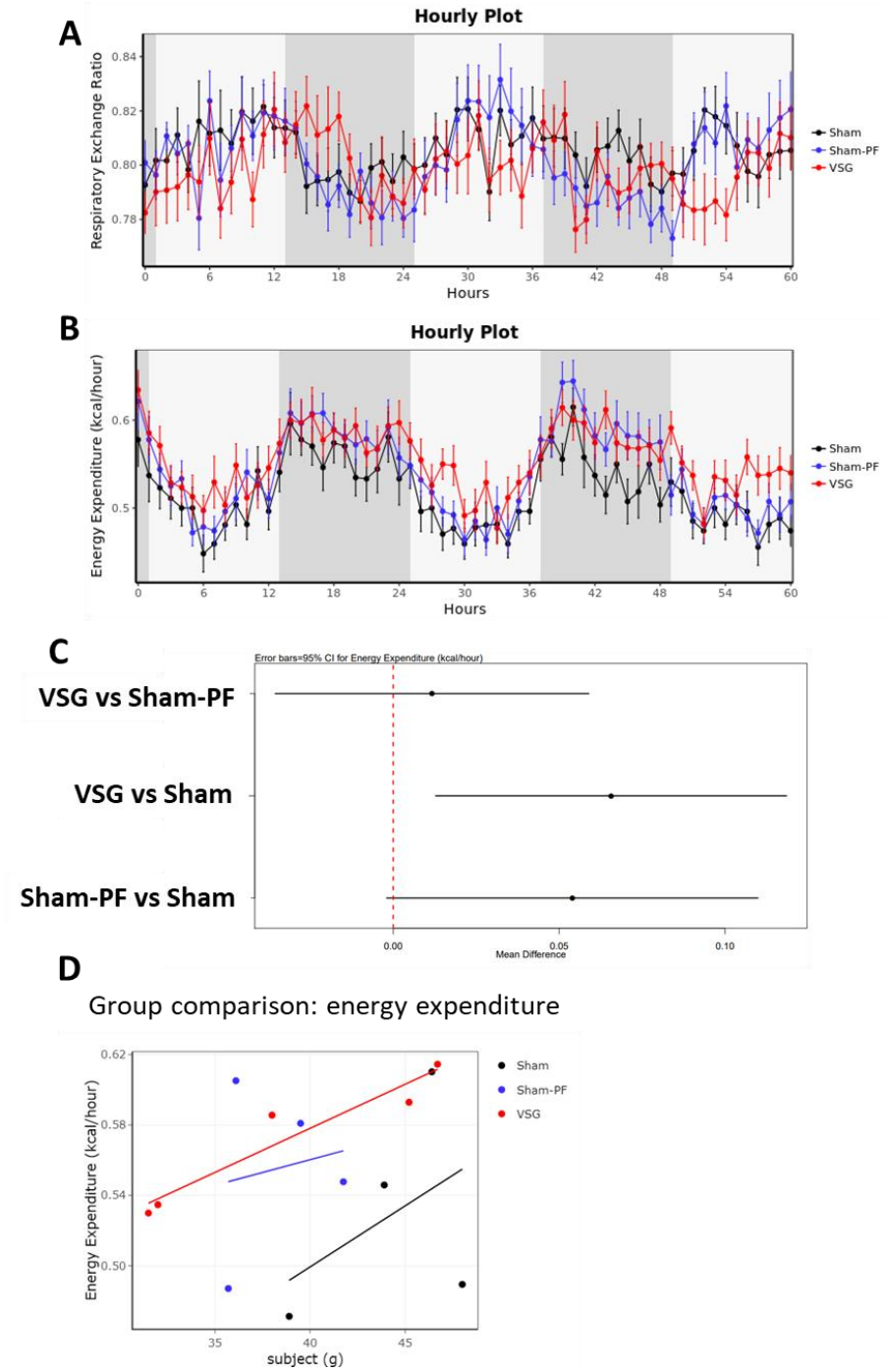

Figure 3-6. Measurements of indirect calorimetry

Hourly graph of (A) respiratory exchange ratio and (B) energy expenditure. (C) The intergroup difference of energy expenditure by general linear model and (D) relationship between total body weight and energy expenditure.

2. Histologic analysis of peripheral tissues

2.1. VSG improved fatty liver

On the histologic analysis of liver tissues, all mice showed some degree of fatty liver change (Figure 3-7). Compare to sham group, VSG and sham-PF groups had lesser degree of fatty liver. When I graded the non-alcoholic fatty liver disease (NAFLD) activity score, VSG and sham-PF had similar activity score which was lower than sham group with marginal significance ($P = 0.08$). Liver weight was also tended to lower in VSG and sham-PF group.

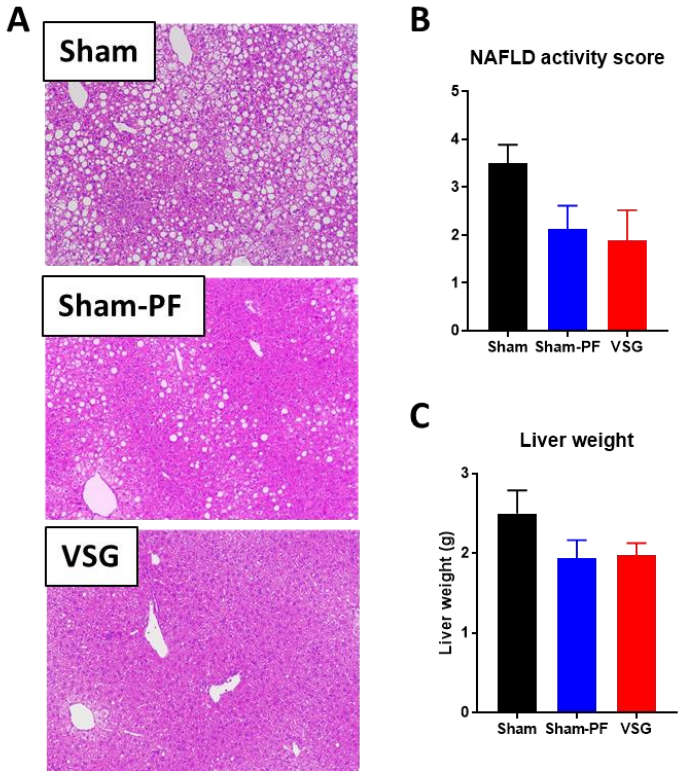

Figure 3-7. Histologic analysis of liver

(A) H&E stain images of liver, (B) NAFLD activity score and (C) liver weight at sacrifice.

2.2. VSG decreased inflammation in adipose tissue

On the histologic analysis of epididymal adipose tissue, mean size of adipocyte was not different among the groups (Figure 3-8). However, sham had more inflammatory infiltration than sham-PF and VSG. The number of crown-like structure was significantly lower in sham-PF and VSG than sham group.

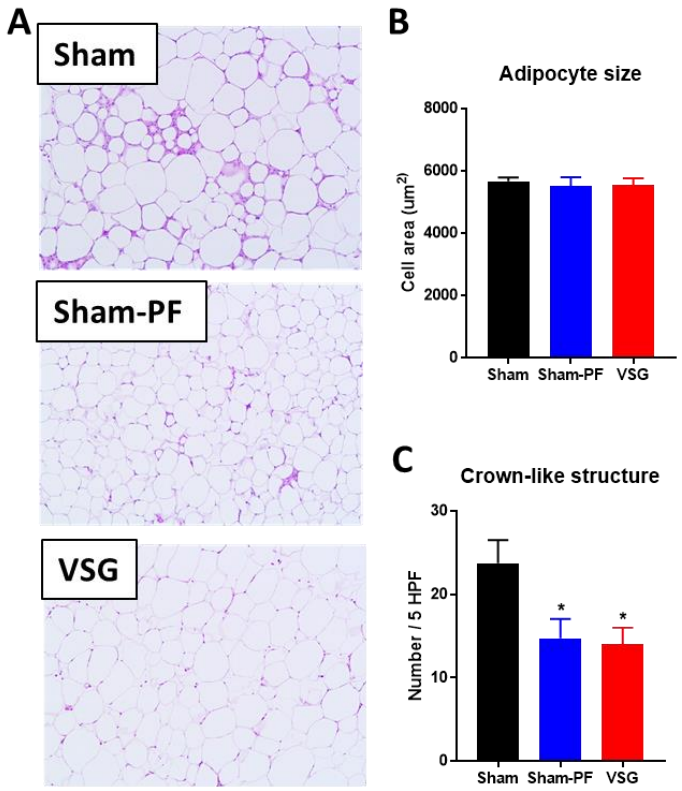

Figure 3-8. Histologic analysis of epididymal adipose tissue

(A) H&E stain images of adipose tissue, (B) mean size of adipocyte and (C) number of crown-like structure per high power field. *P <0.05 for sham vs. VSG

3. Transcriptome analysis of peripheral tissues

3.1. Liver

After the RNA sequencing of the liver in three groups, I compared the gene expressions in the three comparisons: sham-PF vs. sham, VSG vs. sham-PF and VSG vs. sham. First, PCA plot showed that sham-PF and sham samples were close together, while VSG samples were distant (Figure 3-9). The intragroup heterogeneity was higher in VSG group than sham or sham-PF group. The volcano plot and venn diagram summarizes the number of DEGs in the three comparisons. The number of DEG was highest in the comparison of VSG vs. sham-PF, and lowest in the comparison of sham-PF vs. sham. These results suggested that the sham and sham-PF group were similar and VSG group was distinct from the two groups.

Then, I analyzed enriched gene ontology and KEGG pathway in the list of DEG which was common in VSG vs. sham-PF and VSG vs. sham to find out which pathway is distinctive in VSG group. In the up-regulated DEGs, immune-related processes were enriched including the highest p-value of immune system process among gene ontology biologic process. In the down-regulated DEGs, metabolic processes were enriched including the highest p-value of lipid metabolic processes. KEGG pathways enriched in the down-regulated DEGs were also related with metabolism processes especially the processes related with the detoxification of chemical, drugs or xenobiotics.

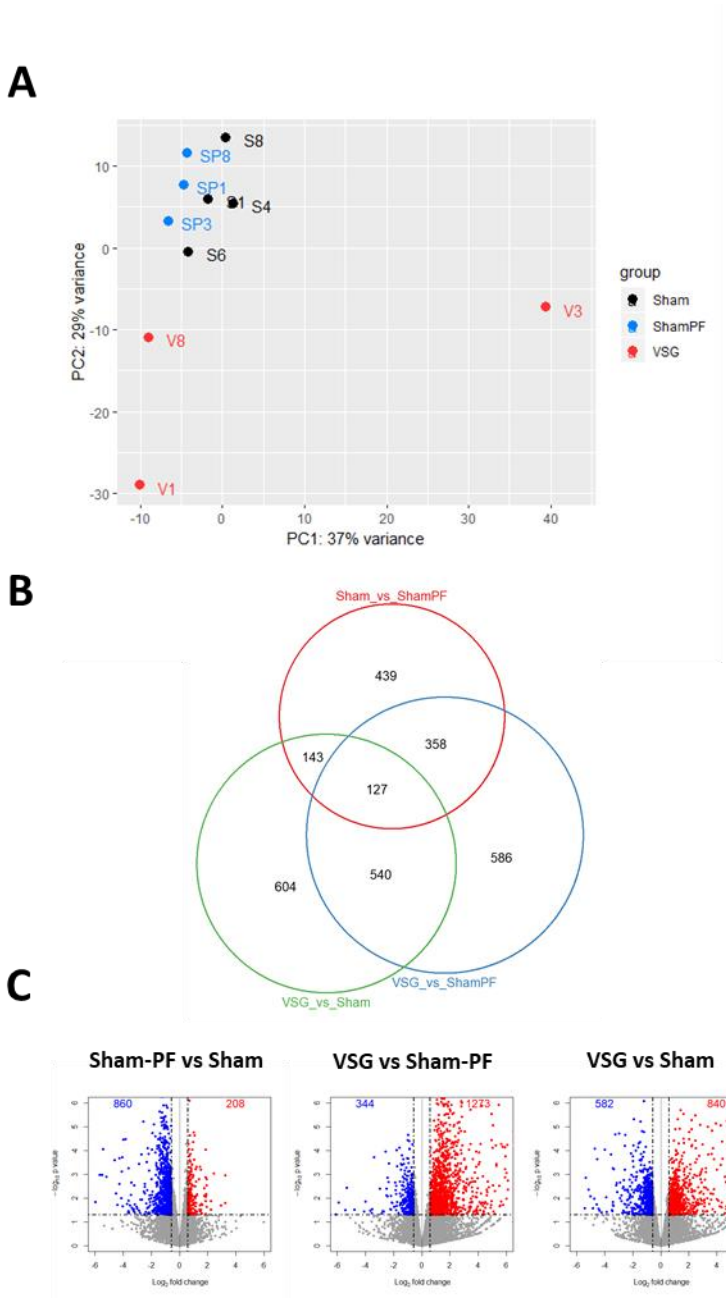

Figure 3-9. Transcriptomic analysis of liver

(A) PCA plot of the three groups, (B) venn diagram showing the number of DEGs in each comparison, and (C) volcano plot showing the p value and fold change of the gens in each comparison.

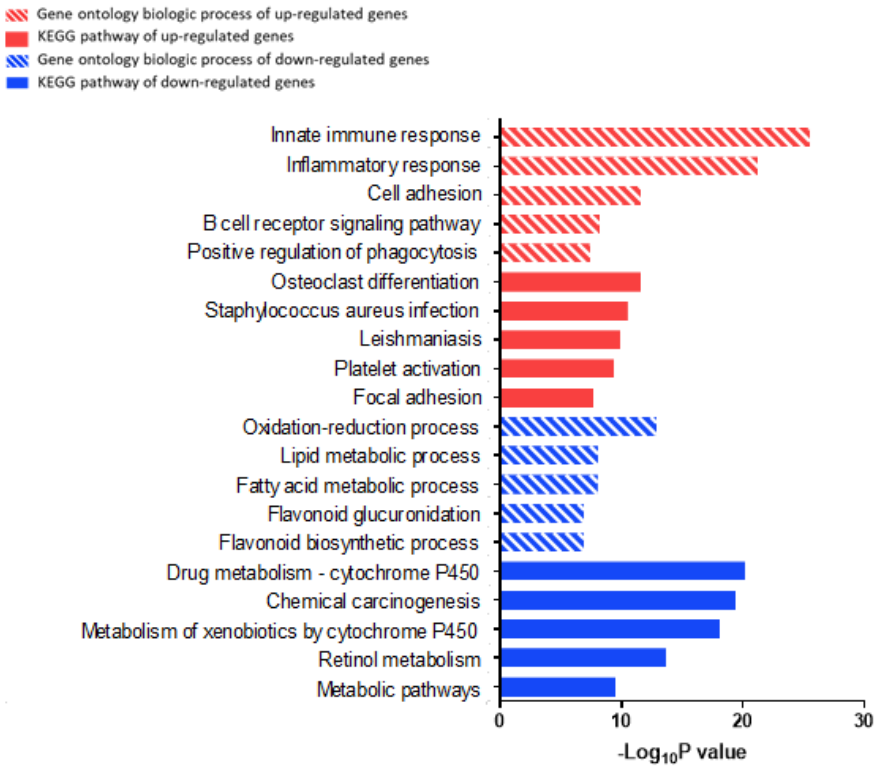

Figure 3-10. Gene ontologies and KEGG pathways enriched in the liver after VSG compared to sham-PF

Gene ontology of biologic process and KEGG pathways significantly enriched in the common DEG of VSG vs sham-PF.

3.2. Adipose tissue

In the transcriptome analysis of the epididymal adipose tissue, I found that the VSG was distinct from the sham and sham-PF groups (Figure 3-10). In the PCA plot, sham and sham-PF were close and VSG were distant from the two groups. Like liver, the intragroup heterogeneity was also higher in VSG group than sham or sham-PF group. As summarized in the volcano plot and venn diagram, the number of DEG was highest in the comparison of VSG vs. sham, and lowest in the comparison of sham-PF vs. sham. The DEG of VSG vs. sham-PF was largely overlapped with that of VSG vs. sham. These results suggested that, like liver, VSG was distinct from the two sham groups.

I analyzed enriched gene ontology and KEGG pathway in the list of DEG which was common in VSG vs. sham-PF and VSG vs. sham. The most distinct result was that immune-related processes were enriched in the up-regulated DEGs. Although the significance level was lower than above mentioned pathways, adhesion and extracellular matrix related pathways were enriched in the down regulated DEGs.

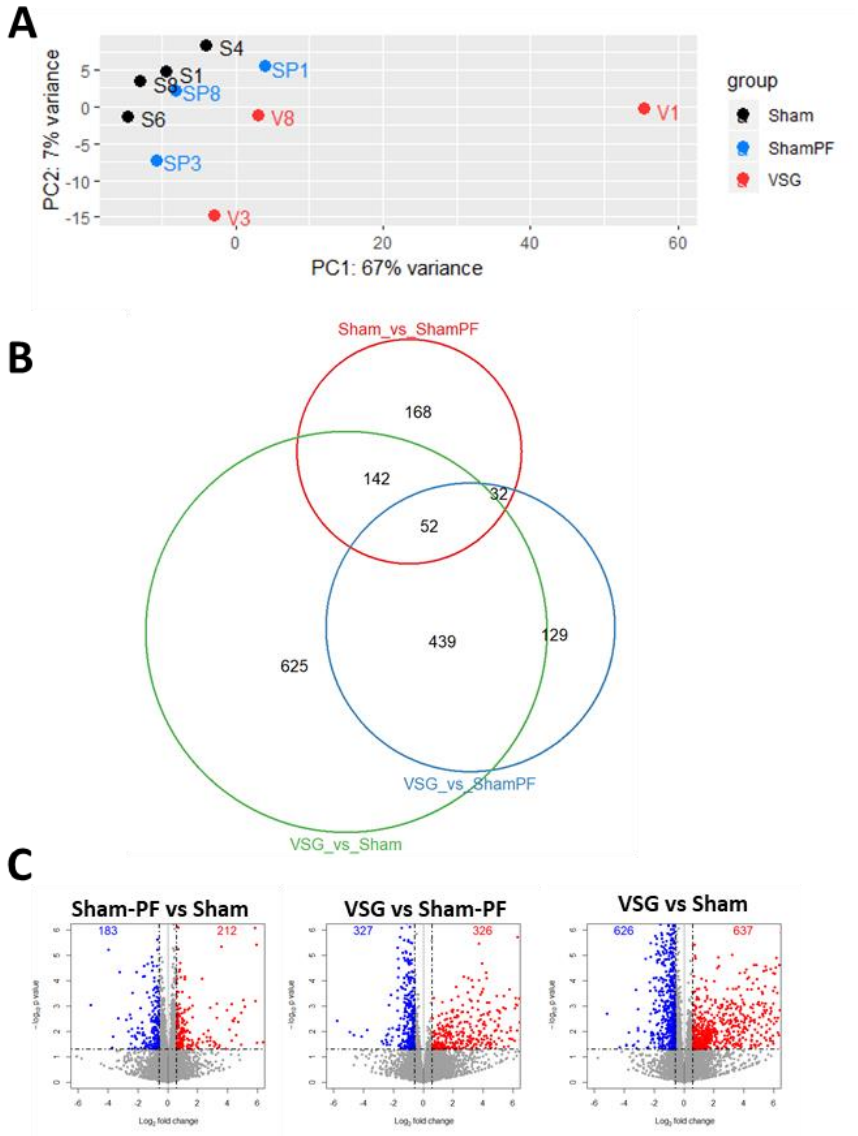

Figure 3-11. Transcriptome analysis of adipose tissue

(A) PCA plot of the three groups, (B) venn diagram showing the number of DEGs in each comparison, and (C) volcano plot showing the p value and fold change of the gens in each comparison.

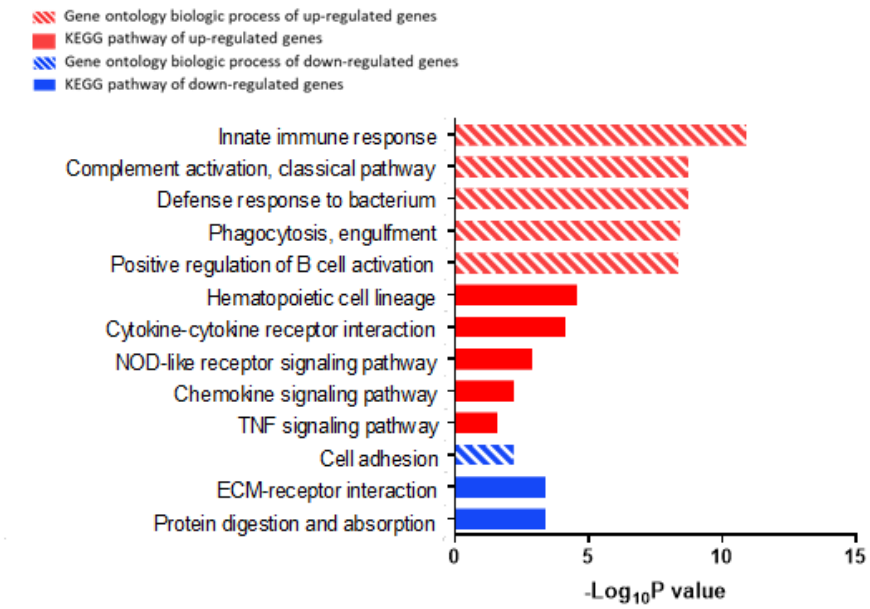

Figure 3-12. Gene ontologies and KEGG pathways enriched in the adipose tissue after VSG compared to sham-PF

Gene ontology of biologic process and KEGG pathways significantly enriched in the common DEG of VSG vs sham-PF.

3.3. Muscle

Unlike liver and adipose tissue, the transcriptome analysis of muscle tissue showed no clear clustering of the samples in each group (Figure 3-11). The number was higher in VSG vs. sham and VSG vs. sham-PF than Sham-PF vs. sham comparison. However, the total number of DEG in the analysis of muscle tissue was much smaller than that of liver or adipose tissue. These suggested that the gene expression in muscle was not altered by VSG as much as in liver or adipose tissue.

Despite of the smaller changes in the gene expression overall, the enrichment analysis showed similar result as liver or fat that the immune response was enriched in the up-regulated DEGs.

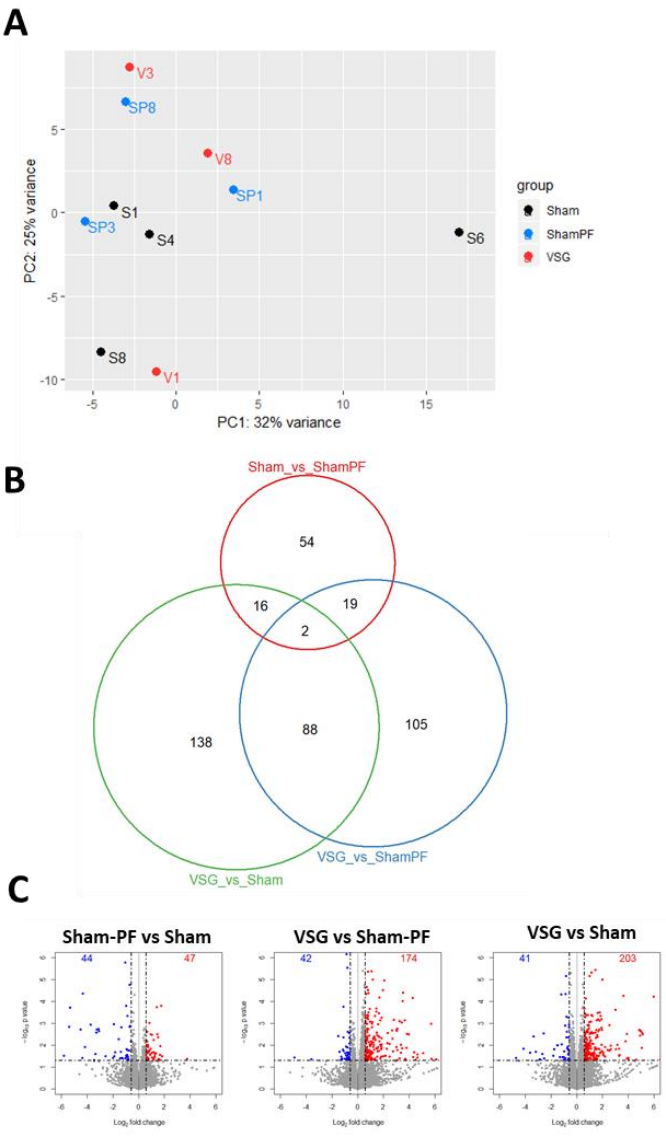

Figure 3-13. Transcriptome analysis of muscle tissue

(A) PCA plot of the three groups, (B) venn diagram showing the number of DEGs in each comparison, and (C) volcano plot showing the p value and fold change of the gens in each comparison.

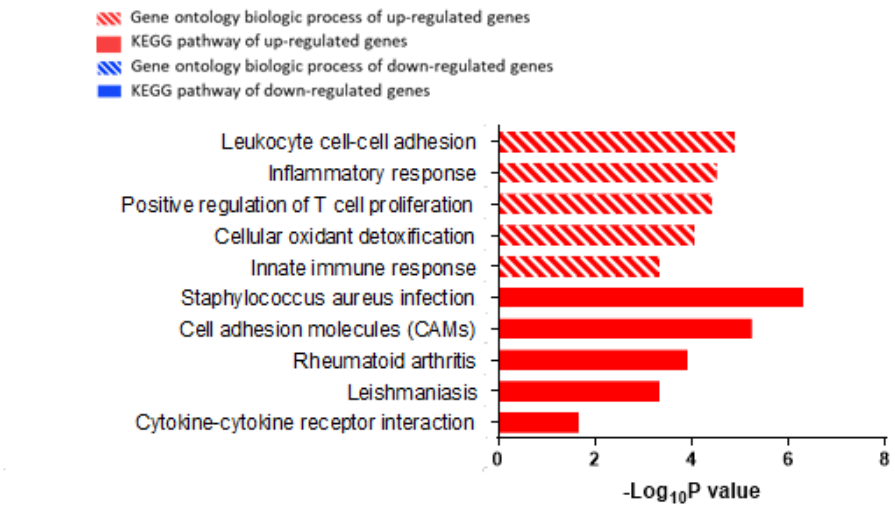

Figure 3-14. Gene ontologies and KEGG pathways enriched in the muscle after VSG compared to sham-PF

Gene ontology of biologic process and KEGG pathways significantly enriched in the common DEG of VSG vs sham-PF.

4. Inter-organ comparison of transcriptome analysis

I tried to figure out the similarity and the difference in the transcriptome analysis of the three organs to see which was shared by the three organs and which was distinctive in each organ.

To perform gene-level comparison, I compared the DEGs in the comparison of VSG vs. sham-PF among the three organs (Figure 3-12). Only the small number of DEGs were shared by the three organs, and only about 10% of DEGs of each organ were shared by any two organs. However, when I performed pathway-level comparison, I could find more similarities among the organs. The most distinctive pathway that shared by the three organs was that the immune-related processes were enriched in the un-regulated DEGs.

A

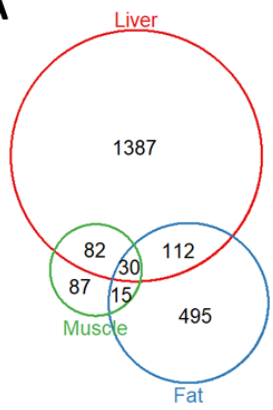

B

Shared DEGs		
Adgre4	Ighm	Ltf
Aif1	Ighv11-2	Marcksl1
Aoah	Ighv1-26	Mmp9
Cd300e	Igkc	Ngp
Cd300lf	Igkv1-110	S100a9
Clec4a1	Igkv1-135	Siglece
Cxcl13	Iglc2	Slc15a3
Fgr	Il1b	Snca
Hbb-bs	Itgax	Tmem176a
Hbb-bt	Jchain	Tmem176b

Figure 3-15. Comparative analysis of transcriptome of the liver, fat and muscle

(A) Venn diagram of DEGs in the comparison of VSG and sham-PF in liver, fat and muscle, (B) list of DEGs which were shared by the three organs.

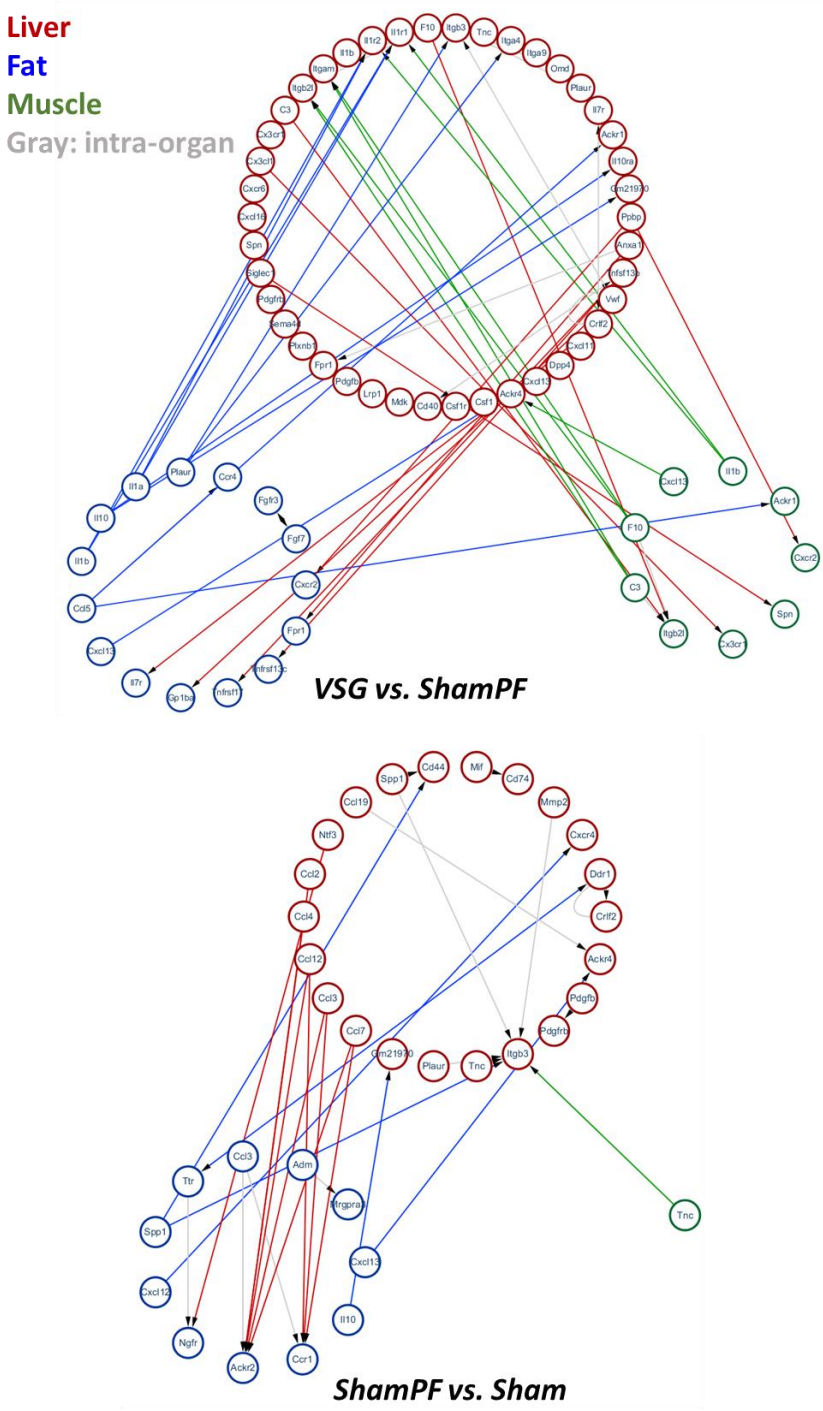

3-16. Networks models of the inter-organ communication in liver, fat and muscle after VSG.

Networks models illustrate the inter-organ communications changed in VSG compared to sham-PF or in sham-PF compared to sham. An open database of receptor-ligand relationship (CellPhoneDB by Vento-Tormo R et al. (98)) was used to create the network. Each node denotes a DEG in liver, fat or muscle which is a receptor or ligand. Each edge denotes a receptor-ligand relationship between the two nodes and the direction was set from ligand to receptor. Red nodes and edges represent liver. Green represents muscle and blue represents fat. Gray edges are intra-organ communications.

5. Comparison between RYGB and VSG

RYGB is another popular bariatric surgery. It showed similar metabolic effects in terms of diabetes remission and lowering body weight, the surgical procedure have large differences compared to VSG. RYGB involves bypass of the intestine, unlike VSG. By comparing RYGB and VSG, I can find out the common and unique mechanisms of how bariatric surgery affects metabolism.

I analyzed the public dataset GSE113823 from GEO which was done by Ben-Zvi et al. In this study, Ben-Zvi et al. performed transcriptome analysis of liver, inguinal adipose tissue, and gastrocnemius muscle by RNA sequencing. I downloaded the FASTQ files and performed subsequent analysis.

First, I compared the DEGs of VSG vs. sham-PF in our study with DEGs of RYGB study in each organ. 23.5, 29.1 and 34.1% of the DEGs were shared in liver, adipose tissue and muscle. The number of DEG was larger in RYGB than VSG in all three organs. I then compared the pathways enriched in each organ. I then compared the fold change of each gene between RYGB and VSG. The high correlation in this analysis means that the genes up-regulated or down-regulated in VSG was also similarly up- or down-regulated in RYGB mice. Interestingly, the gene expression fold change was most strongly correlated in liver than adipose tissue or muscle, suggesting that the changes in liver after RYGB and VSG is more similar than adipose tissue or muscle.

Then, I compared the gene ontology enriched in each organ of RYGB and VSG (Figure 3-14, 3-15, 3-16). In liver, fat, and muscle, the immune-related gene ontologies were shared by RYGB and VSG.

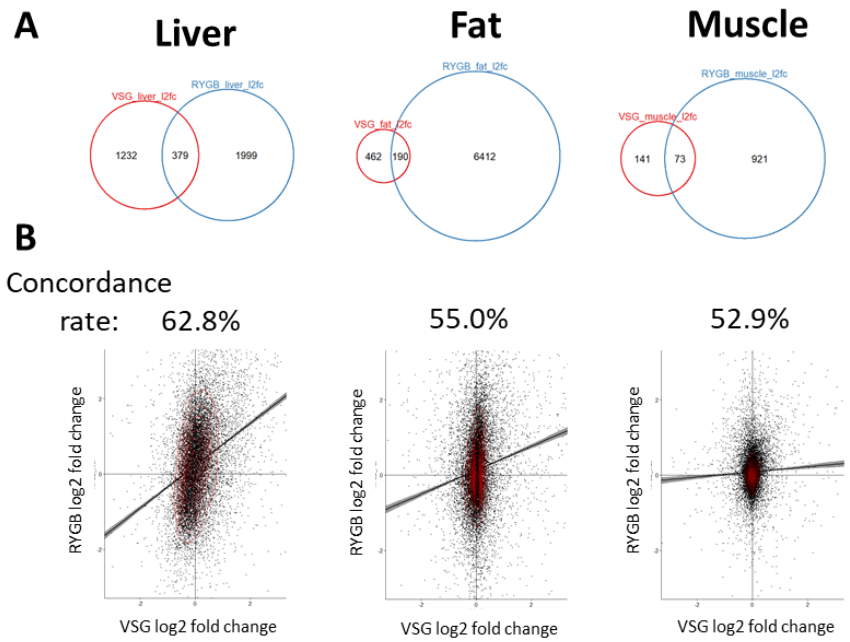

Figure 3-17. Comparative analysis of transcriptome between VSG and RYGB model

(A) Venn diagram of DEGs in the three organs of VSG and RYGB, (B) scatter plot of the log2 fold changes of the genes in VSG and RYGB

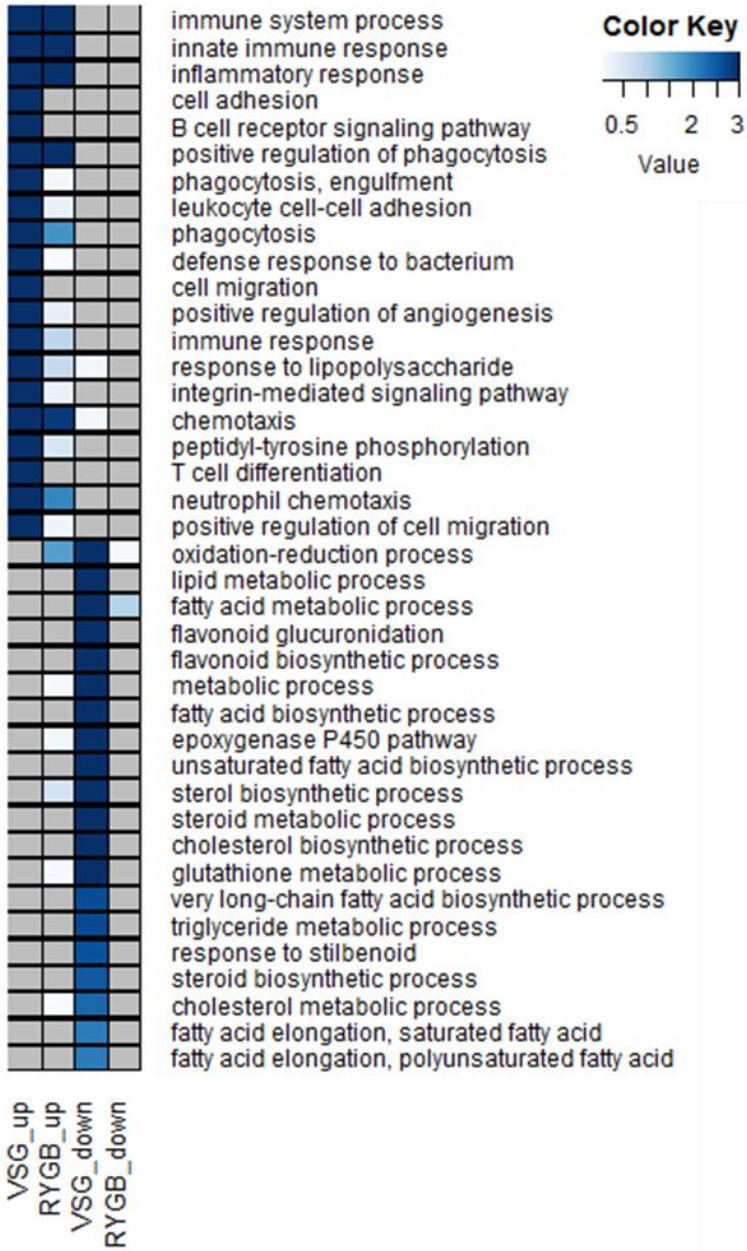

Figure 3-18. Gene ontology biologic process enriched in liver of VSG and RYGB

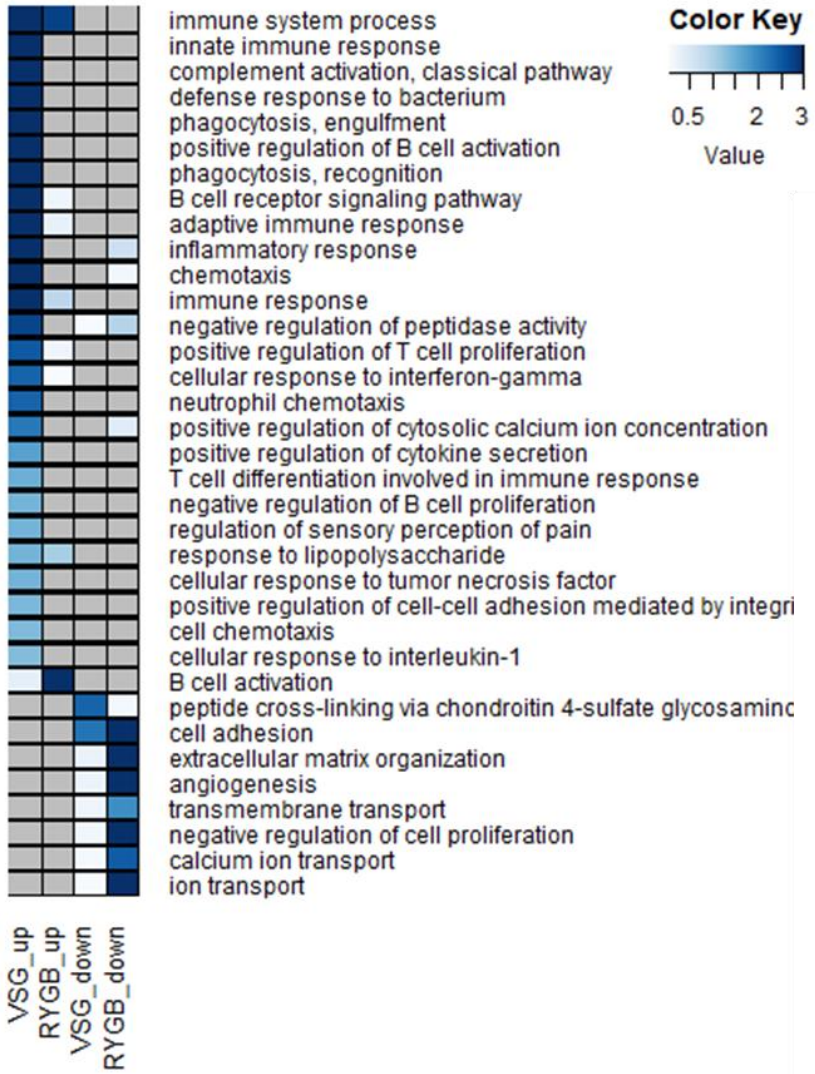

Figure 3-19. Gene ontology biologic process enriched in fat of VSG and RYGB

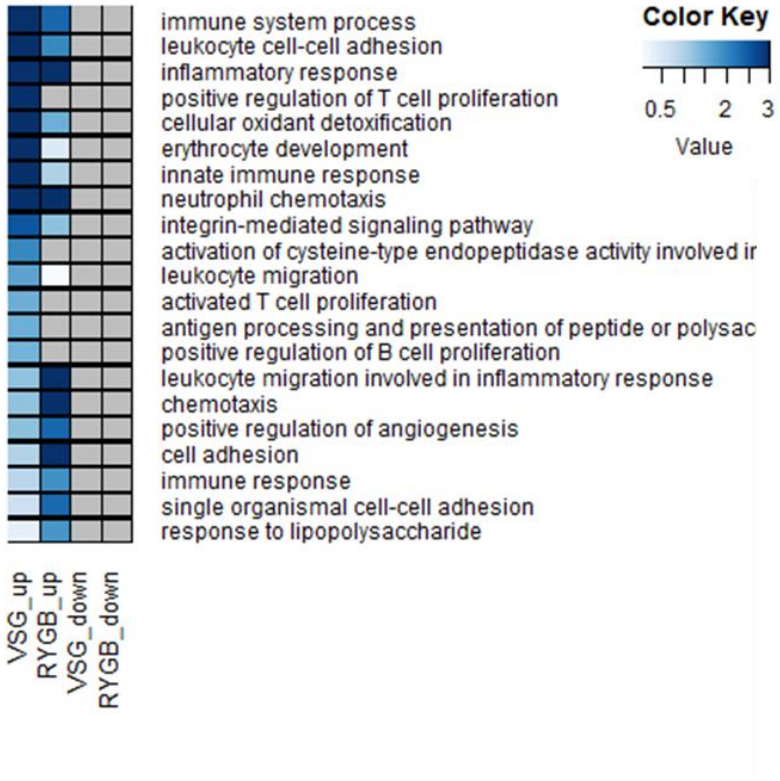

Figure 3-20. Gene ontology biologic process enriched in muscle of VSG and RYGB

6. Immune response in peripheral tissues

6.1. Macrophage with M2-phenotype was increased in VSG than sham-PF

I separated stromal vascular fraction from epididymal adipose tissue and performed flow cytometry to investigate the macrophage. The number of macrophage was marginally increased in VSG than sham-PF (Figure 3-17). The percentage of M2-phenotype was also marginally increased in VSG. The M2 marker gene was decreased in epididymal fat. Mesenteric fat also showed similarly increased M2 marker gene with decreased M1 marker gene. Subcutaneous fat did not showed pattern of increased M2 and decreased M1 marker gene.

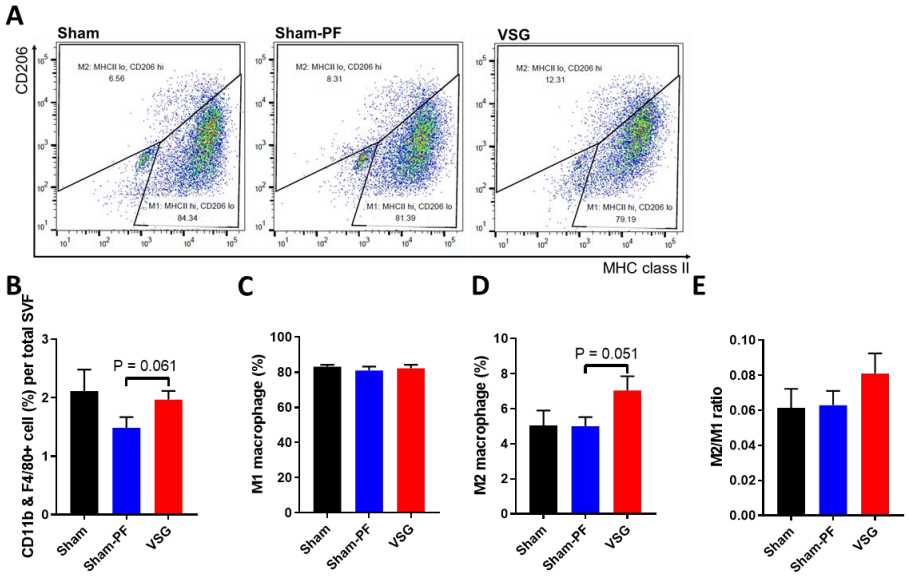

Figure 3-21. Macrophage profiling in stromal vascular fraction of epididymal adipose tissue

(A) Representative graph of M1 and M2-phenotype macrophage flow cytometry analysis in three groups, (B) The percentage of CD11b+ and F4/80+ macrophage, (C) percentage of M1 phenotype macrophage, (D) percentage of M2 phenotype macrophage, (E) ratio of M1/M2 macrophage. *P <0.05 VSG vs. Sham-PF.

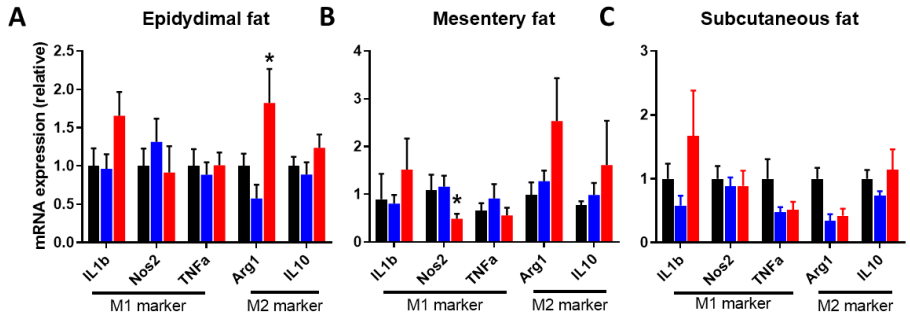

Figure 3-22. Expression of M1/M2 macrophage markers in stromal vascular fraction of epididymal adipose tissue

Expression levels of M1 and M2 marker genes in (A) epididymal fat, (B) mesenteric fat, and (C) inguinal fat. *P <0.05 VSG vs. Sham-PF.

6.2. B cell population was increased in VSG than sham-PF

Cxcl13 gene expression was increased in all the three adipose tissues and liver and muscle (Figure 3-18). I confirmed that the tissue protein level was also increased in VSG than sham-PF. Cxcl13 is a B cell chemoattractrant. Thus, I analyzed the lymphocyte subpoulation in the stromal vascular fraction of epididymal adipose tissue. CD19 positive B cell population was significantly increased in the SVF of epididymal fat.

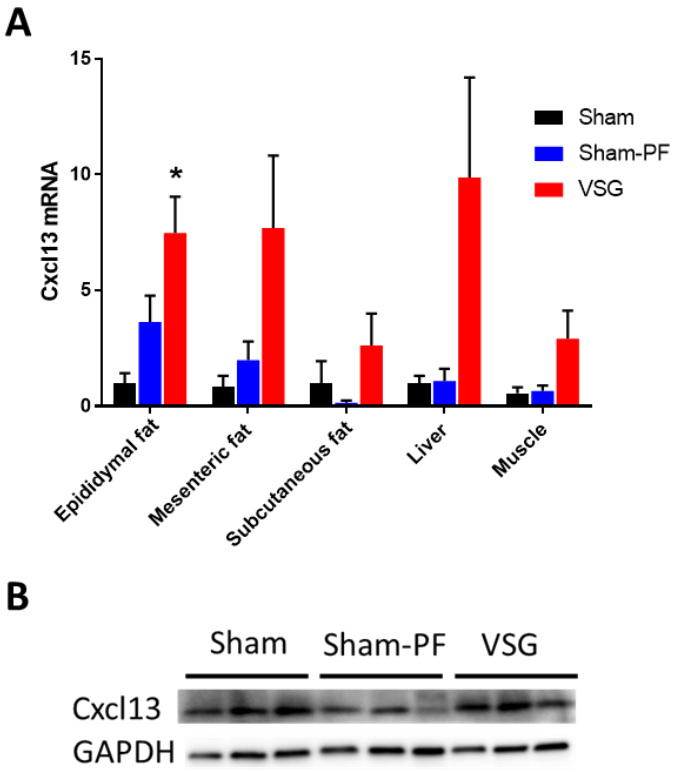

Figure 3-23. Cxcl13 level in adipose tissue

(A) mRNA levels of Cxcl13 in epididymal, mesenteric and subcutaneous adipose tissue, liver, and muscle. (B) Protein quantification of Cxcl13 in epididymal adipose tissue.

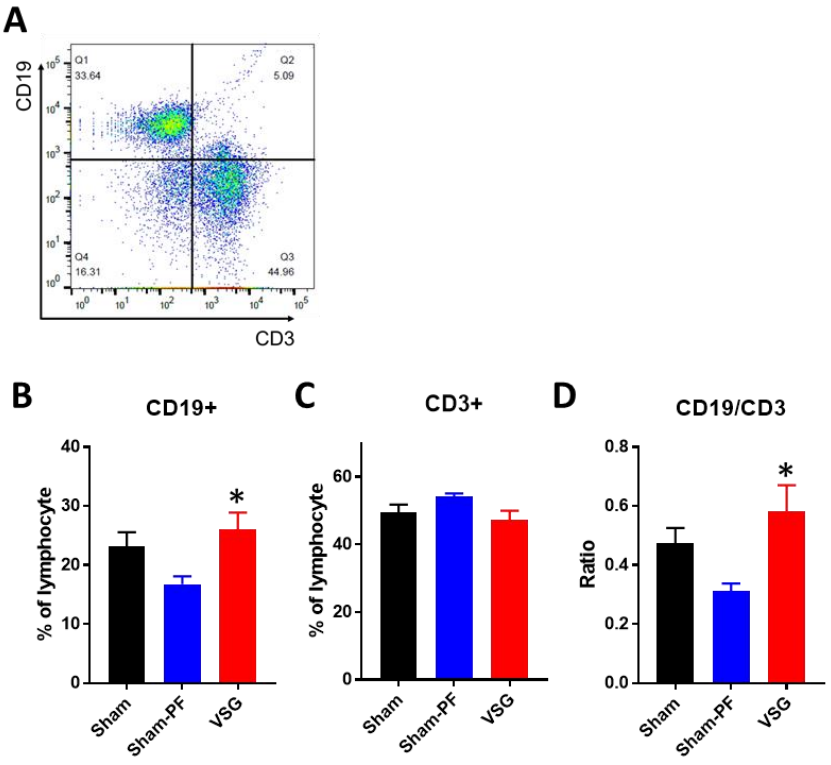

Figure 3-24. Lymphocyte subpopulation into T cell and B cell in adipose tissue

(A) representative graph of T and B cell population in flow cytometry (B) percentage of CD19+ B cell population, (C) CD3+ T cell population in lymphocytes and (D) ratio of CD19/CD3 cells

Discussion of chapter 2

I matched the food intake between VSG and sham-PF, not the body weight. However, the body weight of the two groups were similar in our study. The energy expenditure was not different between VSG and sham-PF. Thus, in terms of energy homeostasis, these results can be interpreted as that VSG induces body weight loss mainly by reducing food intake. Interestingly, the reduced food intake was only apparent during the early postoperative period. This pattern of early decrease in food intake and later catch-up to the level of control group was consistently shown for rodent model of metabolic surgery (34, 99). This means that even though the stomach volume was largely reduced, VSG mice can eat as much as sham mice. Thus, these support that the restriction of food intake does not work on VSG, rather the homeostatic regulation of food intake is changed after VSG. The weight loss induced by VSG are resulted from the lower food intake for only 3 weeks after surgery in our study. Sham mice had compensatory hyperphagia after initiation of solid food, but this was not seen in VSG mice. This can be interpreted as that VSG mice had new set point of body weight after surgery.

In our study, the weight-loss independent effect of VSG on glucose tolerance was not larger than weight-loss dependent effects. The glucose tolerance was not different between VSG and sham-PF during IPGTT. This suggests that gut-factor explains the difference in the plasma glucose level between VSG and sham-PF during OGTT. GLP-1 is well characterized as

having a significant role in this gut factor after VSG. Postprandial GLP-1 secretion increased significantly in our study, too.

The weight-loss independent effects on gene expression of peripheral tissues were larger than the weight-loss dependent effects. Shown by PCA plot, clustering analysis and number of DEGs, VSG group was distinct from sham or sham-PF. The difference of VSG from sham or sham-PF was bigger than the difference between sham and sham-PF. To focus on these weight-loss independent effects, I further looked at the enriched pathways in DEG of VSG vs. sham-PF. Interestingly, the immune-related pathways were consistently enriched in the three organs, suggesting VSG induces a distinct immunologic process in peripheral organs.

I compared our transcriptome analysis results with that of RYGB mouse model studied by Ben-Zvi et al. (100). At the gene level comparison, only 20~30% of DEGs in each organ of VSG was shared by RYGB. Interestingly, when compare the gene expression changes brought by VSG and RYGB in each organ at whole genome level. The correlation of gene expression changes was highest in liver, which suggests that the physiology of liver is more common than adipose tissue and muscle in VSG and RYGB.

In my study, VSG reduced body weight and improved glucose tolerance in diet-induced obese mice. This improvement was partially explained by the weight loss when I compared the VSG with matched sham-PF. Augmented insulin secretion after oral glucose load along with increased GLP-1 secretion was only observed in VSG mice, not in sham-PF mice. Insulin sensitivity was improved after both VSG and pair-feeding, but slightly more

after VSG. Through transcriptome analysis of liver, fat and muscle, I could find that, unlike the degree of metabolic difference between VSG and sham-PF, gene expression profile of liver, fat, and muscle was more distinct between VSG and sham-PF than between sham and sham-PF, suggesting that the weight-loss independent effect was more robust for the gene expression profiles of the three tissues. Among various pathways enriched in the DEGs, immune-related pathways were most consistently up-regulated in all three organs. Finally, with flow cytometry analysis, I could capitulate altered immune response that was increased Cxcl13 and B cell population in adipose tissue.

Discussion

1. Summary of the previous studies about the molecular mechanisms of metabolic surgery

There have been numerous studies to investigate the role of a specific molecular pathway in metabolic surgery. By comparing the effects of VSG in wild type and transgenic mice models, the contribution of a specific molecular pathway in metabolic surgery was tested (Table).

Table 4-1. Results of the studies investigated the role of specific molecular pathways in VSG using transgenic mouse model. NR, not reported; KO, knock out.

Author	Year	Journal	Animal model	Model description	Body weight	Food intake	Glucose	Insulin sensitivity	Insulin secretion	Other effects
Joram D. Mul, Randy J. Seeley, et al.	2012	Am J Physiol Endocrinol Metab	MC4R KO rat	MC4R mutantation is a model of genetic obesity	Higher baseline weight in KO Similar degree of weight reduction by VSG in KO and WT	Higher baseline food intake in KO Similar degree of reduction by VSG in KO and WT	Higher baseline glucose in KO Similar degree of reduction by VSG in KO and WT	Similar improvement	NR	
Hilary E. Wilson-Pérez, Randy J. Seeley, et al.	2013	Diabetes	GLP1r KO mouse		Lower baseline weight in KO Similar effect of VSG in KO and WT	Similar effect of VSG in KO and WT (Early post-op reduction in food intake)	Higher baseline glucose level in KO Similar post-op glucose level in WT and KO VSG mice	NR	Similar improvement in KO and WT	
Adam P.Chambers, Randy J.Seeley, et al.	2013	Gastroenterology	Ghrelin KO mouse	No detectable circulating Ghrelin	Lower baseline weight in KO Similar effect of VSG in KO and WT	Similar effect of VSG in KO and WT (Early post-op reduction in food intake)	Similar baseline and post-op glucose level in WT and KO VSG mice	NR	NR	
Myronovych A, Kohli R., et al.	2014	Obesity	Small heterodimer partner (SHP) KO, SHP Tg mouse	SHP is an orphan nuclear receptor which regulates metabolic processes in the liver, including BA, lipid, glucose homeostasis	Similar baseline weight, similar effect of VSG in KO and WT	Similar baseline weight, similar effect of VSG in KO and WT	Similar baseline and post-op glucose level in WT and KO VSG mice (only fasting level was reported)	NR	NR	

Karen K. Ryan, Randy J. Seeley, et al.	2014	Nature	FXR KO mouse		Lower baseline weight in KO No effect of VSG in KO	No early post-op reduction in KO	Fasting glucose was increased in KO VSG than KO sham No difference in AUC of glucose between KO VSG and KO sham	NR	NR	Gut microbiome change was attenuated in KO
Arble DM, Randy J. Seeley, et al.	2015	Int J Obes	ClockΔ19 mouse	Circadian disruption model	Higher baseline weight in KO Similar degree of weight reduction by VSG in KO and WT	Higher baseline food intake in KO Slightly lower reduction by VSG in KO	No significant improvement (AUC of glucose)	NR	Less improvement	
Anne K McGavigan, Bethany P Cummings, et al.	2015	Gut	TGR5 KO mouse		Similar baseline weight, similar effect of VSG in KO and WT	Similar effect of VSG in KO and WT (Lower cumulative food intake)	Similar baseline and post-op glucose level in WT and KO VSG mice	Similar improvement in WT and KO	NR	Hepatic insulin signaling was attenuated in KO VSG Less improvement in bile acid pool in KO
Arble DM, Sandoval DA, et al.	2016	Surg Obes Relat Dis	Magel2 KO mouse	Mouse model of Prader-Willi syndrome	Similar baseline weight, similar effect of VSG in KO and WT	Similar effect, lower fat preference maintained	Similar baseline and post-op glucose level in WT and KO VSG mice	NR	NR	
Lili Ding, Wendong Huang, et al.	2016	Hepatology	TGR5 KO mouse		Similar baseline weight in KO and WT The effect of VSG was much attenuated in KO	Similar effect of VSG in KO and WT (Early post-op reduction in food intake)	Similar baseline glucose level in KO and WT Improvement of glucose tolerance was diminished, but	Improvement diminished	Improvement diminished	Bile acid change was attenuated in KO

							still with a lower trend			
Darline Garibay, Bethany P. Cummings, et al.	2016	Endocrinology	β cell specific GLP1r KO mouse		Similar baseline weight, similar effect of VSG in KO and WT	Similar baseline weight, similar effect of VSG in KO and WT	VSG improved AUC of glucose both in KO and WT KO VSG had higher glucose than WT VSG	NR	Less improvement	
Jonathan D. Douros, David A. D'Alessio, et al.	2018	Diabetes	β cell specific GLP1r KO mouse		Similar baseline weight, similar effect of VSG in KO and WT	Similar baseline weight, similar effect of VSG in KO and WT	Higher baseline glucose in KO Similar degree of reduction by VSG in KO and WT	NR	NR	
Frikke-Schmidt H, Randy J. Seeley, et al.	2019	Mol Metabolism	GDF15 KO, GFRAL KO mouse	GDF15 induces anorexia	Similar baseline weight, similar effect of VSG in KO and WT	Similar effect, lower fat preference was maintained	NA	NR	NR	

As noted from the table 4-1, bile acid and its receptors, FXR and TGR5, are the only candidates with positive results as a molecular target of metabolic surgery up to now (101). Bile acid facilitates the absorption of lipid, and is recycled through enterohepatic circulation. After RYGB and VSG, the enterohepatic circulation of bile acid is changed and, as a result, the bile acid pool in the systemic circulation and intestinal lumen is changed. Addition to its role in lipid absorption, bile acid also has an endocrine function with various metabolic effects being signaled through the farnesoid X receptor (FXR) and G-protein coupled bile acid receptor (GPBAR, TGR5). FXR regulates bile acid synthesis by modulating the enzyme CYP7A1, and is also directly related to glucose and lipid metabolism. In the liver, FXR activation results in increased glycogen synthesis and decreased gluconeogenesis (102, 103). TGR5 is expressed in various cells including endothelial cells, monocytes and enteroendocrine cells, which results in attenuation of macrophage activation (104) and stimulation of GLP-1 secretion from intestinal L-cells (105).

As summarized in Table 4-1, there is direct evidence that FXR and TGR5 signaling have important role in the metabolic effects of metabolic surgery. In FXR knock out mice, VSG could not induce weight loss and improved glucose tolerance compared to control sham mice (34). In TGR5 knock out mice, the effects of VSG were not diminished entirely; weight loss effect was similar as in wild type mice, but glucose tolerance effect was less than in wild type mice (99). These studies emphasize the role of bile acid signaling in the metabolic improvements after metabolic surgery. However, somewhat contradictory results were reported on the attempts to use FXR as a

therapeutic target of metabolic diseases. Using FXR agonist not absorbed systematically, intestinal FXR agonism prevented diet-induced obesity and improved glucose metabolism (106). In contrast to this, intestinal FXR antagonist also prevented diet induced obesity and improved glucose tolerance in mice fed high fat diet (107). FXR is a nuclear receptor expressed in various types of cells and exerts pleiotropic effects differentially in each organ (108). Thus, it is still difficult to conclude the role of FXR in the glucose metabolism and metabolic surgery.

2. Candidates for the molecular target of metabolic surgery suggested in current study

I employed systematic unbiased approach to the transcriptome of the distal small intestine of IT rat model using microarray, and the transcriptome of liver, fat, and skeletal muscle of VSG mouse model using RNA sequencing. With this approach, I could explore the gene expression profile brought by metabolic surgery in these organs, and this gene expression profile can give us insights for the mechanism of metabolic surgery in molecular level.

2.1. Extracellular matrix and immune response are the two major component altered in the distal small intestine after IT

In the transcriptome analysis of the transposed distal ileum, numerous genes were found to be differentially expressed by IT. Among these genes, two key components were noted, extracellular matrix protein, and immune response

genes, cytokines and chemokines. Extracellular matrix proteins are related to the structural adaptation of the transposed ileum, and cytokines and chemokines are related to the immune adaptation.

Only a few studies have shown direct evidence relating structural adaptation of the intestine with glucose metabolism in animal models of RYGB or VSG (68). However, several potential mechanisms may explain the roles of structural changes in metabolic improvement after bariatric surgery. The increase in villi length and ileum diameter tremendously increase the luminal surface area, which allows efficient absorption of nutrients. A rapid rise in plasma glucose levels after oral ingestion and exaggerated postprandial insulin secretion are consistently observed in patients who have undergone RYGB or VSG (22). Increased luminal surface area might contribute to these changes. Another potential mechanism is the change in gut permeability. The up-regulation of laminin (*Lama2* and *Lamc1*) and collagens (*Col4a1* and *Col1a2*), which are the major components of the basement membrane, could enhance the structural integrity of the intestine, thereby reducing gut permeability.

The immune adaptation was apparent at postoperative week 4. Cytokines including *Il1a, Il1b, Il17a,* and *Il22* and chemokines including *Ccl3, Ccl5, Ccl17, Cxcl1, Cxcl19, Ccl19* were up-regulated. The intestine serves an important role in immune system. The immune response primed in the intestine can affect the whole body immune response. Among the cytokines, *Il1b, Il17a* and *Il22* suggests the possible activation of Th17 cells (109). Th17 cells play an important role in maintaining mucosal barrier and regulates mucosal immunity against fungi and bacteria in the intestine (109). Interestingly, a

specific gut microbiota promotes Th17 differentiation (110), and the composition of gut microbiota affects the development of Th17 in the intestine (111), which suggests a potential role of Th17 in the host-gut microbiome interaction. In addition, there is a more direct evidence that suggests a role of intestinal Th17 cell in metabolism. The number of Th17 cells were reduced in the small intestine of high fat diet-fed mice (112). Intriguingly, transfer of gut-tropic Th17 cells to those mice decreased body weight and improved glucose metabolism, which was accompanied by the expansion of commensal gut microbes (112).

In current analysis, *Tlr2* and *Tlr4* were also upregulated in the transposed ileum. Toll-like receptors are involved in the interaction between gut microbiota and host (113). *Tlr2* mediates gut microbiota's stimulation of epithelial proliferation in the small intestinal mucosa (114). Gut microbiota is known to play an important role in the pathogenesis of T2DM, and also mediates key effects of bariatric surgery (115). The changes in various immunologic signals including TLRs might mediate the altered interaction between gut microbiota and host, and potentially involve in glucose metabolism.

2.2. Immune response is the common pathway affected by VSG in the liver, fat and muscle

In VSG mouse model, I analyzed the gene expression profile of the three organs involved in glucose metabolism, liver, fat and muscle. First, the results of RNA sequencing were inspected in each organ. Interestingly, the difference between VSG and sham-PF was larger than the difference between

sham-PF and sham. Thus, I focused on the DEGs in the comparison between VSG and sham-PF. In the enrichment analysis of gene ontology and KEGG pathways, immune response-related gene ontology and pathways were commonly enriched in up-regulated DEGs of all the three organs. For the next step, when compared the DEGs of the three organs, *Cxcl13* and several immunoglobulin genes were commonly up-regulated in the three organs. Interestingly, in the analysis of the RNA sequencing results of RYGB mouse model, *Cxcl13* was also commonly up-regulated in liver, fat and muscle. *Cxcl13* is a chemokine selectively acts on B cells. *Cxcl13* and immunoglobulin genes suggests the possibility of B cell response was enhanced after VSG. For more detailed characterization of immune response changed after VSG, the immune cell population in the SVF of adipose tissue was examined. In the analysis of lymphocytes population, the B cell population was significantly increased after VSG.

The inflammatory response examined under the H&E histology was clearly reduced after VSG than sham, which was the reduced number of crown-like structure in adipose tissue and attenuated fatty degeneration in liver. However, several immune response-related genes were up-regulated in all the three organs, and specific immune cell population, B cell, was increased in adipose tissue after VSG. Although, the role of B cell in adipose tissue is not well characterized yet, these results suggest the possibility that immune response is not all detrimental for metabolism, otherwise some of them including B cell response might have beneficial effects on metabolism.

3. Review of previous studies involving the immune system with metabolic surgery

3.1. The immune response is not always decreased after metabolic improvements induced by metabolic surgery

Obesity and diabetes are considered as chronic low grade inflammatory diseases (116). Obese subjects have increased systemic level of proinflammatory cytokine. Adipose tissue is also infiltrated with inflammatory cells, and cellular necrosis is increased in obese subjects (117). T2DM is also well-known to be associated with increased inflammatory response (118). The systematic level of proinflammatory cytokines are increased in T2DM patients. Weight loss by low calorie diet can reverse these chronic inflammatory responses. The systemic level of cytokines and inflammatory response in peripheral tissues are all reduced after achieving weight loss by low calorie diet (119). This is also confirmed by decreased expression of proinflammatory genes in peripheral tissues. Thus, it can be expected that metabolic surgery induces metabolic improvements and, then, decrease of inflammatory response in peripheral tissues. However, there are several evidences show that some immune response is upregulated after metabolic surgery.

Hagman et al. investigated the changes in systemic level of inflammatory cytokines and immune cell density in adipose tissue of patients underwent RYGB or VSG (120). After 1 year, patients showed in average 35 kg weight loss, but the number of neutrophil, dendritic cell, macrophage and T cell were increased in subcutaneous adipose tissue. The level of c-reactive

protein (CRP) was significantly reduced more than half. In a meta-analysis of systemic level of inflammatory markers after metabolic surgeries, the level of CRP and IL-6 was decreased significantly, but the level of TNF-α was not significantly changed (121). Similarly, in another meta-analysis of inflammation in adipose tissue after metabolic surgeries, the results were inconsistent for the gene expression levels of TNF-α, IL-1b, IL-6 and MCP-1 (122). Lips et al. compared RYGB and very low calorie diet (VLCD) on inflammatory cytokine and immune cell infiltration of adipose tissue. They found that the IL-4 was higher in VLCD, but TNF-α, number of T-cell and B-cell were higher in RYGB than VLCD (123). In addition, in animal study, Frikke-Schmidt et al. compared the effects of VSG to sham and sham pair fed group (124). Interestingly, number of T cells and macrophages were increased in epididymal fat after VSG compared to sham and sham PF. Number of adipose tissue dendritic cell was lower in VSG group. Collectively, these results suggest that systemic level of cytokines or chemokines, and infiltration of immune cells and expression of inflammatory cytokines in adipose tissue are not consistently decreased by metabolic surgery. Different immune responses are differentially affected by metabolic surgery.

3.2. The possible link between B cell and glucose metabolism

In chapter 2, the immune response was the common gene ontology enriched in all the three organs. Among the 30 genes included in the DEGs in the three organs, *Cxcl13* and immunoglobulin genes were noted. Cxcl13 is a chemokine belonging to CXC chemokine family. It is selectively chemotactic

for B cells. Cxcl13 is required for the formation of B cell follicle. It is secreted by immune cells including T cell and monocytes to incorporate B cells. Interestingly, there are some evidences that other cell types can also secret Cxcl13. The 3T3-L1 adipocyte cell line increased gene expression of Cxcl13 during maturation (125, 126). In addition, Cxcl13 was expressed in primary mouse myocyte when cultured in vitro and myogenesis was induced (127). Another interesting report is that plasma cells reside in adipose tissue and Fc receptors are expressed in adipocytes which was investigated in human subcutaneous adipose tissue sample (128). In addition, by incubation with Fc moiety of IgG, the immune gene, IL1b and IL6 expression was reduced in adipocytes and lipogenesis was stimulated as much as insulin treatment.

In vivo studies investigated the role of B-cell in adipose tissue and glucose metabolism was done using various mouse models. B cells are accumulated in visceral adipose tissue of high fat-fed mice. Mice lacking B cells (immunoglobulin μ heavy chain knockout mice) were protected from glucose intolerance even after high fat feeding (129). Injection of IgG to these B cell null mice, the glucose tolerance was deteriorated. In addition, high fat-fed mice treated with CD20 antibody to deplete B cells showed improved glucose tolerance (129). These suggested that the B cells in adipose tissue promote insulin resistance through production of pathogenic antibodies. In addition, in more recent studies, B cell subtype might have differential impact on adipose tissue inflammation and glucose metabolism. Regulatory B cells negatively control adipose tissue inflammation (130), while B2 subtype promote insulin resistance and adipose tissue inflammation (131).

4. Suggestions for further investigation

Current study suggested possible candidates for the molecular target of metabolic surgery. About Cxcl13 and B cell response, I confirmed the change in cellular level using tissue flow cytometry. However, I could not demonstrate the impact of that pathway in the effects of VSG. For confirmatory results, experimental studies using inhibitor of the specific pathway or knock out model of the target gene is necessary.

RNA sequencing and microarray can analyze the expression of mRNAs in whole transcriptomic level. However, this bulk transciptome analysis cannot differentiate whether the changes are caused by the changes in the intracellular level of each mRNAs or the changes in the number of the cells express each mRNAs. In other words, I cannot differentiate the intracellular change with changes of cell composition. Single cell RNA sequencing can overcome this limitation. Using cDNA library tagged with labels specific for each cell, I can discriminate the changes of the mRNA expression in cell level, not tissue level.

These two approaches and focus on the role of immune system in the metabolic surgery would be a future direction to elucidate the fundamental mechanism of metabolic surgery.

Acknowledgement

Professor Young Min Cho was the advisor of this thesis. Prof. Cho contributed to build the concept of this study, design the study scheme, discuss study results, and edit the manuscript. Eun Hye Choi contributed to the animal surgery and postoperative care. Tae Jung Oh contributed to the animal surgery. Sehyun Chae and Daehee Hwang contributed to the microarray analysis. Hyung Jung Lee, Woochan Lee and Jong-Il Kim contributed to the RNA sequencing analysis. Byung Soo Kong contributed to discuss study results.

Reference

1. World Health Organization. Obesity and overweight 2016 [Available from: https://www.who.int/news-room/fact-sheets/detail/obesity-and-overweight.

2. Korean Ministry of Health and Welfare. Korea Health Statistics 2017 [Available from: http://www.index.go.kr/unify/idx-info.do?idxCd=4040.

3. Bluher M. Obesity: global epidemiology and pathogenesis. Nature reviews Endocrinology. 2019.

4. Bray GA, Kim KK, Wilding JPH. Obesity: a chronic relapsing progressive disease process. A position statement of the World Obesity Federation. Obesity reviews : an official journal of the International Association for the Study of Obesity. 2017;18(7):715-23.

5. Diagnosis and classification of diabetes mellitus. Diabetes care. 2004;27 Suppl 1:S5-s10.

6. 2. Classification and Diagnosis of Diabetes: Standards of Medical Care in Diabetes-2019. Diabetes care. 2019;42(Suppl 1):S13-s28.

7. Colditz GA, Willett WC, Rotnitzky A, Manson JE. Weight gain as a risk factor for clinical diabetes mellitus in women. Annals of internal medicine. 1995;122(7):481-6.

8. Derosa G, Maffioli P. Anti-obesity drugs: a review about their effects and their safety. Expert opinion on drug safety. 2012;11(3):459-71.

9. Bessesen DH, Van Gaal LF. Progress and challenges in anti-obesity pharmacotherapy. The lancet Diabetes & endocrinology. 2018;6(3):237-48.

10. Carls G, Huynh J, Tuttle E, Yee J, Edelman SV. Achievement of Glycated Hemoglobin Goals in the US Remains Unchanged Through 2014. Diabetes therapy : research, treatment and education of diabetes and related disorders. 2017;8(4):863-73.

11. Won JC, Lee JH, Kim JH, Kang ES, Won KC, Kim DJ, et al. Diabetes Fact Sheet in Korea, 2016: An Appraisal of Current Status. Diabetes & metabolism journal. 2018;42(5):415-24.

12. Phillips BT, Shikora SA. The history of metabolic and bariatric surgery: Development of standards for patient safety and efficacy. Metabolism: clinical and experimental. 2018;79:97-107.

13. Kremen AJ, Linner JH, Nelson CH. An experimental evaluation of the nutritional importance of proximal and distal small intestine. Annals of surgery. 1954;140(3):439-48.

14. Printen KJ, Mason EE. Gastric surgery for relief of morbid obesity. Archives of surgery (Chicago, Ill : 1960). 1973;106(4):428-31.

15. Wilkinson LH, Peloso OA. Gastric (reservoir) reduction for morbid obesity. Archives of surgery (Chicago, Ill : 1960). 1981;116(5):602-5.

16. Kuzmak LI. A Review of Seven Years' Experience with Silicone Gastric Banding. Obesity surgery. 1991;1(4):403-8.

17. Angrisani L, Santonicola A, Iovino P, Formisano G, Buchwald H, Scopinaro N. Bariatric Surgery Worldwide 2013. Obesity surgery. 2015;25(10):1822-32.

18. Moshiri M, Osman S, Robinson TJ, Khandelwal S, Bhargava P, Rohrmann CA. Evolution of bariatric surgery: a historical perspective. AJR

American journal of roentgenology. 2013;201(1):W40-8.

19. Ren CJ, Patterson E, Gagner M. Early results of laparoscopic biliopancreatic diversion with duodenal switch: a case series of 40 consecutive patients. Obesity surgery. 2000;10(6):514-23; discussion 24.

20. Gumbs AA, Gagner M, Dakin G, Pomp A. Sleeve gastrectomy for morbid obesity. Obesity surgery. 2007;17(7):962-9.

21. Olbers T, Lonroth H, Fagevik-Olsen M, Lundell L. Laparoscopic gastric bypass: development of technique, respiratory function, and long-term outcome. Obesity surgery. 2003;13(3):364-70.

22. Madsbad S, Dirksen C, Holst JJ. Mechanisms of changes in glucose metabolism and bodyweight after bariatric surgery. The lancet Diabetes & endocrinology. 2014;2(2):152-64.

23. Chang SH, Stoll CR, Song J, Varela JE, Eagon CJ, Colditz GA. The effectiveness and risks of bariatric surgery: an updated systematic review and meta-analysis, 2003-2012. JAMA surgery. 2014;149(3):275-87.

24. Sjostrom L, Narbro K, Sjostrom CD, Karason K, Larsson B, Wedel H, et al. Effects of bariatric surgery on mortality in Swedish obese subjects. The New England journal of medicine. 2007;357(8):741-52.

25. Courcoulas AP, King WC, Belle SH, Berk P, Flum DR, Garcia L, et al. Seven-Year Weight Trajectories and Health Outcomes in the Longitudinal Assessment of Bariatric Surgery (LABS) Study. JAMA surgery. 2018;153(5):427-34.

26. Schauer PR, Bhatt DL, Kirwan JP, Wolski K, Aminian A, Brethauer SA, et al. Bariatric Surgery versus Intensive Medical Therapy for Diabetes - 5-

Year Outcomes. The New England journal of medicine. 2017;376(7):641-51.

27. Ashrafian H, Bueter M, Ahmed K, Suliman A, Bloom SR, Darzi A, et al. Metabolic surgery: an evolution through bariatric animal models. Obesity reviews : an official journal of the International Association for the Study of Obesity. 2010;11(12):907-20.

28. Sumithran P, Prendergast LA, Delbridge E, Purcell K, Shulkes A, Kriketos A, et al. Long-term persistence of hormonal adaptations to weight loss. The New England journal of medicine. 2011;365(17):1597-604.

29. Sudan R, Sudan R, Lyden E, Thompson JS. Food cravings and food consumption after Roux-en-Y gastric bypass versus cholecystectomy. Surgery for obesity and related diseases : official journal of the American Society for Bariatric Surgery. 2017;13(2):220-6.

30. Mans E, Serra-Prat M, Palomera E, Sunol X, Clave P. Sleeve gastrectomy effects on hunger, satiation, and gastrointestinal hormone and motility responses after a liquid meal test. The American journal of clinical nutrition. 2015;102(3):540-7.

31. Ochner CN, Stice E, Hutchins E, Afifi L, Geliebter A, Hirsch J, et al. Relation between changes in neural responsivity and reductions in desire to eat high-calorie foods following gastric bypass surgery. Neuroscience. 2012;209:128-35.

32. Mathes CM, Spector AC. Food selection and taste changes in humans after Roux-en-Y gastric bypass surgery: a direct-measures approach. Physiology & behavior. 2012;107(4):476-83.

33. Stearns AT, Balakrishnan A, Tavakkolizadeh A. Impact of Roux-en-Y

gastric bypass surgery on rat intestinal glucose transport. American journal of physiology Gastrointestinal and liver physiology. 2009;297(5):G950-7.

34. Ryan KK, Tremaroli V, Clemmensen C, Kovatcheva-Datchary P, Myronovych A, Karns R, et al. FXR is a molecular target for the effects of vertical sleeve gastrectomy. Nature. 2014;509(7499):183-8.

35. Ding L, Sousa KM, Jin L, Dong B, Kim BW, Ramirez R, et al. Vertical sleeve gastrectomy activates GPBAR-1/TGR5 to sustain weight loss, improve fatty liver, and remit insulin resistance in mice. Hepatology (Baltimore, Md). 2016;64(3):760-73.

36. Grayson BE, Schneider KM, Woods SC, Seeley RJ. Improved rodent maternal metabolism but reduced intrauterine growth after vertical sleeve gastrectomy. Science translational medicine. 2013;5(199):199ra12.

37. Odstrcil EA, Martinez JG, Santa Ana CA, Xue B, Schneider RE, Steffer KJ, et al. The contribution of malabsorption to the reduction in net energy absorption after long-limb Roux-en-Y gastric bypass. The American journal of clinical nutrition. 2010;92(4):704-13.

38. Mahawar KK, Sharples AJ. Contribution of Malabsorption to Weight Loss After Roux-en-Y Gastric Bypass: a Systematic Review. Obesity surgery. 2017;27(8):2194-206.

39. Fox W, Borgert A, Rasmussen C, Kallies K, Klas P, Kothari S. Long-term micronutrient surveillance after gastric bypass surgery in an integrated healthcare system. Surgery for obesity and related diseases : official journal of the American Society for Bariatric Surgery. 2019.

40. Knowler WC, Pettitt DJ, Savage PJ, Bennett PH. Diabetes incidence

in Pima indians: contributions of obesity and parental diabetes. American journal of epidemiology. 1981;113(2):144-56.

41. Lipton RB, Liao Y, Cao G, Cooper RS, McGee D. Determinants of incident non-insulin-dependent diabetes mellitus among blacks and whites in a national sample. The NHANES I Epidemiologic Follow-up Study. American journal of epidemiology. 1993;138(10):826-39.

42. Campbell PJ, Gerich JE. Impact of obesity on insulin action in volunteers with normal glucose tolerance: demonstration of a threshold for the adverse effect of obesity. The Journal of clinical endocrinology and metabolism. 1990;70(4):1114-8.

43. Knowler WC, Fowler SE, Hamman RF, Christophi CA, Hoffman HJ, Brenneman AT, et al. 10-year follow-up of diabetes incidence and weight loss in the Diabetes Prevention Program Outcomes Study. Lancet (London, England). 2009;374(9702):1677-86.

44. Rubino F, Schauer PR, Kaplan LM, Cummings DE. Metabolic surgery to treat type 2 diabetes: clinical outcomes and mechanisms of action. Annual review of medicine. 2010;61:393-411.

45. Kirk E, Reeds DN, Finck BN, Mayurranjan SM, Patterson BW, Klein S. Dietary fat and carbohydrates differentially alter insulin sensitivity during caloric restriction. Gastroenterology. 2009;136(5):1552-60.

46. Jackness C, Karmally W, Febres G, Conwell IM, Ahmed L, Bessler M, et al. Very low-calorie diet mimics the early beneficial effect of Roux-en-Y gastric bypass on insulin sensitivity and beta-cell Function in type 2 diabetic patients. Diabetes. 2013;62(9):3027-32.

47. Bradley D, Magkos F, Klein S. Effects of bariatric surgery on glucose homeostasis and type 2 diabetes. Gastroenterology. 2012;143(4):897-912.

48. Chambers AP, Jessen L, Ryan KK, Sisley S, Wilson-Perez HE, Stefater MA, et al. Weight-independent changes in blood glucose homeostasis after gastric bypass or vertical sleeve gastrectomy in rats. Gastroenterology. 2011;141(3):950-8.

49. Abu-Gazala S, Horwitz E, Ben-Haroush Schyr R, Bardugo A, Israeli H, Hija A, et al. Sleeve Gastrectomy Improves Glycemia Independent of Weight Loss by Restoring Hepatic Insulin Sensitivity. Diabetes. 2018;67(6):1079-85.

50. Myronovych A, Kirby M, Ryan KK, Zhang W, Jha P, Setchell KD, et al. Vertical sleeve gastrectomy reduces hepatic steatosis while increasing serum bile acids in a weight-loss-independent manner. Obesity (Silver Spring, Md). 2014;22(2):390-400.

51. Douros JD, Niu J, Sdao S, Gregg T, Fisher-Wellman K, Bharadwaj M, et al. Sleeve gastrectomy rapidly enhances islet function independently of body weight. JCI insight. 2019;4(6).

52. Pories WJ, Swanson MS, MacDonald KG, Long SB, Morris PG, Brown BM, et al. Who would have thought it? An operation proves to be the most effective therapy for adult-onset diabetes mellitus. Annals of surgery. 1995;222(3):339-50; discussion 50-2.

53. Pournaras DJ, Osborne A, Hawkins SC, Vincent RP, Mahon D, Ewings P, et al. Remission of type 2 diabetes after gastric bypass and banding: mechanisms and 2 year outcomes. Annals of surgery. 2010;252(6):966-71.

54. Service GJ, Thompson GB, Service FJ, Andrews JC, Collazo-Clavell ML, Lloyd RV. Hyperinsulinemic hypoglycemia with nesidioblastosis after gastric-bypass surgery. The New England journal of medicine. 2005;353(3):249-54.

55. Matthews DR, Hosker JP, Rudenski AS, Naylor BA, Treacher DF, Turner RC. Homeostasis model assessment: insulin resistance and beta-cell function from fasting plasma glucose and insulin concentrations in man. Diabetologia. 1985;28(7):412-9.

56. Rao RS, Yanagisawa R, Kini S. Insulin resistance and bariatric surgery. Obesity reviews : an official journal of the International Association for the Study of Obesity. 2012;13(4):316-28.

57. DeFronzo RA, Tobin JD, Andres R. Glucose clamp technique: a method for quantifying insulin secretion and resistance. The American journal of physiology. 1979;237(3):E214-23.

58. Bojsen-Moller KN, Dirksen C, Jorgensen NB, Jacobsen SH, Serup AK, Albers PH, et al. Early enhancements of hepatic and later of peripheral insulin sensitivity combined with increased postprandial insulin secretion contribute to improved glycemic control after Roux-en-Y gastric bypass. Diabetes. 2014;63(5):1725-37.

59. Bradley D, Magkos F, Eagon JC, Varela JE, Gastaldelli A, Okunade AL, et al. Matched weight loss induced by sleeve gastrectomy or gastric bypass similarly improves metabolic function in obese subjects. Obesity (Silver Spring, Md). 2014;22(9):2026-31.

60. Dirksen C, Jorgensen NB, Bojsen-Moller KN, Jacobsen SH, Hansen

DL, Worm D, et al. Mechanisms of improved glycaemic control after Roux-en-Y gastric bypass. Diabetologia. 2012;55(7):1890-901.

61. Lindqvist A, Spegel P, Ekelund M, Garcia Vaz E, Pierzynowski S, Gomez MF, et al. Gastric bypass improves beta-cell function and increases beta-cell mass in a porcine model. Diabetes. 2014;63(5):1665-71.

62. Wilson-Perez HE, Chambers AP, Ryan KK, Li B, Sandoval DA, Stoffers D, et al. Vertical sleeve gastrectomy is effective in two genetic mouse models of glucagon-like Peptide 1 receptor deficiency. Diabetes. 2013;62(7):2380-5.

63. Chambers AP, Kirchner H, Wilson-Perez HE, Willency JA, Hale JE, Gaylinn BD, et al. The effects of vertical sleeve gastrectomy in rodents are ghrelin independent. Gastroenterology. 2013;144(1):50-2.e5.

64. Mul JD, Begg DP, Alsters SI, van Haaften G, Duran KJ, D'Alessio DA, et al. Effect of vertical sleeve gastrectomy in melanocortin receptor 4-deficient rats. American journal of physiology Endocrinology and metabolism. 2012;303(1):E103-10.

65. Frikke-Schmidt H, Hultman K, Galaske JW, Jorgensen SB, Myers MG, Jr., Seeley RJ. GDF15 acts synergistically with liraglutide but is not necessary for the weight loss induced by bariatric surgery in mice. Molecular metabolism. 2019;21:13-21.

66. Oh TJ, Ahn CH, Cho YM. Contribution of the distal small intestine to metabolic improvement after bariatric/metabolic surgery: Lessons from ileal transposition surgery. Journal of diabetes investigation. 2016;7 Suppl 1:94-101.

67. Shaw D, Gohil K, Basson MD. Intestinal mucosal atrophy and

adaptation. World journal of gastroenterology. 2012;18(44):6357-75.

68. Seeley RJ, Chambers AP, Sandoval DA. The role of gut adaptation in the potent effects of multiple bariatric surgeries on obesity and diabetes. Cell metabolism. 2015;21(3):369-78.

69. Kohli R, Kirby M, Setchell KD, Jha P, Klustaitis K, Woollett LA, et al. Intestinal adaptation after ileal interposition surgery increases bile acid recycling and protects against obesity-related comorbidities. American journal of physiology Gastrointestinal and liver physiology. 2010;299(3):G652-60.

70. Oh TJ, Lee HJ, Cho YM. Ileal Transposition Decreases Plasma Lipopolysaccharide Levels in Association with Increased L Cell Secretion in Non-obese Non-diabetic Rats. Obesity surgery. 2016;26(6):1287-95.

71. Strader AD, Vahl TP, Jandacek RJ, Woods SC, D'Alessio DA, Seeley RJ. Weight loss through ileal transposition is accompanied by increased ileal hormone secretion and synthesis in rats. American journal of physiology Endocrinology and metabolism. 2005;288(2):E447-53.

72. Bolstad BM, Irizarry RA, Astrand M, Speed TP. A comparison of normalization methods for high density oligonucleotide array data based on variance and bias. Bioinformatics (Oxford, England). 2003;19(2):185-93.

73. Lee HJ, Suk JE, Patrick C, Bae EJ, Cho JH, Rho S, et al. Direct transfer of alpha-synuclein from neuron to astroglia causes inflammatory responses in synucleinopathies. The Journal of biological chemistry. 2010;285(12):9262-72.

74. Hwang D, Rust AG, Ramsey S, Smith JJ, Leslie DM, Weston AD, et al. A data integration methodology for systems biology. Proceedings of the National Academy of Sciences of the United States of America.

2005;102(48):17296-301.

75. Storey JD, Tibshirani R. Statistical significance for genomewide studies. Proceedings of the National Academy of Sciences of the United States of America. 2003;100(16):9440-5.

76. Huang da W, Sherman BT, Lempicki RA. Systematic and integrative analysis of large gene lists using DAVID bioinformatics resources. Nature protocols. 2009;4(1):44-57.

77. Bader GD, Betel D, Hogue CW. BIND: the Biomolecular Interaction Network Database. Nucleic Acids Res. 2003;31(1):248-50.

78. Peri S, Navarro JD, Kristiansen TZ, Amanchy R, Surendranath V, Muthusamy B, et al. Human protein reference database as a discovery resource for proteomics. Nucleic acids research. 2004;32:D497-D501.

79. Stark C, Breitkreutz BJ, Reguly T, Boucher L, Breitkreutz A, Tyers M. BioGRID: a general repository for interaction datasets. Nucleic acids research. 2006;34:D535-D9.

80. Chatr-Aryamontri A, Ceol A, Palazzi LM, Nardelli G, Schneider MV, Castagnoli L, et al. MINT: the molecular INTeraction database. Nucleic acids research. 2007;35:D572-D4.

81. Shimoyama M, De Pons J, Hayman GT, Laulederkind SJ, Liu W, Nigam R, et al. The Rat Genome Database 2015: genomic, phenotypic and environmental variations and disease. Nucleic Acids Res. 2015;43(Database issue):D743-50.

82. Cline MS, Smoot M, Cerami E, Kuchinsky A, Landys N, Workman C, et al. Integration of biological networks and gene expression data using

Cytoscape. Nature Protocols. 2007;2(10):2366-82.

83. Kanehisa M, Goto S, Sato Y, Furumichi M, Tanabe M. KEGG for integration and interpretation of large-scale molecular data sets. Nucleic Acids Res. 2012;40(Database issue):D109-14.

84. Schuppan D, Riecken EO. Molecules of the extracellular matrix: potential role of collagens and glycoproteins in intestinal adaptation. Digestion. 1990;46 Suppl 2:2-11.

85. Culnan DM, Albaugh V, Sun M, Lynch CJ, Lang CH, Cooney RN. Ileal interposition improves glucose tolerance and insulin sensitivity in the obese Zucker rat. American journal of physiology Gastrointestinal and liver physiology. 2010;299(3):G751-60.

86. Ikezawa F, Shibata C, Kikuchi D, Imoto H, Miura K, Naitoh T, et al. Effects of ileal interposition on glucose metabolism in obese rats with diabetes. Surgery. 2012;151(6):822-30.

87. Cummings BP, Bettaieb A, Graham JL, Kim J, Ma F, Shibata N, et al. Bile-acid-mediated decrease in endoplasmic reticulum stress: a potential contributor to the metabolic benefits of ileal interposition surgery in UCD-T2DM rats. Disease models & mechanisms. 2013;6(2):443-56.

88. Cummings BP, Strader AD, Stanhope KL, Graham JL, Lee J, Raybould HE, et al. Ileal interposition surgery improves glucose and lipid metabolism and delays diabetes onset in the UCD-T2DM rat. Gastroenterology. 2010;138(7):2437-46, 46.e1.

89. Gaitonde S, Kohli R, Seeley R. The role of the gut hormone GLP-1 in the metabolic improvements caused by ileal transposition. The Journal of

surgical research. 2012;178(1):33-9.

90. Cho YM, Fujita Y, Kieffer TJ. Glucagon-like peptide-1: glucose homeostasis and beyond. Annual review of physiology. 2014;76:535-59.

91. Yusta B, Baggio LL, Estall JL, Koehler JA, Holland DP, Li H, et al. GLP-1 receptor activation improves beta cell function and survival following induction of endoplasmic reticulum stress. Cell metabolism. 2006;4(5):391-406.

92. O'Connor TP, Lam MM, Diamond J. Magnitude of functional adaptation after intestinal resection. The American journal of physiology. 1999;276(5 Pt 2):R1265-75.

93. Liou AP, Paziuk M, Luevano JM, Jr., Machineni S, Turnbaugh PJ, Kaplan LM. Conserved shifts in the gut microbiota due to gastric bypass reduce host weight and adiposity. Science translational medicine. 2013;5(178):178ra41.

94. Kellett GL, Helliwell PA. The diffusive component of intestinal glucose absorption is mediated by the glucose-induced recruitment of GLUT2 to the brush-border membrane. The Biochemical journal. 2000;350 Pt 1:155-62.

95. Cani PD, Holst JJ, Drucker DJ, Delzenne NM, Thorens B, Burcelin R, et al. GLUT2 and the incretin receptors are involved in glucose-induced incretin secretion. Molecular and cellular endocrinology. 2007;276(1-2):18-23.

96. Mace OJ, Schindler M, Patel S. The regulation of K- and L-cell activity by GLUT2 and the calcium-sensing receptor CasR in rat small intestine. The Journal of physiology. 2012;590(12):2917-36.

97. Schauer PR, Kashyap SR, Wolski K, Brethauer SA, Kirwan JP, Pothier

CE, et al. Bariatric surgery versus intensive medical therapy in obese patients with diabetes. The New England journal of medicine. 2012;366(17):1567-76.

98. Vento-Tormo R, Efremova M, Botting RA, Turco MY, Vento-Tormo M, Meyer KB, et al. Single-cell reconstruction of the early maternal-fetal interface in humans. Nature. 2018;563(7731):347-53.

99. McGavigan AK, Garibay D, Henseler ZM, Chen J, Bettaieb A, Haj FG, et al. TGR5 contributes to glucoregulatory improvements after vertical sleeve gastrectomy in mice. Gut. 2017;66(2):226-34.

100. Ben-Zvi D, Meoli L, Abidi WM, Nestoridi E, Panciotti C, Castillo E, et al. Time-Dependent Molecular Responses Differ between Gastric Bypass and Dieting but Are Conserved Across Species. Cell metabolism. 2018;28(2):310-23.e6.

101. Albaugh VL, Banan B, Ajouz H, Abumrad NN, Flynn CR. Bile acids and bariatric surgery. Molecular aspects of medicine. 2017;56:75-89.

102. Cipriani S, Mencarelli A, Palladino G, Fiorucci S. FXR activation reverses insulin resistance and lipid abnormalities and protects against liver steatosis in Zucker (fa/fa) obese rats. Journal of lipid research. 2010;51(4):771-84.

103. Li T, Owsley E, Matozel M, Hsu P, Novak CM, Chiang JY. Transgenic expression of cholesterol 7alpha-hydroxylase in the liver prevents high-fat diet-induced obesity and insulin resistance in mice. Hepatology (Baltimore, Md). 2010;52(2):678-90.

104. Lou G, Ma X, Fu X, Meng Z, Zhang W, Wang YD, et al. GPBAR1/TGR5 mediates bile acid-induced cytokine expression in murine

Kupffer cells. PloS one. 2014;9(4):e93567.

105. Habib AM, Richards P, Rogers GJ, Reimann F, Gribble FM. Co-localisation and secretion of glucagon-like peptide 1 and peptide YY from primary cultured human L cells. Diabetologia. 2013;56(6):1413-6.

106. Fang S, Suh JM, Reilly SM, Yu E, Osborn O, Lackey D, et al. Intestinal FXR agonism promotes adipose tissue browning and reduces obesity and insulin resistance. Nature medicine. 2015;21(2):159-65.

107. Jiang C, Xie C, Lv Y, Li J, Krausz KW, Shi J, et al. Intestine-selective farnesoid X receptor inhibition improves obesity-related metabolic dysfunction. Nature communications. 2015;6:10166.

108. Massafra V, Pellicciari R, Gioiello A, van Mil SWC. Progress and challenges of selective Farnesoid X Receptor modulation. Pharmacology & therapeutics. 2018;191:162-77.

109. Blaschitz C, Raffatellu M. Th17 cytokines and the gut mucosal barrier. Journal of clinical immunology. 2010;30(2):196-203.

110. Ivanov, II, Frutos Rde L, Manel N, Yoshinaga K, Rifkin DB, Sartor RB, et al. Specific microbiota direct the differentiation of IL-17-producing T-helper cells in the mucosa of the small intestine. Cell host & microbe. 2008;4(4):337-49.

111. Gaboriau-Routhiau V, Rakotobe S, Lecuyer E, Mulder I, Lan A, Bridonneau C, et al. The key role of segmented filamentous bacteria in the coordinated maturation of gut helper T cell responses. Immunity. 2009;31(4):677-89.

112. Hong CP, Park A, Yang BG, Yun CH, Kwak MJ, Lee GW, et al. Gut-

Specific Delivery of T-Helper 17 Cells Reduces Obesity and Insulin Resistance in Mice. Gastroenterology. 2017;152(8):1998-2010.

113. Yiu JH, Dorweiler B, Woo CW. Interaction between gut microbiota and toll-like receptor: from immunity to metabolism. Journal of molecular medicine (Berlin, Germany). 2017;95(1):13-20.

114. Hormann N, Brandao I, Jackel S, Ens N, Lillich M, Walter U, et al. Gut microbial colonization orchestrates TLR2 expression, signaling and epithelial proliferation in the small intestinal mucosa. PloS one. 2014;9(11):e113080.

115. Tremaroli V, Karlsson F, Werling M, Stahlman M, Kovatcheva-Datchary P, Olbers T, et al. Roux-en-Y Gastric Bypass and Vertical Banded Gastroplasty Induce Long-Term Changes on the Human Gut Microbiome Contributing to Fat Mass Regulation. Cell metabolism. 2015;22(2):228-38.

116. Hotamisligil GS. Inflammation and metabolic disorders. Nature. 2006;444(7121):860-7.

117. Wentworth JM, Naselli G, Brown WA, Doyle L, Phipson B, Smyth GK, et al. Pro-inflammatory CD11c+CD206+ adipose tissue macrophages are associated with insulin resistance in human obesity. Diabetes. 2010;59(7):1648-56.

118. Lontchi-Yimagou E, Sobngwi E, Matsha TE, Kengne AP. Diabetes mellitus and inflammation. Current diabetes reports. 2013;13(3):435-44.

119. Esposito K, Pontillo A, Di Palo C, Giugliano G, Masella M, Marfella R, et al. Effect of weight loss and lifestyle changes on vascular inflammatory markers in obese women: a randomized trial. Jama. 2003;289(14):1799-804.

120. Hagman DK, Larson I, Kuzma JN, Cromer G, Makar K, Rubinow KB, et al. The short-term and long-term effects of bariatric/metabolic surgery on subcutaneous adipose tissue inflammation in humans. Metabolism: clinical and experimental. 2017;70:12-22.

121. Rao SR. Inflammatory markers and bariatric surgery: a meta-analysis. Inflammation research : official journal of the European Histamine Research Society [et al]. 2012;61(8):789-807.

122. Labrecque J, Laforest S, Michaud A, Biertho L, Tchernof A. Impact of Bariatric Surgery on White Adipose Tissue Inflammation. Canadian journal of diabetes. 2017;41(4):407-17.

123. Lips MA, van Klinken JB, Pijl H, Janssen I, Willems van Dijk K, Koning F, et al. Weight loss induced by very low calorie diet is associated with a more beneficial systemic inflammatory profile than by Roux-en-Y gastric bypass. Metabolism: clinical and experimental. 2016;65(11):1614-20.

124. Frikke-Schmidt H, Zamarron BF, O'Rourke RW, Sandoval DA, Lumeng CN, Seeley RJ. Weight loss independent changes in adipose tissue macrophage and T cell populations after sleeve gastrectomy in mice. Molecular metabolism. 2017;6(4):317-26.

125. Kusuyama J, Komorizono A, Bandow K, Ohnishi T, Matsuguchi T. CXCL3 positively regulates adipogenic differentiation. Journal of lipid research. 2016;57(10):1806-20.

126. Kabir SM, Lee ES, Son DS. Chemokine network during adipogenesis in 3T3-L1 cells: Differential response between growth and proinflammatory factor in preadipocytes vs. adipocytes. Adipocyte. 2014;3(2):97-106.

127. Griffin CA, Apponi LH, Long KK, Pavlath GK. Chemokine expression and control of muscle cell migration during myogenesis. Journal of cell science. 2010;123(Pt 18):3052-60.

128. Palming J, Gabrielsson BG, Jennische E, Smith U, Carlsson B, Carlsson LM, et al. Plasma cells and Fc receptors in human adipose tissue--lipogenic and anti-inflammatory effects of immunoglobulins on adipocytes. Biochemical and biophysical research communications. 2006;343(1):43-8.

129. Winer DA, Winer S, Shen L, Wadia PP, Yantha J, Paltser G, et al. B cells promote insulin resistance through modulation of T cells and production of pathogenic IgG antibodies. Nature medicine. 2011;17(5):610-7.

130. Nishimura S, Manabe I, Takaki S, Nagasaki M, Otsu M, Yamashita H, et al. Adipose Natural Regulatory B Cells Negatively Control Adipose Tissue Inflammation. Cell metabolism. 2013;18(5):759-66.

131. Ying W, Wollam J, Ofrecio JM, Bandyopadhyay G, El Ouarrat D, Lee YS, et al. Adipose tissue B2 cells promote insulin resistance through leukotriene LTB4/LTB4R1 signaling. The Journal of clinical investigation. 2017;127(3):1019-30.

국문 초록

비만은 현대사회에서 가장 큰 의료 부담을 야기하는 질병의 하나로써 다양한 대사, 심혈관, 근골격 질환 그리고 종양과 연관되어 있다. 특히 제 2 형 당뇨병은 이러한 비만의 동반 질환 중에서 가장 대표적인 질병으로 환자들의 삶의 질 저하와 사망률의 증가로 이어진다. 현재까지 많은 연구와 노력에도 불구하고 비만과 당뇨 치료법들은 한계점은 가지고 있다. 비교적 최근에 도입된 대사 수술은 위장관계 수술을 통하여 체중을 감소시키고 나아가 당대사를 호전시키고자 하는 치료법이다. 현재까지 개발된 어떠한 약물치료에 비하여 대사 수술은 더 강력한 혈당 저하 및 체중감소 효과를 보이며, 이러한 효과는 10 년이상 오래 유지됨이 밝혀졌다. 특히, 대사 수술은 당뇨 약제를 중단하여도 정상 혈당이 유지되는 당뇨 관해를 유도할 수도 있다고 알려졌다. 이러한 대사 수술의 기전을 연구함으로써 비만과 당뇨병을 치료할 수 있는 새로운 방향을 제시할 수 있을 것으로 기대된다.

이를 위하여, 본 연구에서 두 종류의 대사 수술 동물 모델을 연구하였다. 먼저 회장 전치술 렛트 모델을 통해서 대사 수술에서 원위 회장의 역할 및 수술 후 장의 적응 변화를 살펴보았다. 회장 전치술은 후위부 회장의 일부를 수술적으로 십이지장 다음으로 위치시켜 대사 수술에서 말단부 회장의 역할을 연구하고자 하는 수술법이다. 회

장전치술을 고지방사료 섭취로 비만을 유도한 식이 유발 비만 렛트에서 시행하여 대사적인 효과를 살펴보았다. 회장전치술은 혈당을 감소시켰는데, 특히 식후 인슐린과 GLP-1 분비 증가를 통하여 이를 일으키는 것으로 생각되었다. 또한 이러한 변화는 췌장 베타세포의 증가와 동반되었다. 다음으로 전치된 회장에서의 유전자 발현 변화를 분석하였다. 회장 전치술 후에 1주, 4주가 지나고 회장 조직을 채취하고 마이크로어레이 분석을 시행하여 유전자 발현을 살펴보았다. 흥미롭게도, 1 주와 4 주의 유전자 발현사이에 큰 차이가 있어 회장 전치술 후 초기에 회장에서 매우 역동적인 적응 변화가 일어남을 알 수 있었다. 추가적인 유전자 경로 분석 및 네트워크 분석을 통하여 첫 1주에는 구조적인 적응이, 4주에는 대사적인 적응과 면역학적인 적응이 주된 반응임을 알 수 있었다.

다음으로, 당대사에 중요한 간, 지방, 근육 조직에서의 변화를 살펴보기 위하여 마우스에서 위소매절제술을 시행하여 연구하였다. 식이유도 비만 마우스에서 위소매절제술을 시행한 뒤 간, 지방, 근육 조직을 채취하여 RNA 시퀀싱 분석을 통해 유전자 발현의 차이를 비교하였다. 또한 이를 sham 수술 대조군 뿐만 아니라 sham 수술 후 위소매절제술 수술과 동일한 식이를 섭취하도록 한 pair-fed 그룹과도 비교하여 위소매절제술의 효과에서 체중 감소 독립적인 부분을 확인하고자 하였다. 이러한 실험을 통하여 위소매절제술이 간, 지방, 근육에 모두 유전자 발현 변화를 유도하는데, 특히 이러한 차이는

단순한 식이 제한을 통해 체중 감소를 유도한 pair-fed 마우스에서 대조군과 비교한 차이보다 훨씬 크게 나타나서 위소매절제술의 간, 지방, 근육에 대한 효과 중 체중감소 독립적인 기전에 중요함을 알 수 있었다. 또한 면역 반응과 관련된 유전자들이 세가지 조직에서 모두 공통적으로 변화되어 있었다.

본 연구를 통해서 장에서는 수술 후 다이나믹한 적응 변화가 일어남을 알 수 있었고 말초에서 당을 대사하는 간, 지방, 근육 조직에서는 체중감소 독립적인 유전자 발현 변화가 크게 일어남을 알 수 있었다. 이러한 변화 중 면역 반응과 연관된 유전자 발현 변화가 모두 공통적으로 나타나서 대사 수술 후 면역 반응의 변화가 중요한 역할을 할 가능성을 시사하였다.

주요어 : 대사수술, 비만, 당뇨, 회장 전치술, 위소매절제술, 마이크로어레이, RNA 시퀀싱, 장 적응 변화

학 번 : 2016-30012